NASA TECHNICAL NOTE

NASA TN D-6199

FLUTTER SUPPRESSION USING ACTIVE CONTROLS BASED ON THE CONCEPT OF AERODYNAMIC ENERGY

by E. Nissim

Langley Research Center
Hampton, Va. 23365

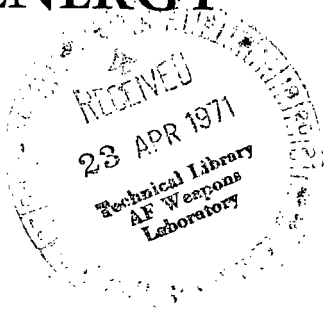

NATIONAL AERONAUTICS AND SPACE ADMINISTRATION • WASHINGTON, D. C. • MARCH 1971

1. Report No.	2. Government Accession No.	3. Recipient's Catalog No.
NASA TN D-6199		

4. Title and Subtitle	5. Report Date
FLUTTER SUPPRESSION USING ACTIVE CONTROLS BASED ON THE CONCEPT OF AERODYNAMIC ENERGY	March 1971
	6. Performing Organization Code
7. Author(s)	8. Performing Organization Report No.
E. Nissim	L-7525
	10. Work Unit No.
9. Performing Organization Name and Address	126-14-14-02
NASA Langley Research Center Hampton, Va. 23365	11. Contract or Grant No.
	13. Type of Report and Period Covered
12. Sponsoring Agency Name and Address	Technical Note
National Aeronautics and Space Administration Washington, D.C. 20546	14. Sponsoring Agency Code

15. Supplementary Notes

This research was accomplished while the author held a National Research Council Postdoctoral Resident Research Associateship at NASA Langley Research Center. Author is now Associate Professor, Technion, Israel Institute of Technology, Haifa, Israel.

16. Abstract

The problem of flutter suppression is treated from an energy point of view, whereby the energy dissipated per cycle of oscillations is reduced to a quadratic form involving a diagonal matrix of energy eigenvalues which are of aerodynamic origin only. A simplified binary bending-torsion flutter of a wing strip is investigated by several systems: leading-edge (L.E.) control surface, trailing-edge (T.E.) control surface, and combined leading-edge—trailing-edge (L.E.-T.E.) control surfaces. In each case the control surfaces are allowed to be driven by a linear sensor, a rotational sensor, and a combined linear-rotational sensor system. The results show that the flutter of the wing strip can be suppressed, a single control law being used, over a wide range of reduced frequencies, irrespective of the mass of the system, its stiffness, center-of-gravity location, elastic axis, the mode of vibration, and the Mach number (in the subsonic range). Parameters affecting the implementation of the control law, such as power requirements, phase lags, and amplitude gains, are investigated. The extension of the results to three-dimensional flow cases is discussed and the use of the flutter suppressor as a gust alleviator is also considered.

17. Key Words (Suggested by Author(s))	18. Distribution Statement
Flutter suppression Gust alleviation Modal suppression Active control system Aeroelasticity	Unclassified – Unlimited

19. Security Classif. (of this report)	20. Security Classif. (of this page)	21. No. of Pages	22. Price*
Unclassified	Unclassified	114	$3.00

*For sale by the National Technical Information Service, Springfield, Virginia 22151

CONTENTS

FLUTTER SUPPRESSION USING ACTIVE CONTROLS BASED ON THE CONCEPT OF AERODYNAMIC ENERGY

By E. Nissim*
Langley Research Center

SUMMARY

The problem of flutter suppression is treated from an energy point of view, whereby the energy dissipated by the system per cycle is reduced to a quadratic form involving a diagonal matrix of energy eigenvalues which are of aerodynamic origin only. A simplified binary bending-torsion flutter of a wing strip is investigated by several systems: leading-edge (L.E.) control surface, trailing-edge (T.E.) control surface, and combined leading-edge—trailing-edge (L.E.-T.E.) control surfaces. In each case the control surfaces are allowed to be driven by a linear sensor, a rotational sensor, and a combined linear-rotational sensor system. The results show that the flutter of the wing strip can be suppressed, a single control law being used, over a wide range of reduced frequencies irrespective of the mass of the system, its stiffness, center-of-gravity location, elastic axis, the mode of vibration, and the Mach number (in the subsonic range). The leading-edge—trailing-edge control system driven by linear-rotational sensors system is shown to be the most efficient system. Estimates are made for the power required to drive the proposed leading-edge—trailing-edge system and the parameters affecting the implementation of the control law (such as phase lags and amplitude gains) are investigated. A broad discussion is also included regarding application of the flutter-suppressing system to three-dimensional wings, the parameters affecting the reduction of the number of control systems required to suppress flutter, and the use of the flutter suppressors as gust alleviators. The analytical developments are given in several appendixes and the results obtained are illustrated in figures and charts.

INTRODUCTION

The recent technological advances made in the field of control systems and the increased reliability of control system components offer a new way of treating the problem of flutter instability. This approach consists of a rapidly responding control system

*NRC-NASA Resident Research Associate, now Associate Professor, Technion, Israel Institute of Technology, Haifa, Israel.

which is actuated by the motion of the main surface and which leads to an appropriate deflection of the control surface. In this way, use is made of control-surface aerodynamic forces to combat flutter instability. Such a system is referred to as an active control system.

Attempts to use active controls were made in recent years mainly in conjunction with problems associated with gust alleviation (the objective being to reduce the rigid-body response to turbulence) and with mode stabilization (the objective being to reduce structural dynamic response to gusts).

The study, design, and test of gust-alleviation systems have been explored over a number of decades and although they have been shown to be effective and technically feasible (refs. 1 to 4) they have lagged in practical application. Mode stabilization, to reduce structural response, is akin to the problem of flutter suppression. It has been seriously considered only during the past decade, and has culminated with the installation of active systems on the B-52 aircraft to control the response of the rigid-body mode and one elastic mode (first aft body bending) to gust inputs. (See refs. 5 and 6.) No attempt will be made to review the extensive literature in the field of gust alleviation with mode stabilization (for excellent reviews, see refs. 7 and 8) and mention will only be made of some of the contributions and results which have direct bearing on flutter suppression.

Flutter suppression implies, essentially, the control of structural modes only. Therefore, mode stabilization methods are of prime importance in flutter suppression. Associated problems can be classified within a few categories as follows:

(a) The determination of the contribution of the different structural modes to a given arbitrary deformation of the aircraft

(b) The determination of a control law which will actuate the control surfaces in a certain fashion, proportional to the participation of the structural mode in the given deformation, and give rise to a stable control system. An unstable control system can arise, for example, when a signal sensed from one structural mode gives rise to a control force which actuates a second structural mode and which in turn gives rise to a force which drives the first structural mode. This condition is known as control system induced instability and is caused by the sensor-force couplings.

(c) The determination that the control forces arising from the determined control law are of the type to stabilize the motion sensed

(d) The determination that the stabilized system is insensitive to changes in flight configuration, altitude, Mach number and mode shapes

Different approaches and methods were proposed and studied for the solution of the problems mentioned in (a), (b), and (c). These methods include multisensor systems for modal observation, force-sensor modal decoupling networks (very sensitive to changes in flight configuration), or mode discriminating sensors to avoid control system induced instability, and aerodynamic damping forces for mode stabilization. Linear optimal control theory has recently been used (ref. 9) to provide a systematic way of treating the problem of control system instability and to increase the control-force stabilization effectiveness. However, the control law which is derived by this method, and which depends on the location of the sensors, cannot often be attained by real systems. Furthermore, it requires as many control surfaces as modes considered. Recently, Wykes (ref. 10) suggested the identically located accelerometer and force (ILAF) scheme to insure control system stability and made use of control "aerodynamic damping" forces (that is, control deflection proportional to linear velocity) for modal stabilization.

These procedures permit some measure of optimization of a specific system at a specific flight condition (that is, flight configuration, altitude, and Mach number) and for specifically defined mode shapes. However, the problem common to all mode stabilization control systems is a tendency to be very sensitive to changing flight conditions. Thus, an optimized control system at one flight condition may either show degradation or even give rise to adverse effects at another flight condition. (See ref. 10.) Furthermore, even the optimization procedures used for a specific flight condition may often lead to control systems which are difficult to realize in practice. Wykes (ref. 10) has used only aerodynamic "damping" forces with the ILAF concept and in so doing he imposed a severe limitation on the optimization technique. It should also be remembered that extensive literature exists (refs. 11 to 13) showing that addition of positive damping can turn a stable elastic system into an unstable one. It is therefore concluded that the approaches to mode stabilization do not appear to offer an appropriate basis for flutter-suppression investigations and that a new approach is desirable.

Mention should be made here, prior to any elaboration on a new approach, of two experimental works carried out with the objective of increasing the flutter speed by the use of active control systems. (See refs. 14 and 15.) It is not believed, however, that these experiments were methodically planned, and they therefore resulted in very minor changes in flutter speed that were often accompanied by poor controllability. It seems that extensive analytical work which will lead to deeper understanding of the basic parameters affecting the suppression of flutter by active controls is required before new experiments are made.

The approach taken in this paper is based on aerodynamic energy considerations and is formulated in a manner insuring lack of sensitivity to changing flight conditions. Conceptual studies of some basic control systems are made and their relative merit

determined. Figures are furnished partly to illustrate the results and partly to supply information for general preliminary design considerations.

SYMBOLS

b	semichord length
C_{ij}	element i,j, of control law matrix $[C]$
C_k	scalar multiplier of $[G]$ matrix
d	representative oscillatory amplitude
f_β, f_δ	generalized forces in β and δ coordinates and required to establish a desired control law
G_{ij}	element i,j, of the control law matrix $[G]$
$h, \bar{h}$	bending displacement, positive in down direction
h_1, h_2	bending amplitudes defined by sketch (o)
h_s	h at $x = x_s$
$i = \sqrt{-1}$	
k	reduced frequency, $\frac{\omega b}{V}$
l_1, l_2, l_3, l_4, l_8	distance defined in sketch (B2)
M	Mach number
$m_1 = \pi \rho b^4 s$	
n	number of degrees of freedom of elastic system
$\overline{P}$	energy dissipated by system per cycle

$\overline{P}_1$ power required to drive control surfaces

$Q_h, Q_\alpha, Q_\beta, Q_\delta$ generalized aerodynamic force along h, α, β, and δ, respectively

S_{max} maximum stress at a specified location

s reference length or wing semispan

t time

V flight speed

$W_h, W_\alpha, W_\beta, W_\delta$ virtual work along coordinates h, α, β, and δ, respectively

x downstream coordinate measured from midchord point

x_s value of x at which the sensor is located divided by b

$\bar{y}, \bar{z}$ leading-edge displacements of the control surfaces defined in equations (B9) and (B10)

$\alpha, \bar{\alpha}$ oscillatory angle of attack of wing, or oscillatory amplitude, positive in nose-up direction

α_s value of α at $x = x_s$

β, δ leading-edge and trailing-edge control surface deflections, respectively, positive directions defined in sketch (B1)

λ eigenvalue of $[U]$

λ_i ith eigenvalue of $[U]$

ρ fluid density

ω oscillatory frequency

Matrices:

$[A_R], [A_I]$ real and imaginary part, respectively, of aerodynamic matrix A

$[B]$ inertia matrix

$\left.\begin{matrix}[B_1], [B_2], \\ [B_3], [B_4]\end{matrix}\right\}$ submatrices of $[B]$ defined by equations (C2)

$[C]$ control law matrix

$[C_o], [C_1], [C_2]$ control law matrices defined by equation (9)

E structural stiffness matrix

$\left.\begin{matrix}[E_1], [E_2], \\ [E_3], [E_4]\end{matrix}\right\}$ structural stiffness submatrices defined by equations (C2)

$\{F\}$ column matrix of forces

$[F_1]$ force matrix defined by equation (C4)

$[G]$ control law matrix

$[G_o], [G_1], [G_2]$ control law matrices defined by equation (10)

$[H]$ complex aerodynamic matrix defined by equation (B16)

$\left.\begin{matrix}[H_1], [H_2], \\ [H_3], [H_4]\end{matrix}\right\}$ submatrices of $[H]$ defined by equations (C2)

$\left.\begin{matrix}[N_{S1}], [N_{S2}], \\ [N_{A1}], [N_{A2}]\end{matrix}\right\}$ matrices defined in equations (D9)

$[Q_R], [Q_I]$ real and imaginary part, respectively, of energy eigenvector modal matrix

$\{q\}$ complex response vector

$\{q_F\}$ value of $\{q\}$ at flutter speed

$\{q_o\}$ complex amplitudes of response vector

$\{q_R\}, \{q_I\}$ real and imaginary part of $\{q_o\}$

$[U]$ aerodynamic energy matrix defined by equation (A9)

$[\Lambda]$ diagonal matrix of eigenvalues of $[U]$

$\{\xi_R\}, \{\xi_I\}$ real and imaginary parts, respectively, of generalized energy coordinates

$\{\eta\}$ eigenvector of $[U]$

Other notations:

$|\ |$ absolute value

$[\ ]^T$ or ^{T} transposed matrix

$*$ complex conjugate

$[\ ]$ row matrix

$\{\ \}$ column matrix

Subscripts:

min minimum

max maximum

opt optimum

r reference

Dots over symbols denote derivatives with respect to time.

THE ENERGY APPROACH TO FLUTTER SUPPRESSION

Basic Requirements for a Flutter-Suppression System

In determining a new approach to the problem of flutter suppression, the following goals were set:

(1) To provide some analytical means which will insure, during the process of optimization, minimum sensitivity of control system effectiveness to flight conditions

(2) To provide a simple analytical model which will yield some insight into the mechanism of flutter suppression by active controls and still retain the essence of the problem

The simplest possible flutter model is the bending-torsion flutter of a rigid two-dimensional strip. The idea of using such a model, although very attractive, seems to present some inherent difficulties. For example, what should the inertia matrix or the elastic matrix values be? What values should be assigned to parameters such as mass ratio or elastic-axis location and how could these results be correlated, even within some approximation such as aerodynamic strip theory, to a three-dimensional wing? These points should be carefully considered before discarding such a simple model. The natural question which follows is how do the values of inertia or elastic terms, for example, affect the flutter instability? Clearly, these terms affect the natural frequency and the natural mode shapes of the oscillating strip and the variation of these parameters over a wide range of values will yield, for each frequency of oscillation, a wide range of mode shapes which represent, in essence, different combinations of bending and torsional displacements. Since the frequency is itself a parameter, this statement implies infinite combinations of frequency and mode shapes. It may therefore be possible to accomplish this result by a direct variation rather than indirectly (through inertia or elastic terms). Indeed, since a wing is a continuous system, one isolated strip on the wing can vibrate at many frequencies and many mode shapes and therefore, this variation of frequencies and mode-shape combinations is also essential for the extension of the results to a three-dimensional wing. Similarly, the sensitivity to changes in flight conditions reduces in essence to the effect of changing the mode-shape—frequency combinations. Hence, the requirement that the binary system be insensitive to flight conditions implies that the increase in stability of the binary system be independent of the mode shapes over a wide range of frequencies. There remains now to determine an appropriate approach which will allow an easy variation of frequencies and mode shapes and indicate their effect on the stability of the binary flutter system. At this stage, an energy approach seems to be the natural outgrowth of these requirements. This is true since one can expect that the work done per cycle by the system will depend on the aerodynamic forces (which are

functions of the reduced frequency for any given Mach number) and mode shapes only, whereas the magnitude and sign of the work done per cycle indicate the state of stability of the system.

The Energy Analysis

In this section the energy concept is developed (the details are presented in appendix A) without imposing any restrictions on the size of the system and the nature of the aerodynamic forces. The results obtained apply to three-dimensional wings as well as to the two-dimensional model described.

Let

$$\{F\} = -\omega^2\left[B + \pi\rho b^4 s\left(A_R + iA_I\right)\right]\{q\} + [E]\{q\} \tag{1}$$

where, at flutter,

$$\{F\} = 0$$

and ω represents the frequency of oscillation; $[B]$, the mass matrix; $[A_R]$ and $[A_I]$, the real and imaginary parts of the aerodynamic matrix, respectively; $[E]$, the stiffness matrix; ρ, the density of the fluid; s, a reference length; b, a reference semichord length; and $\{q\}$, the response vector.

As shown in appendix A, the work $\overline{P}$ done by the system on its surrounding per cycle can be written as (eq. (A7))

$$\overline{P} = \frac{1}{2}\pi^2\rho b^4 s\omega^2\left\lfloor q_R - q_I\right\rfloor\left[-\left(A_I^T + A_I\right) + i\left(A_R - A_R^T\right)\right]\left\{q_R + iq_I\right\} \tag{2}$$

where (from eq. (A2))

$$\{q\} = \{q_o\}e^{i\omega t} = \left\{q_R + iq_I\right\}e^{i\omega t} \tag{3}$$

The sign of $\overline{P}$ is of importance in the determination of stability, and therefore, it will be advantageous to convert equation (2) to a more convenient form. As shown in appendix A (eq. (A15)), $\overline{P}$ can be reduced to the form

$$\overline{P} = \frac{1}{2}\pi^2\rho b^4\omega^2 s\left(\left\lfloor\xi_R\right\rfloor[\Lambda]\{\xi_R\} + \left\lfloor\xi_I\right\rfloor[\Lambda]\{\xi_I\}\right) \tag{4}$$

or

$$\overline{P} = \frac{1}{2}\pi^2\rho b^4\omega^2 s\left[\lambda_1\left(\xi_{R1}^2 + \xi_{I1}^2\right) + \lambda_2\left(\xi_{R2}^2 + \xi_{I2}^2\right) + \ldots \lambda_n\left(\xi_{Rn}^2 + \xi_{In}^2\right)\right] \tag{5}$$

where $\left[\Lambda\right]$ is a diagonal matrix of the eigenvalues λ_i, necessarily real, of the Hermitian matrix (eq. (A9))

$$\left[U\right] = \left[-\left(A_I + A_I^T\right) + i\left(A_R - A_R^T\right)\right] \tag{6}$$

and where the vectors $\left\{\xi_R\right\}$ and $\left\{\xi_I\right\}$ are defined by the transformation (eq. (A10))

$$\left\{q_o\right\} = \left[Q_R + iQ_I\right]\left\{\xi_R + i\xi_I\right\} \tag{7}$$

The matrix $\left[Q_R + iQ_I\right]$ is a square modal matrix of the principal eigenvectors. Equation (5) contains some very interesting features:

(1) The work $\overline{P}$ done per cycle has been brought to a principal quadratic form (which involves a diagonal matrix) in terms of the system responses. Hence, the sign of $\overline{P}$ will be independent of the values of the responses provided it is possible to render all the λ terms positive.

(2) The values of λ are determined from the aerodynamic matrices only. They depend on the assumed modes but are independent of the response of the system. The values of λ will, however, depend on the reduced frequency of oscillation and Mach number. In this way, complete decoupling has been achieved between the aerodynamic inputs and the response of the system.

It can now be seen that a necessary and sufficient condition for the suppression of flutter for arbitrary values of responses $\left(\xi_R \text{ and } \xi_I\right)$ is that all the λ terms be positive. This requirement which stresses the arbitrary nature of the response of the system is a severe one in most cases. This statement is true since the values of the ξ terms of a particular system (in a specified flight configuration) may be such as to render $\overline{P}$ in equation (5) positive despite the existence of some negative values of λ. It is essential, however, to introduce this requirement to insure the dissipation of energy under any conceivable flight condition. The objective of the following work will be to find a relation between the main surface oscillatory displacements to the control surface deflections to insure that the smallest value of λ $\left(\text{that is, } \lambda_{min}\right)$ of the simplified flutter model becomes and remains positive and assumes adequately large values over a wide range of reduced frequencies and Mach numbers.

It is interesting to note here that several investigators have, in the past, used an energy approach to treat various aeroelastic problems (refs. 13, 16, and 17) while they restricted the energy expressions to real variables only. It now appears that the use of complex notation throughout the analysis, as shown in the appendix, is advantageous in that it leads to a diagonalized quadratic expression.

Control System Law for the Simplified Flutter Model

The two-dimensional rigid strip shown in sketch (a) has two degrees of freedom, translation (bending) and rotation (torsion). Therefore, two control surfaces are required in order to maintain precise control of the two degrees of freedom of the main surface. The main surface is thus allowed to have both leading-edge (L.E.) and trailing-edge (T.E.) control surfaces (the choice of a leading-edge—trailing-edge control system is further

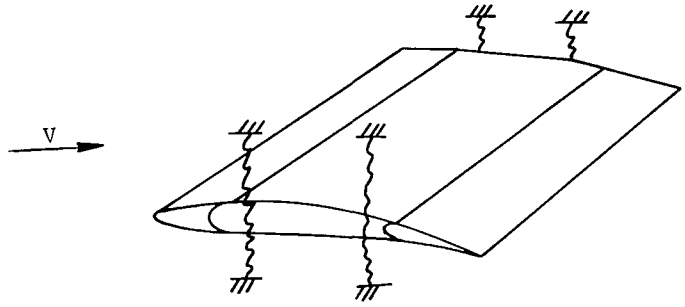

Sketch (a)

discussed in a subsequent section of this paper). It is possible to see, at this stage, that eight parameters (four for each control surface) exist which permit a general deflection of the control surfaces with respect to the motion of the main surface. These deflections are:

(1) Deflection of the T.E. control surface actuated by the in-phase displacement of the main surface

(2) Deflection of the T.E. control surface actuated by the out-of-phase displacement of the main surface

(3) Deflection of the T.E. control surface actuated by the in-phase twist of the main surface

(4) Deflection of the T.E. control surface actuated by the out-of-phase twist of the main surface

The additional four parameters similarly relate to the actuation of the L.E. control surface by the in-phase and out-of-phase (90^{o} phase lead) movements of the main surface. This relation can be put in matrix form by using the notation illustrated in sketch (b), that is,

$$\begin{Bmatrix} \beta \\ \delta \end{Bmatrix} = \begin{bmatrix} C_{11} & C_{12} \\ C_{21} & C_{22} \end{bmatrix} \begin{Bmatrix} h/b \\ \alpha \end{Bmatrix} + i \begin{bmatrix} G_{11} & G_{12} \\ G_{21} & G_{22} \end{bmatrix} \begin{Bmatrix} h/b \\ \alpha \end{Bmatrix} \tag{8}$$

Equation (8) represents a control law, where the C and G terms are essentially the gearing ratios between the motion of the main surface and the deflection of the control surfaces.

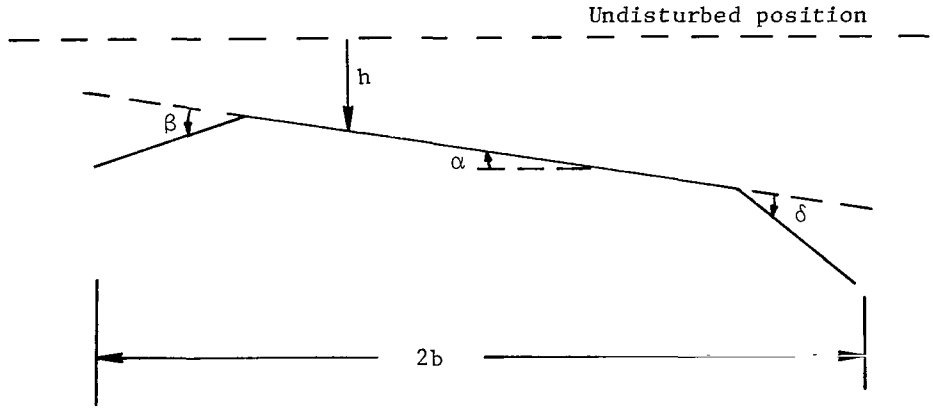

Sketch (b)

No attempt is made at this stage to consider the practical feasibility of mechanizing the control law. Such considerations are left for a later stage of this work, after gaining some insight into the relative importance of the different control parameters.

It is possible to increase the number of parameters by letting the C and G terms in equation (8) be functions of the reduced frequency. An expansion of the C and G values in terms of reduced frequency will be of the form

$$[C] = [C_o] + k[C_1] + k^2[C_2] + \ldots \tag{9}$$

$$[G] = [G_o] + k[G_1] + k^2[G_2] + \ldots \tag{10}$$

It should, however, be noted that the aerodynamic coefficients of both the main surface and the control surfaces are quadratic in k^{-1} and the coefficients vary only slowly with the reduced frequency k. Therefore, a quadratic representation of C and G should be sufficient to represent all the coefficients of the main surface for all practical purposes. Hence, equation (8) can be looked upon as a special form of equations (9) and (10) and can be expected to yield good results at low reduced frequencies. The matrices $[C_2]$ and $[G_2]$ will affect the aerodynamic derivatives of the main surface mainly through the control surface aerodynamic inertia terms, and these values are known to be very small

in wing flutter at the normal range of frequencies. It can therefore be concluded that although equation (8) will be used throughout the present work, one might consider the use of the following equations if a high range of reduced frequencies needs to be considered:

$$\left[C\right] = \left[C_o\right] + k\left[C_1\right] \tag{11}$$

$$\left[G\right] = \left[G_o\right] + k\left[G_1\right] \tag{12}$$

In the following discussion, it will be assumed that $\left[C\right] = \left[C_o\right]$ and $\left[G\right] = \left[G_o\right]$.

Analysis of the Simplified Flutter Model

The first step in the analysis is to determine the aerodynamic matrices which lead to the formation of the aerodynamic energy matrix $\left[U\right]$ defined by equation (6). The treatment of the L.E. control surface presents no special problems since, effectively, it is equivalent to a deflection of a large T.E. control surface. A detailed derivation of the two-dimensional generalized aerodynamic forces per unit span is presented in appendix B. The aerodynamic forces per unit span have the form (eq. (B17))

$$\begin{Bmatrix} Q_h \\ Q_\alpha \\ Q_\beta \\ Q_\delta \end{Bmatrix} = \pi\rho b^4\omega^2\left[H\right]\begin{Bmatrix} h/b \\ \alpha \\ \beta \\ \delta \end{Bmatrix} \tag{13}$$

where $\left[H\right]$ represents the matrix of aerodynamic coefficients, Q represents generalized forces, and the subscript refers to the degree of freedom upon which these forces act. Substitution of the control law defined by equation (8) into equation (13) yields

$$\begin{Bmatrix} Q_h \\ Q_\alpha \\ Q_\beta \\ Q_\delta \end{Bmatrix} = \pi\rho b^4\omega^2\left(\begin{bmatrix} H_1 + H_2C \\ H_3 + H_4C \end{bmatrix} + i\begin{bmatrix} H_2G \\ H_4G \end{bmatrix}\right)\begin{Bmatrix} h/b \\ \alpha \end{Bmatrix} \tag{14}$$

where

$$\left[H\right] \equiv \left[\begin{array}{c:c} H_1 & H_2 \\ \hdashline H_3 & H_4 \end{array}\right]$$

Hence H_1, H_2, H_3, and H_4 are 2×2 submatrices of $[H]$. The generalized forces Q_β and Q_δ need to be known only when evaluating the power required by the control system to establish the control law defined by equation (8). The bending-torsion aerodynamic forces can therefore be written as

$$\begin{Bmatrix} Q_h \\ Q_\alpha \end{Bmatrix} = \pi\rho b^4\omega^2 [A_R + iA_I] \begin{Bmatrix} h/b \\ \alpha \end{Bmatrix} \tag{15}$$

where

$$[A_R + iA_I] = [H_1 + H_2C + iH_2G] \tag{16}$$

Equation (16) shows how $[C]$ and $[G]$ affect the value of the matrices $[A_R]$ and $[A_I]$. Finally, substitution of the values of $[A_R]$ and $[A_I]$ into equation (6) yields the required matrix $[U]$ which, in turn, yields the energy eigenvalues.

Mention should be made here that the derivation of $[U]$ for the simplified model implies that the control surfaces represent irreversible systems, that is, they can be deflected by the control system only and are not affected by other forces.

As a first step, $[U]$ was calculated herein by using aerodynamic derivatives pertinent to Mach number $M = 0$, derived from potential theory solutions of Theodorsen, Garrick, Küssner, and Schwartz, and summarized in references 18 to 21. In a later stage, Mach number effects were considered in calculating $[U]$ by solving, numerically, Possio's integral equation (ref. 22) with the two-dimensional compressible kernel. An extensive comparison with the numerical results appearing in references 23 and 24 has shown that, in all cases, the accuracy of the numerical results was within 3 percent.

Optimization Procedure

The eigenvalue solution of the simplified flutter model yields two values of λ, the smaller of which is designated by λ_{min}. Imagine now that λ_{min} is plotted against k^{-1} for different values of a particular control parameter, for example, C_{ij}. The optimization procedure was initially programed to determine the smallest value of λ_{min} at each value of a specific C_{ij} (or G_{ij}) as shown in sketch (c). Comparison was then made between points such as 1, 2, and 3 and the optimized value of C_{ij} was defined as that value which produced the largest minimum value of λ_{min} (that is, $C_{ij} = r_3$ in sketch (c)). The deficiencies inherent in this definition of optimum values made it impossible to implement in practice.

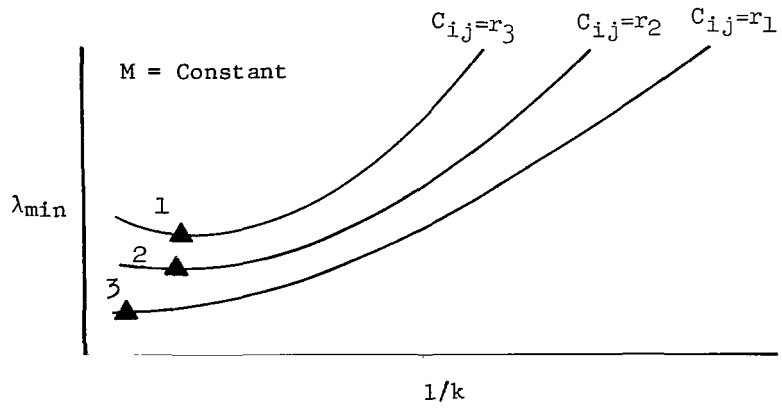

Sketch (c)

Sketch (d) illustrates how one may be misled to choose the value of $C_{ij} = r_2$ as optimum, on the basis of this definition, whereas the overall performance of $C_{ij} = r_1$ is superior.

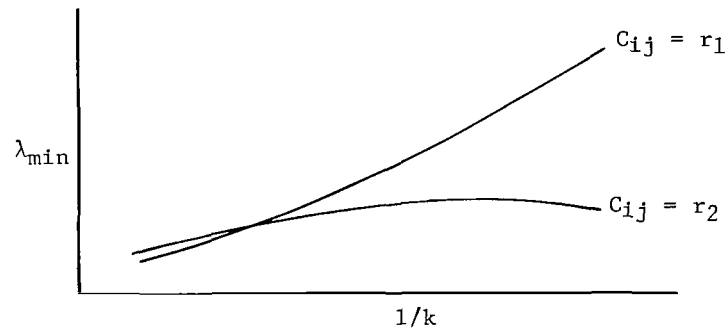

Sketch (d)

The optimization with respect to the control parameters was therefore redefined to yield the values of the control parameters which give rise to maximum area under the curve of λ_{min} against k^{-1}. This definition has possible theoretical deficiencies, such as shown in sketch (e). Practice has shown that this definition is workable and that, unlike the curve in the sketch, the curves are well behaved. The optimization procedure

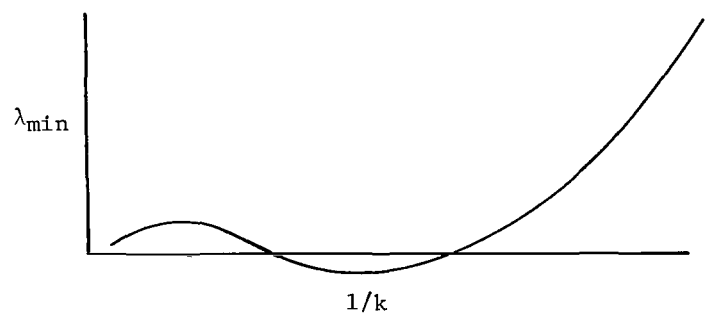

Sketch (e)

consists of the variation of a single control parameter at a time, all the other control parameters being kept constant. The value of the control parameter which yields the largest area under the curve of λ against k^{-1} is then assigned to the parameter and another control parameter varied in a similar fashion. This whole procedure is repeated until convergence of the values of the control parameters is reached. Experience has shown that convergence is reached after 3 to 4 parameter sweeps. It is, however, advisable to accompany each optimization with a plot of the optimized λ_{min} against k^{-1} curve, together with sensitivity curves which indicate the effect of the off-design values of $[C]$ and $[G]$.

Data and Scope of Optimization

The binary flutter model was allowed 20 percent chord L.E. and T.E. control surfaces. No variation was allowed in these values and they were kept constant throughout the investigation. Similarly, a reference point for sensing the motion of the main surface was kept constant at 30 percent of the chord (measured from the leading edge). This point (x = -0.4b) simulates the location of the sensors on the wing. If it should be desired to relate the results to another sensor location ($x = x_S b$), then the following transformation may be used to modify the optimized values of $[C]$ and $[G]$:

$$\left.\begin{aligned} \alpha &= \alpha_S \\ h &= h_S - \alpha(x_S + 0.4)b \end{aligned}\right\} \tag{17}$$

or, in matrix form

$$\begin{Bmatrix} h/b \\ \alpha \end{Bmatrix} = \begin{bmatrix} 1 & -x_S - 0.4 \\ 0 & 1 \end{bmatrix} \begin{Bmatrix} h_S/b \\ \alpha_S \end{Bmatrix} \tag{18}$$

The optimum control law will then assume the form:

$$\begin{Bmatrix} \beta \\ \delta \end{Bmatrix} = [C + iG]_{opt} \begin{bmatrix} 1 & -x_S - 0.4 \\ 0 & 1 \end{bmatrix} \begin{Bmatrix} h_S/b \\ \alpha_S \end{Bmatrix} \tag{19}$$

or

$$\begin{Bmatrix} \beta \\ \delta \end{Bmatrix} = [C + iG]_S \begin{Bmatrix} h_S/b \\ \alpha_S \end{Bmatrix} \tag{20}$$

where

$$\left[C + iG\right]_s = \left[C + iG\right]_{opt}\begin{bmatrix} 1 & -x_s - 0.4 \\ 0 & 1 \end{bmatrix} \tag{21}$$

The flutter model was optimized over a wide range of reduced frequencies ($0.0128 \leqq k \leqq 19.5$).

The numerical work which follows was carried out in four stages:

(1) Stage 1, optimization at $M = 0$: Optimization of λ_{min} with respect to $\left[C\right]$ and $\left[G\right]$ at $M = 0$. Comparative studies of optimum conditions were made for T.E. control system, L.E. and T.E. controls, and L.E. control only (optimization carried out, in all cases, for both single-sensor control law and a double-sensor control law).

(2) Stage 2, power requirement: Rough assessment of the power required to drive the optimized control system and its sensitivity to the control parameters.

(3) Stage 3, compressibility effects: Mach number sensitivity of λ_{min}, $\left[C\right]_{opt}$ and $\left[G\right]_{opt}$.

(4) Stage 4, some practical aspects of the optimized control laws: The practical achievement of the control law from both a block-diagram point of view and performance point of view, together with off-design sensitivities.

The work was organized to determine the possibilities offered by the analysis and to look for any deficiencies which might make the results impractical. Allowance was also made for possible interactions between the different stages requiring some compromising results. Where interactions were light, no reoptimization followed since it was felt that slight refinements should be left to a later stage.

OPTIMIZATION AT ZERO MACH NUMBER

Ranges of Optimization

The variations of the control parameters were confined, in this stage, within the following ranges, to insure small control deflections:

$$-0.5 \leqq C_{11} \leqq 0.5$$

$$-1.0 \leqq C_{12} \leqq 1.0$$

$$-0.5 \leqq C_{21} \leqq 0.5$$

$$-2.5 \leqq C_{22} \leqq 2.5$$

$$-0.5 \leqq G_{11} \leqq 0.5$$

$$-1.0 \leqq G_{12} \leqq 1.0$$

$$-0.5 \leqq G_{21} \leqq 0.5$$

$$-2.5 \leqq G_{22} \leqq 2.5$$

As can be seen, the L.E. control surface was allowed a somewhat smaller range of variations than the T.E. control surface. Some of these ranges were changed at subsequent stages, on the basis of the results already obtained. Figure 1 shows the variations of λ_{min} and λ_{max} with k^{-1} for a wing strip having no control surfaces (or $[C] = [G] = 0$). It can be seen that λ_{min} is negative throughout the range of k ($0.0128 \leqq k \leqq 19.5$) and that λ_{max} is positive throughout the same range of k. Figure 1 represents the basic values of λ and any improvements due to control deflections should be determined by comparison with this figure.

Results for Trailing-Edge Control Only

The optimized values of $[C]$ and $[G]$ for the case where only a T.E. control surface was allowed are

$$[C] = \begin{bmatrix} 0 & 0 \\ -0.35 & -1.9 \end{bmatrix}$$

$$[G] = \begin{bmatrix} 0 & 0 \\ 0.35 & 0.1 \end{bmatrix}$$

The graphical descriptions of these $[C]$ and $[G]$ values are illustrated in sketches (f) and (g).

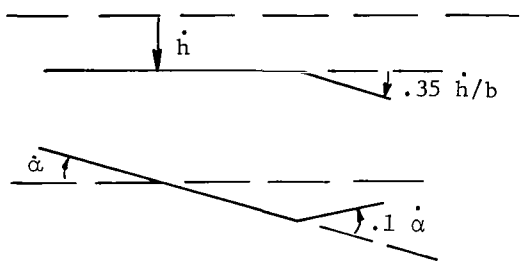

Sketch (f)

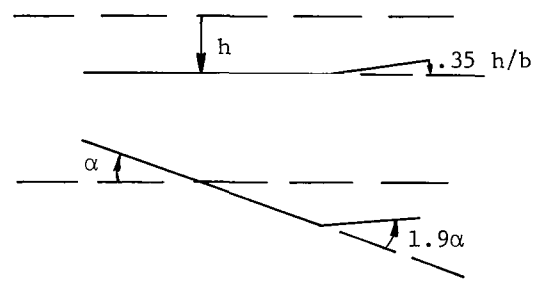

Sketch (g)

Figure 2 shows the variations of λ_{min} with k^{-1} around these optimum values of $[C]$ and $[G]$. Figure 3 shows a similar variation of λ_{max} with k^{-1} around the optimum values of $[C]$ and $[G]$.

The following points emerging from these figures are worth noting:

(1) The value of $(\lambda_{min})_{opt}$ is only marginally positive (except at high k values) and is highly sensitive to off-design values

(2) The most sensitive control parameters are C_{22} and G_{22}

(3) The values of C_{22} which improve λ_{min} cause λ_{max} to deteriorate

(4) There is an optimum value of the parameter G_{21} which, essentially, gives rise to aerodynamic damping. (See fig. 2(c).) This result is consistent with the observations of Wykes (ref. 10) concerning the effects of damping

Figures 4 and 5 are basically identical to figures 2 and 3 except for the magnified k^{-1} scale.

By referring back to sketches (f) and (g), it is interesting to note that the main effect of the in-phase deflection of the control surface is to counteract any lift buildup; that is, the lift increase due to the angle of attack α is opposed by the forces created by the deflection of the T.E. control surface. Furthermore, the out-of-phase deflection of the T.E. control surface increases the damping in bending, on one hand, while the torsional damping is reduced on the other. It can therefore be seen that flutter suppression is achieved by both reducing the energy input into the system and increasing the dissipation of energy.

Comparison can also be made between this T.E. control system, which requires two sensors (to determine α and h/b), and a T.E. control system which makes use of one sensor only. The control law of such a single-sensor T.E. control system may assume either of the following forms.

$$\left\{\begin{array}{l} \begin{Bmatrix} \beta \\ \delta \end{Bmatrix} = \left(\begin{bmatrix} 0 & 0 \\ C_{21} & 0 \end{bmatrix} + i \begin{bmatrix} 0 & 0 \\ G_{21} & 0 \end{bmatrix} \right) \begin{Bmatrix} h/b \\ \alpha \end{Bmatrix} \\ \begin{Bmatrix} \beta \\ \delta \end{Bmatrix} = \left(\begin{bmatrix} 0 & 0 \\ 0 & C_{22} \end{bmatrix} + i \begin{bmatrix} 0 & 0 \\ 0 & G_{22} \end{bmatrix} \right) \begin{Bmatrix} h/b \\ \alpha \end{Bmatrix} \end{array}\right\} \tag{22}$$

Figure 2 shows the reduction in λ_{min} caused by either letting C_{21} and G_{21} approach zero. It can thus be seen that the system having the two sensors is superior to any single-sensor system.

Results for Leading- and Trailing-Edge Control Surfaces

The optimized values of $[C]$ and $[G]$ for this case, where the system was allowed to have both L.E. and T.E. control surfaces and was activated by two sensors, are

$$[C] = \begin{bmatrix} 0.5 & 1.0 \\ -0.05 & -1.7 \end{bmatrix}$$

$$[G] = \begin{bmatrix} -0.5 & 1.0 \\ 0.45 & 0.2 \end{bmatrix}$$

Illustration of the physical meaning of these $[C]$ and $[G]$ values is shown in sketches (h) and (i). Figure 6 shows the variation of λ_{min} with k^{-1} around these optimum values of $[C]$ and $[G]$ whereas figure 7 shows a similar variation of λ_{max}. An identical representation but with a magnified k^{-1} scale is shown in figure 8.

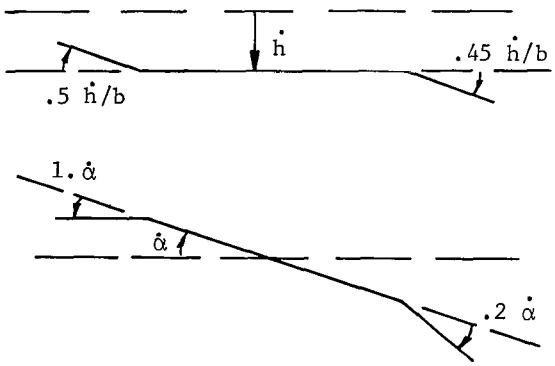

Sketch (h)

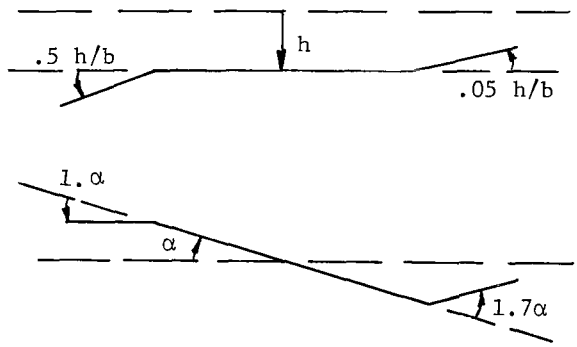

Sketch (i)

A study of figures 6 to 8 yields the following points which are worth summarizing:

(1) The optimum value of λ_{min} is large and positive over the whole range of k^{-1}.

(2) The off-design sensitivity of the optimized values of $[C]$ and $[G]$ is greatly reduced as compared with the T.E. control surface only.

(3) The most sensitive control parameters which affect both λ_{min} and λ_{max} (in practically opposite fashions) are, as before, C_{22} and G_{22}.

(4) The parameter G_{12} mainly affects λ_{min} whereas the parameter G_{21} mainly affects λ_{max}.

(5) The parameters C_{11}, C_{12}, C_{21}, and G_{11} have only very small effect on both λ_{min} and λ_{max}.

(6) A variation of G_{21} can reduce λ_{max} to the point where $\lambda_{max} = \lambda_{min}$. Further variation of G_{21} may cause the interchange between λ_{max} and λ_{min}. Hence, there must be a critical value of G_{21} below which, the variation of G_{21} will greatly affect λ_{min}.

(7) The parameters C_{11}, C_{12}, G_{11}, and G_{12} have optimum values coinciding with the limits of their range of variation; thus, an expanded range might improve the results.

The preceding sketch of the activated (optimized) oscillating strip shows again that the in-phase control deflections counteract any lift buildup whereas the out-of-phase control deflection provides both bending and torsional damping forces.

Once again, the effectiveness of a single activating sensor was tested. Figures 9 and 10 show typical results of a variation around such an optimized system. Note that the rotational sensor activates all the important control parameters except G_{21}. A rotational sensor only reduces effectively to letting $C_{11} = C_{21} = G_{11} = G_{21} = 0$ and thus causes (through G_{21}) the interchange between λ_{min} and λ_{max}. Clearly, the two-sensor system is the more effective sensing system and shows a very large effect on λ_{min}.

Leading-Edge Control Surface Only

An investigation into the effectiveness of an optimized L.E. control surface activated only by two sensors was made. A typical variation of λ_{min} around the optimum values of $[C]$ and $[G]$, shown in figure 11, indicates that a L.E. control surface, on its own, is effectively of very little use.

Subsequent Considerations

To cut down the amount of work in the following investigation, and on the basis of the results obtained so far, it was decided to consider only the two most promising systems: the L.E.-T.E. system and the system comprising the T.E. control only. Furthermore, each of these systems will always be considered as being activated by two sensors.

Remarks on the Comparison Between the Two-Controls System and the Single-Control System

It is felt, at this stage, that the use of both L.E. and T.E. control systems requires an additional justification. This is true since it may be argued that an unfair comparison has been made in the simplified flutter model, where an attempt was made to control a two-degrees-of-freedom system by a single control surface (T.E. only) and thus justify the L.E.-T.E. control system. It may further be argued that the introduction of two T.E.

control surfaces, suitably controlled, may produce some improvements similar to those of the L.E.-T.E. control system. Sketch (j) shows two such T.E. control surfaces controlling the bending-torsion degrees of freedom of the strip.

On the basis of the aerodynamic strip theory, one can divide the strip shown in sketch (j) into two strips each having a single T.E. control surface. Since these two strips perform an identical oscillation, any optimization technique, including the energy approach, will yield

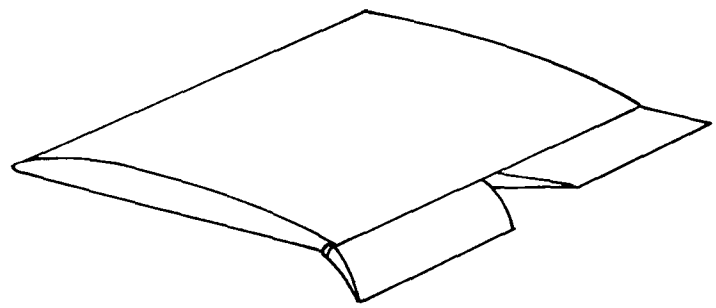

Sketch (j)

identical control laws for these two control surfaces. Hence, the two control surfaces effectively oscillate as a single T.E. control surface, the performance of which has already been investigated. It can therefore be stated, on the basis of this argument and the results presented in this work, that the L.E.-T.E. control system is superior to a T.E. control system.* The physical reason for this superiority lies in the fact that the T.E. control surface has combined beneficial-detrimental effects on the system. On one hand, the T.E. control surface is very powerful in decoupling the aerodynamic nonsymmetrical cross terms, but on the other hand, it reduces both the aerodynamic damping in torsion and the torsional aerodynamic stiffness term (this latter term will be later shown to affect the nonactivated strips on an elastic wing). The optimization results reflect the compromise obtained between these conflicting effects. The L.E. control surface, although very ineffective in decoupling the nonsymmetrical aerodynamic terms, provides a means of adding aerodynamic damping in pitch and positive torsional aerodynamic stiffness terms. Hence, these two control surfaces supplement each other and can yield good results if properly used.

*This result appears to be self-explanatory. It has, however, an additional importance in that it points out that two T.E. control systems, when located on a wing, will be more efficient if the elastic deformations at the controls locations are widely different. Two adjoining T.E. controls can therefore be expected to be relatively inefficient at the low frequencies (leading to almost identical elastic deformation at the two adjoining sections) whereas at high frequencies they may be expected to be more efficient.

POWER REQUIREMENT

Preliminary Considerations

In evaluating the power required when activating the control surfaces, some further definition of the fluttering system has to be made. To avoid analyzing very specific systems where force-response amplitude and phase characteristics are of prime importance, it was decided to generalize somewhat the problem by attempting to assess the upper bound of the power requirement. This assessment can be made by assuming that the force-response-phase relationship is such as to require maximum power. Furthermore, only the peak power requirement will be evaluated as compared with average power required per cycle. The detailed analysis of the power requirement, presented in appendix C, shows that the upper power bound $\overline{P}_{1,max}$ can be written (eq. (C11))

$$\overline{P}_{1,max} = \omega \left| \left| h_o/b \right|, \left| \alpha_o \right| \right| \left[\left[C^T + iG^T \right] \right] \left[\left[F_1 \right] \right] \left\{ \begin{matrix} \left| h_o/b \right| \\ \left| \alpha_o \right| \end{matrix} \right\} \tag{23}$$

where

$$\left.\begin{aligned} h &= h_o e^{i\omega t} \\ \alpha &= \alpha_o e^{i\omega t} \end{aligned}\right\} \tag{24}$$

The notation $|\ |$ means the modulus of the complex number, and $\left[F_1\right]$ denotes the sum of the 2×2 inertia, elastic, and aerodynamic matrices which appear in the equations of motion relating to the control surfaces. (See eq. (C4).) The $\left[F_1\right]$ matrix has inertia terms (both structural and aerodynamic) proportional to ω^2, structural elastic constant terms, aerodynamic stiffness terms proportional to velocity square V^2 and aerodynamic damping terms proportioned to ωV. Initial results have shown that the aerodynamic stiffness terms (proportional to V^2) contribute most to the power requirement. Hence, the value of $\overline{P}_{1,max}$ will, approximately, be proportional to ωV^2 and to the response squared.

Gust power-spectral input considerations indicate that low frequencies, where both the input power and the response are large, should be critical from the point of view of the power requirement. Similar conclusions can be reached if a uniform cantilevered beam is considered to oscillate to produce a specified maximum stress S_{max} at a specified location. The inertia loading is proportional to $\omega^2 d$, where d is a representative oscillatory amplitude. Hence,

$$d \propto \frac{S_{max}}{\omega^2}$$

Thus, since

$$\overline{P}_{1,max} \propto \omega d^2 V^2$$

and using this relation yields

$$\overline{P}_{1,max} \propto \omega \left(\frac{S_{max}}{\omega^2}\right)^2 V^2$$

or

$$\overline{P}_{1,max} \propto \frac{S_{max}^2}{\omega^3} V^2$$

Thus, it is again shown that low frequencies will, in general, be critical when the power requirement is considered.

Data for Power Estimate

The flutter model was assigned the following values to estimate $\overline{P}_{1,max}$:

Wing chord, 3.048 meters (10 feet)

Velocity, 243.84 meters/sec (800 ft/sec)

Altitude, sea level

L.E. control, 20 percent chord

T.E. control, 20 percent chord

$|h_o/b| = 0.2$

$h_o = 0.3048$ meter = 1 foot

$|\alpha_o| = 0.044$ radian = 2.5^o

$\omega = 12$ radians/second

$$[C] = \begin{bmatrix} 0.5 & 1.0 \\ -0.05 & 1.7 \end{bmatrix}$$

$$[G] = \begin{bmatrix} -0.5 & 1.0 \\ 0.45 & 0.2 \end{bmatrix}$$

Mass ratio, 4.

$$[B_3] = \begin{bmatrix} 0.04 & -0.018666 \\ 0.04 & 0.050666 \end{bmatrix}$$

$$[B_4] = \begin{bmatrix} 0.010666 & 0 \\ 0 & 0.010666 \end{bmatrix}$$

$$[E_3] = \begin{bmatrix} 0 & 0 \\ 0 & 0 \end{bmatrix}$$

$$[E_4] = \begin{bmatrix} 0 & 0 \\ 0 & 0 \end{bmatrix}$$

and where $[B_3]$, $[B_4]$, $[E_3]$, and $[E_4]$ are defined in appendix C. This flutter example was extracted from reference 25. The control surfaces were allowed inertia values appropriate to flat-plate-type controls.

Effect of Power Requirement

Figure 12 shows the variation of the power requirement with the variation of the control surface parameters around their optimum value. The upper curve represents the total upper bound for the power required to actuate a unit span of the wing. The other two curves represent the decomposition of this power into its L.E. control and T.E. control constituents. The following conclusions can be determined from figure 12:

(1) The value of $\overline{P}_{1,max}$ per unit span is very sensitive to the values of C_{11}, C_{21}, and G_{11}. If it is remembered that these parameters have negligible effect on λ_{min}, one can see that the values of 32.3 kW/m (13.2 hp/ft) can be reduced by about 21.6 kW/m (8.84 hp/ft) if $C_{11} = C_{21} = G_{11} = 0$.

(2) All the other parameters, except G_{21}, which mainly affect λ_{max} contribute little to the power requirement. The parameter C_{12} is later shown to be of great importance and it is worth noting that it has a very small effect on $\overline{P}_{1,max}$.

It seems therefore, rather unexpectedly, that all the important parameters (C_{12} and those affecting λ_{min}) contribute little to the power requirement whereas the parasitic terms which do not affect λ_{min} and G_{21} and which affect λ_{max} have a large effect on the power requirement.

Reoptimization and Reevaluation of the Power Requirement With Unimportant Control Parameters Set to Zero

On the basis of the forementioned results, it was decided to reoptimize $[C]$ and $[G]$ by constraining $C_{11} = C_{12} = C_{21} = G_{11} = 0$ and by extending the range of G_{12} to $-1.5 \leqq G_{12} \leqq 1.5$.

The optimized values obtained were

$$[C] = \begin{bmatrix} 0 & 0 \\ 0 & -1.8 \end{bmatrix}$$

$$[G] = \begin{bmatrix} 0 & 1.5 \\ 0.4 & 0.2 \end{bmatrix}$$

Figure 13 shows the large reduction in power requirement due to these changes. The value of 32.3 kW/m (13.2 hp/ft) was thus reduced to 10.7 kW/m (4.36 hp/ft).

Some additional 25 percent reduction in power can be obtained by using L.E. aerodynamic balance obtained by shifting the hinge by 5 percent chord. Figures 14 and 15 show the improvement obtained in both λ_{min} and λ_{max}. This improvement followed the increased range of G_{12}, which, in turn, was increased because of the elimination of C_{11} and G_{11} and, for the time being, C_{12}. Sensitivity tests around those new values of $[C]$ and $[G]$ (the figures are not presented here, except for fig. 16) did not show any new features which have not already been seen in previous figures.

It can therefore be concluded that the results obtained are very efficient in terms of power requirement and that these upper bounds are small in value and therefore cannot present major problems in practical applications.

COMPRESSIBILITY EFFECTS

The simplified flutter model was optimized with respect to $[C]$ and $[G]$ under the constraints that $C_{11} = C_{12} = C_{21} = G_{11} = 0$ for $M = 0.5$, $M = 0.7$, $M = 0.8$, $M = 0.85$, and $M = 0.9$. For the case of T.E. control only, no constraints were imposed. In both cases negligible changes in $[C]$ and $[G]$ were obtained for all Mach numbers; hence, it can be concluded that the optimized control law remains invariant with Mach number.

The curves of λ_{min} at the optimized values of the control parameters show changes with Mach numbers. Figure 16 shows such a variation of a T.E. control system whereas figure 17 shows similar variation of the L.E.-T.E. control system. It can be

seen that Mach number effect is beneficial for the whole k range of the L.E.-T.E. system, whereas the T.E. system shows some improvement, at the high k range, with Mach number increase, and a deterioration at the lower range of reduced frequencies.

It may be noted that the curves of λ against k^{-1} for the $M = 0$ case were computed by using a numerical aerodynamic solution. It can be seen that the agreement with the closed-form solutions shown earlier is generally good, except for the very high values of k. (See fig. 17.) At the very high values of k, the closed-form solution for $M = 0$ yields positive λ values throughout the whole k range whereas the numerical solution yields negative λ_{min} values for $k > 4.6$. In the case of the T.E. system, both the numerical and analytical solutions yield negative λ_{min} values for the high ranges of k. (See fig. 16.) Another point of interest lies in the effect of compressibility on λ_{min} at high k values. Both figures 16 and 17 show that at high k, all the $M \neq 0$ curves coincide. It can thus be concluded that the compressibility effect is beneficial throughout the whole range of k values.

SOME PRACTICAL ASPECTS OF THE OPTIMIZED CONTROL LAWS

Preliminary Discussion

In forming the block diagrams representing how the optimized control laws can be achieved, it was assumed that the control surfaces' hinge moments are parameters which vary rapidly with flight conditions and which may show substantial deviations from theoretical values. It was therefore decided to form a control system which does not require any knowledge of the hinge moments, provided the power requirement is adequate. Figures 18 and 19 show the block diagram of such T.E. and L.E.-T.E. control systems, respectively. It can be seen that the feedback loop error function is based on the difference between the actual control deflection and the desired deflection as determined through the optimized control laws. Two main problems present themselves at this stage:

(1) How can the frequency ω be determined in order to perform the required division shown in the block diagrams and how sensitive will the system be to errors in its determination?

(2) The feedback control loop is, essentially, a second-order system having its resonance frequency and damping coefficients. It can therefore be expected that phase lags and amplitude changes will be incurred between the desired and actual control deflections and that these phase lags and amplitudes will be a function of the frequency of oscillation.

It is therefore necessary to investigate how sensitive the system is to these variations and whether practical systems or system components can meet any ensuing requirements. Figure 20 shows the effect of phase lags for the T.E. control system whereas

figure 21 shows similar variation of the L.E.-T.E. control system at $M = 0.9$. How sensitive the system is to phase lags at the low range of reduced frequencies can clearly be seen. Figure 21, for example, shows that a large positive value of λ_{min} can be changed into a negative value by a mere 20^{o} of phase lag. On the other hand, at high reduced frequencies, the phase lag effect becomes much smaller (see fig. 20) and becomes negligible at values of $k > 1$. This result indicates that the feedback control loop needs to be designed to have a high resonance frequency, relative to the lowest structural frequency, when flutter is expected to occur at the low range of reduced frequencies. Lower relative feedback loop resonance frequencies are required when flutter occurs at the high ranges of reduced frequencies. The effects of the phase lags were investigated at various Mach numbers; in every case a similar pattern of variation as in these figures was shown.

Amplitude Effects

Figure 22 shows a typical variation of the amplitude effects due to the feedback loop for a L.E.-T.E. control system at $M = 0.9$. It can be seen, once again, that the low reduced frequency range shows a very great sensitivity to amplitude gains whereas some beneficial effects can be seen at the high range of reduced frequencies for moderate values of amplitude gains. These results correlate with the phase-lag results for the resonance frequency of the feedback loop. Furthermore, it shows that an intermediate value of damping is required. Too high a damping value will lead to both a rapid variation of phase lags and reduction in amplitude with frequency increase, whereas too light a damping, although yielding small variations in phase lags, will cause large amplitude variations.

The T.E. control system behaves in a similar manner as can be seen from figure 23.

Sensitivity of Optimized System to the Determination of the Frequency

The determination of the frequency, through the determination of the period of oscillation, in a manner shown in figure 24, was suggested by Harley Brixey of the Boeing Co., Wichita, Kansas. This method yields directly the $1/\omega$ term which serves as a multiplier in the controls block diagrams. For a multifrequency signal, it has a tendency to yield an average frequency. The problem therefore reduces to the effect on λ_{min} of multiplying the whole $[G]$ matrix by a constant different from 1. Figures 25 and 26 show the results of a constant multiplier of $[G]$ on the optimized λ_{min} curve for the T.E. and L.E.-T.E. control systems, respectively, both at $M = 0$. The T.E. control system shows such a low sensitivity that an error of 200 percent is hardly noticeable in figure 25. At very high values of multipliers, a deterioration in λ_{min}, which starts at the high k values, creeps well into the low k values. Furthermore, the off-design sensitivity, shown in figure 29, becomes very much amplified (the multiplier $C_k = 18$). For multipliers

smaller than 1, the values of λ_{min} become proportionally smaller but remain positive. (See fig. 25.) For the L.E.-T.E. control system, improvement in λ_{min} can be seen in figure 26 for the lower range of k with a deterioration, which becomes relatively large, for large values of C_k and high ranges of reduced frequencies. (See fig. 26.) It can therefore be seen, in all cases, that inaccuracies in the determination of $1/\omega$ of the order of 200 percent to 300 percent (that is, $C_k = 2$ or $C_k = 3$) have little effect on the results. For $C_k < 1$, a reduction in λ_{min} is shown in figure 26 but in all cases, λ_{min} remains positive and still assumes relatively large values. Sensitivity tests for the L.E.-T.E. control system around the optimum values of $[C]$ and $[G]$ for a large multiplier ($C_k = 18$) does show a decrease in sensitivity (see fig. 29 as a representative example) rather than an increase in sensitivity. Similar results pertinent to $M = 0.9$ are shown in figures 27 and 28 for the T.E. and the L.E.-T.E. control systems. These results of the $1/\omega$ effect on λ_{min} shed a new light on the damping terms G and the form of the control law. This effect is discussed in the following section. At this stage, however, it appears that the optimized control law can be achieved in practice by a careful design.

Some Further Consideration of the Control Law G Parameters

The effect of the accuracy of the $1/\omega$ term, discussed in the previous section, has a direct bearing on both the control law and the mechanism of increasing the damping of the motion of the fluttering system. These points are discussed herein.

A different control law.- It has been shown that the division by ω gives rise to some problems, which although they can be brought to a relatively simple solution, warrant some investigation into the possibility of eliminating the need to determine ω.

Consider the simplified control law

$$\begin{Bmatrix} \beta \\ \delta \end{Bmatrix} = [C] \begin{Bmatrix} h/b \\ \alpha \end{Bmatrix} + i[G] \begin{Bmatrix} h/b \\ \alpha \end{Bmatrix}$$

and modify it to

$$\begin{Bmatrix} \beta \\ \delta \end{Bmatrix} = [C] \begin{Bmatrix} h/b \\ \alpha \end{Bmatrix} + [G] \begin{Bmatrix} \dot{h}/b \\ \dot{\alpha} \end{Bmatrix} \tag{25}$$

where the dots represent differentiation with respect to time. Equation (25) can be easily implemented and does not require the determination of ω. Since $\dot{h}/b$ and $\dot{\alpha}$ are dimensional, equation (25) should be reduced to a nondimensional form. This nondimensionalizing is done by dividing the $[G]$ terms by a reference frequency ω_r which lies

within the range of the expected frequencies of the system. Thus, equation (25) can be written, for sinusoidal oscillation, as

$$\begin{Bmatrix} \beta \\ \delta \end{Bmatrix} = [C] \begin{Bmatrix} h/b \\ \alpha \end{Bmatrix} + \frac{1}{\omega_r} [G] \begin{Bmatrix} \dot{h}/b \\ \dot{\alpha} \end{Bmatrix} \tag{26}$$

or, in a different form, as

$$\begin{Bmatrix} \beta \\ \delta \end{Bmatrix} = [C] \begin{Bmatrix} h/b \\ \alpha \end{Bmatrix} + i \frac{\omega}{\omega_r} [G] \begin{Bmatrix} h/b \\ \alpha \end{Bmatrix} \tag{27}$$

Equation (27) is identical to equation (8) except for the factor ω/ω_r. Therefore the effect of the variation of C_k, as discussed in a previous section, is identical to the effect of applying the control law defined by equation (26) and moving to a different C_k curve for different frequencies. (See, for example, fig. 26.) It should be noted that under this definition, ω/ω_r can assume values larger or smaller than 1. Figures 25 and 29(a) which relate to the T.E. control system show that the deterioration of λ_{min} coupled with the high sensitivity to off-design values does not offer any attraction to such a system. On the other hand, the large improvement in λ_{min} at low k values for the L.E.-T.E. control system for $\frac{\omega}{\omega_r} > 1$ and the decrease in the off-design sensitivity makes this simplified control law a very attractive proposition. It may be possible to allow the values of C and G to be dependent on k through the introduction of filters; thus, one could choose a small value of ω_r and yet maintain positive values of λ_{min} at the very high values of ω/ω_r. Some initial work done in this direction yielded some results which proved to be very sensitive to Mach number at high k and high ω/ω_r values. Some further work using some more sophisticated programing which will allow one to cope with the large number of parameters involved in such an optimization is required.

The damping increase.- A second point emerging from the $1/\omega$ analysis indicates that although a maximum value of λ_{min} is obtained by varying a single G_{ij} term, a monotonically increasing λ_{min} can be obtained by varying all the G_{ij} terms by a constant factor (as in the case of the L.E.-T.E. control system) or a shallow decrease in λ_{min} may result (as in the case of the T.E. control system). This behavior was not detected by the optimization procedure since relatively large parametric increments were used there. For k values smaller than 1, the G values contribute mainly to the aerodynamic damping. From existing literature (refs. 11, 12, and 13) an increase in damping, in a single degree of freedom only, of a fluttering system may show some improvement accompanied by subsequent degradation in stability as damping is further increased. It is also known that an increase in damping by a constant factor in all the degrees of freedom

always leads to an increase in stability. On the basis of these results, it appears that for a T.E. control system, a single sensor like Wykes' (ref. 10) linear accelerometer, for example, essentially introduces damping in bending, whereas a two-sensor system is more efficient in that it enables one to provide some small amounts of damping in pitch. The L.E.-T.E. control system allows the control of damping in both degrees of freedom and therefore leads to substantial improvements.

This correlation of results with known effects of linear damping suggests that the effect of linear damping on flutter speed may be explained in terms of the λ terms and that this energy approach may have a wider application than originally was anticipated. Some further possible use of the energy approach will be mentioned in a subsequent section.

GENERAL DISCUSSION AND RESULTS

The Cross Effects Between Active and Nonactive Strips on a Wing

An isolated strip has so far been considered with the objective of transforming it from an energy-absorbing element into an energy-dissipating element. If the intention is to span the wing with such activated strips, then the problem is solved since the whole wing turns into a dissipative system. If the intention, however, is to put a very small number of such strips in some isolated locations along the span, then care must be taken to insure that the nonactivated strips are not adversely affected by the activated ones. In other words, the "neighboring" nonactive strips should not absorb more energy and offset the beneficial effects arising from the dissipative active strips. With this effect in mind, possible sources for such adverse interactions are sought. However, any such source must be of aerodynamic nature since these forces are the only additional forces that the active strips introduce. From these aerodynamic forces, the aerodynamic damping terms and the aerodynamic cross-coupling terms are of prime importance in turning the activated strip into a dissipative element. Therefore, the possible effects of the direct aerodynamic stiffness terms on the nonactive strips of the wing remain to be investigated. These terms do not appear in the matrix $[U]$ since they are eliminated while it is being formed. It should therefore be made clear that any changes made to those direct aerodynamic stiffness terms cannot possibly have any effect on the values of λ_{min}.

Inspection of the optimized oscillation of both the L.E.-T.E. and the T.E. control systems show an upward deflection of the T.E. control with positive values of α (arising because of the negative values of C_{22}) as shown in sketches (k) and (l). This upward deflection gives rise to a large nose-up pitching moment that leads to a negative torsional aerodynamic stiffness term. This negative stiffness term leads to a reduction of the frequencies of the whole wing as the airspeed is increased and thus affects the neighboring

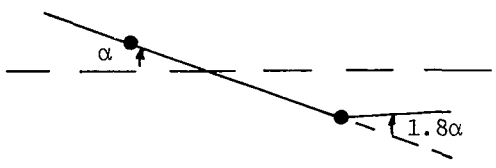

L.E.-T.E. control system

Sketch (k)

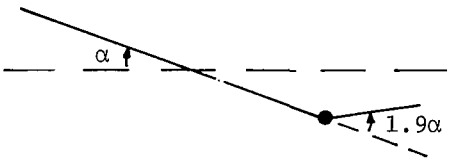

T.E. control system

Sketch (ℓ)

strips in an invariably unfavorable manner. In addition, this condition may result in very low reduced frequencies which could not have been anticipated on the basis of the natural frequencies and velocity of the system; thus, the system is "pushed" outside the k range of optimization.

In the case of the T.E. system, nothing can be done to produce positive aerodynamic torsional stiffness terms. The L.E.-T.E. system, however, offers a simple means of counteracting the nose-up moment by an appropriate deflection of the L.E. control. It is found that a value of $C_{12} \approx 5.6$ eliminates the nose-up moment about the quarter-chord point (aerodynamic center). This value of $C_{12} \approx 5.6$ insures that the aerodynamic torsional stiffness of the oscillation strip can never be negative. For wings having elastic axes location behind the quarter-chord point, the counteraction of the T.E. control to the lift buildup cancels some existing negative aerodynamic torsional stiffness terms. Swept-back wings, however, may show a reduction in their positive aerodynamic torsional stiffness because of this reduction in lift.

In order to minimize any possible cross effects between the activated strips and the nonactivated strips, C_{12} should be assigned a value which will offset the strip nose-up pitching moment about the aerodynamic center caused by the negative values of C_{22} (around $k = 0.5$). It is therefore hoped that by not allowing the system to assume negative aerodynamic stiffness terms and thus maintaining the full structural stiffnesses at all speeds, only a small number of strips will be required to eliminate flutter. The rigid-body modes form an exception to this rule since, in the absence of any structural stiffness terms in these modes, the aerodynamic terms are the sole contributors to the stiffness. The special case of rigid-body modes is discussed in some detail in a subsequent section.

In regard to the aerodynamic bending stiffness, it should be noted that a positive value of C_{21} gives rise to positive bending stiffness and vice versa for negative C_{21}. The L.E.-T.E. optimized control law sets $C_{21} = 0$ and thus leaves the bending stiffness unchanged. The T.E. control law where $C_{21} = -0.35$ incorporates some reduction in the bending stiffness of the system. It can however be modified, if necessary, since its effect on λ_{min} is small.

Suppression of Flutter in Three-Dimensional Wings

The suppression of flutter of a three-dimensional wing can theoretically be treated as a direct extension of the two-dimensional flutter suppression case. This treatment can be done at various levels of sophistication ranging from the simplified strip theory approach which requires some "engineering judgment" to some more elaborate lifting surface theory used in conjunction with a modal approach. These approaches are described in this section.

Consider a wing which flutters at a speed V_F and that it is to be increased to let V_F lie outside the range of speeds 0 to V_R. The first step involves the inspection of the deformation of the wing at V_F with the objective of determining the spanwise location which exhibits the largest product of b^4q^2. (See eq. (A7).) For constant-chord wings, this location may be around the wing tip whereas for tapered wings it will be further inboard. This latter location will form the center line of a L.E.-T.E. strip of length l, governed by the optimized control law. This strip will not only stop absorbing energy but will also dissipate a considerable amount of energy. It is further hoped on the basis of the precautions taken while the direct aerodynamic stiffness terms were considered that the neighboring strips will not extract more energy from the surroundings and thus offset the net energy input into the system. The flutter equations are then solved and the new flutter speed V_{F1} is determined. If V_{F1} still lies within the range 0 to V_R, a second strip is added. This procedure is repeated until the required speed range is cleared. It can be seen that this procedure is possible to accomplish since by spanning the wing with such strips, the whole wing is turned into a dissipative system. The engineering judgment is required to determine the best locations of the strips to keep their number to a minimum.

A second possible approach, still based on aerodynamic strip theory, involves the use of the structural mode shapes to compute the energy matrix $\left[U\right]$. Assume that the system is allowed to have m mode shapes and therefore m values of λ will be obtained. Determine the span l of the L.E.-T.E. control surfaces and optimize λ_{min} with respect to both the control parameters $\left[C\right]$ and $\left[G\right]$ (in much the same way as in the case of the two-dimensional strip) and the spanwise location. Once the optimum control parameters and optimum spanwise location are determined, vary the L.E. control parameter C_{12} to offset the negative torsional aerodynamic stiffness effects due to the optimized value of C_{22}. Determine the important parameters affecting λ_{min} and discard the parasitic terms in the same way as was done for the two-dimensional strip. Reoptimize λ_{min} with respect to the control parameters constraining the value of C_{12} to the specified value and the parasitic control terms to zero, the spanwise location remaining unchanged. At this stage, the flutter equations are solved again and the new value of V_F is checked against V_R. If insufficient increase is obtained, an additional

strip is added in an identical way. Note that a maximum number of $n/2$ strips are required to control the n modes and that if n is sufficiently large, the optimized control law of the strip must be identical to that for the two-dimensional strip results presented. This statement is true since if n is sufficiently large, the mode shapes can be combined in such a way to produce zero deflections at all the $n/2$ strips (which span the wing) except for the active strip treated. Since only a single strip is oscillating under such modal conditions, the optimum control laws must be identical. In this fashion considerable labor can be saved since the optimized results of the two-dimensional strip (with or without the term ω/ω_r) can be used right at the start, and the flutter equations solved for different spanwise control locations to determine the best location. Alternatively, the spanwise station which produces the maximum value of λ_{min} is chosen to be the best location.

A third approach is in essence identical to the modal approach which does not make use of the preoptimized strip results. The only difference lies in the fact that lifting surface aerodynamics, incorporating control forces, are used in evaluating the matrix $[U]$. The strip's values for the control parameters can be used, in this case, to provide the range of values around which the optimum is expected to lie.

It should be stressed here that the number of mode shapes that have to be considered in the analysis depends on the design of the control system. The rule should be that all the modes that actuate the control surfaces have to be considered. It has already been shown (when the ω/ω_r effect was discussed) that a control law which proves to be beneficial at the low range of reduced frequencies may become detrimental at the high ranges of k values. It will, therefore, be incorrect to pursue a flutter analysis involving four modes, for example, on the basis that these are the modes which yield flutter within the range 0 to V_R. It may well be that the control law may deteriorate the higher frequency modes to the extent of producing a flutter speed, at a high k value, within the range 0 to V_R. It is therefore extremely important to make sure that all the modes which lie within the frequency band that actuates the controls are considered. This requirement gives rise to a new problem which relates to the practical implementation of the frequency bounds of the control law. The lower frequency bound can be established by means of a "washout" filter, and no special difficulties arise. The upper bound does give rise to some problems since the introduction of a filter for this purpose is accompanied by large phase lags and amplitude changes, the effect of which has already been shown to be detrimental. It is therefore felt that a very good way of filtering out the high frequencies is through integrations of signals; it should be remembered that the high frequency signals are of less importance because of the integrations of the accelerometer signals. If further reduction of the high frequency signals is required, additional integrations can be performed on the two signals which form the feedback loop error function. This procedure is permissible since the control law (eq. (8)) will still be valid if both sides of the

equations are integrated an equal number of times. In this way the proper bounds are set to embrace the full range of the desired frequencies, and to reduce the high frequency signals to the level of the actuator's friction.

The optimized control law for the L.E.-T.E. control system was applied, analytically, on a large delta-wing-type transport airplane at $M = 0.9$, under NASA contract NAS1-9808. The results showed that a single L.E.-T.E. control system covering 12.5 percent of the wing semispan s and located about $0.1s$ inboard of the wing tip gave rise to 28 percent increase in flutter speed. An additional adjoining L.E.-T.E. strip covering 12.5 percent span and located further inboard led to a complete suppression of flutter in the range of speeds that were considered. (That is, the maximum speed tried was 41 percent greater than the flutter speed of the nonactivated wing. The flutter speed with two active strips appears to be much above this speed, if at all existent.) This result is very encouraging in that it shows that two L.E.-T.E. strips are sufficient to suppress flutter in a real system.

Suppression of Rigid-Body Modes

The suppression of rigid-body modes does not warrant a special treatment from the point of view of λ_{min}, provided the reduced frequency lies within the range of optimization and the phugoid motion is not considered. The reservation concerning the phugoid originates from the energy approach used in this work. It should be noted that in developing the work done per cycle by the system, it has been assumed that the aerodynamic forces are linearly dependent on the attitude of the components of the system. This statement is true for all elastic vibrating modes and it presents a good approximation for all the oscillating rigid-body modes with the exception of the phugoid. The phugoid will not be treated here and the parameters controlling its motion can be readily identified in the control law. With these reservations understood, any strip fitted with the L.E.-T.E. control system will dissipate energy when the airplane moves in a rigid-body mode. Special consideration, however, may have to be made regarding the contribution of the neighboring strips to the energy equation (the assumption being made that the activated strips do not span the wing). For illustrative purposes, consider two types of airplanes: one with sweptback wings and one with "straight" wings.

A wing strip with a L.E.-T.E. control system located around the tip of a sweptback wing is shown in sketch (m). A positive increase in the angle of attack α, which is normally accompanied by an upward increment in lifting force, activates the T.E. control upward to counteract the lift buildup. This reduction in lift due to the activated control deflection introduces a destabilizing moment about the center of gravity of the airplane, or effectively, a relatively large and negative contribution to the rigid-body aerodynamic pitching stiffness (due to the large value of Δx). As already mentioned, since the

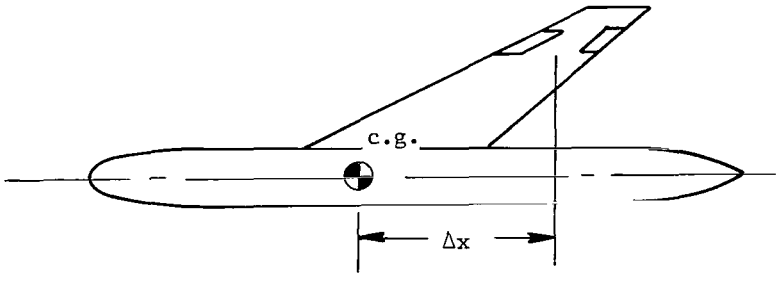

Sketch (m)

aerodynamic stiffness is the only stiffness in pitch, changes leading to its deterioration may affect the response of the rigid airplane in a way which causes the "neighboring" strips to absorb more energy and thus, lead to a net destabilizing effect. It can therefore be seen that a small reduction in lift at a section located far from the center-of-gravity location may cause a large reduction in pitching stiffness. This effect can be readily overcome by the introduction of a linear stiffness term due to C_{21} (which was shown to have a negligible effect on the suppression of flutter). It can thus be seen that a small bending stiffness term (that is, positive C_{21}) introduced at an activated strip located at a large distance behind the center of gravity compensates for this deterioration in stiffness. In nonswept wings, this reduction in lift leads to a negligible change in the rigid-body aerodynamic pitching stiffness. A review of these considerations which essentially deal with avoiding the degradation of the rigid-body modes due to the activation of an isolated strip indicates that this problem is of minor importance (since the washout filter required to suppress the very low frequency range and allow control of the airplane can be designed to filter out the rigid-body frequencies) as compared with the problem which may arise if an attempt is made to control the rigid-body modes to improve their stability.

Assume that it is desired to control, for example, the pitching mode of an elastic aircraft. On the basis of the foregoing results, a L.E.-T.E. control strip at the root of the horizontal tail (for minimum effect on its neighboring strips) will insure the increase in dissipation of the elastic modes of the horizontal tail. Adjustment* of C_{21} will then provide the stiffness control of the rigid-body stiffness in pitch (together with fuselage bending stiffness). Any possible adverse effects on the flutter speed due to possible interaction with the wing may be treated by fitting activated strips on the wing at some appropriate spanwise location in a manner identical to that already described. A canard surface can be treated similar to the horizontal surface. The yaw control also reduces to a similar procedure applied to the vertical-tail stabilizer. Finally, it should be noted that

*When C_{21} is given a value different from zero, C_{11} may be introduced. The reason for this effect is identical to the one which led to the introduction of C_{12} due to the existence of C_{22}. The ratio of C_{11}/C_{21} should therefore be approximately the same as C_{12}/C_{22}.

such active strips, located at the tail surfaces, can be used to compensate any rigid-mode degradation due to the wing's active strips, fitted with the objective of suppressing flutter, such as the case of the sweptback wing previously mentioned.

Gust-Response Problems

The control of the rigid-body modes, as discussed in the preceding section, does not give rise to requirements which are contradictory to those necessary to control the elastic modes. Hence, no difficulties should arise when attempting to control, simultaneously, both the rigid-body and the elastic modes. Since this type of problem falls within the province of gust-response problems, it is evident that the L.E.-T.E. control system, properly adjusted for rigid-body control, should also prove to be a very efficient gust alleviator.

As an example, consider the response of an airplane to a vertical gust. It is known that the gust problems are usually associated with the rigid-body translation of the airplane, whereas others are associated with its elastic response. A L.E.-T.E. control system located near the root of the wing should lead to the dissipation of large amounts of energy due to rigid-body movements. Additional control of rigid-body translation movement can be achieved, if necessary, by introducing aerodynamic translational stiffness through positive values of C_{21}. As noted in the preceding section, the existence of $C_{21} \neq 0$ may lead to the introduction of C_{11}. The problems arising from the elasticity of the airplane are best tackled by fitting a L.E.-T.E. control system at a location near the tip of the wing $\left(C_{11}\right.$ and C_{21} may again be introduced if necessary$\left.\right)$. It should, however, be remembered that although C_{11} and C_{21} have negligible effects on the flutter-suppression characteristics of the system, the penalty they introduce in terms of power requirements is by no means negligible.

Effect of Chordwise Deformations

The results obtained so far relate to wings with rigid chords. The extension of the analysis to a chordwise flexible strip can be made at various degrees of sophistication. In the following discussion, only the simplest possible extension is indicated. It is assumed that the chordwise deformation can be approximated by three straight lines representing the L.E. control surface, the main wing surface, and the T.E. control surface. This approximation is illustrated in sketch (n). The problem thus reduces to determining the control deflection due to the deformation and comparing that deflection, in a feedback loop, with the desired deflection determined through the control law. This result can be achieved in a simple manner by employing four sensors: two linear accelerometers and two rotational accelerometers. The two linear accelerometers were located near the control surface hinges at points 1 and 2 indicated in sketch (o). The

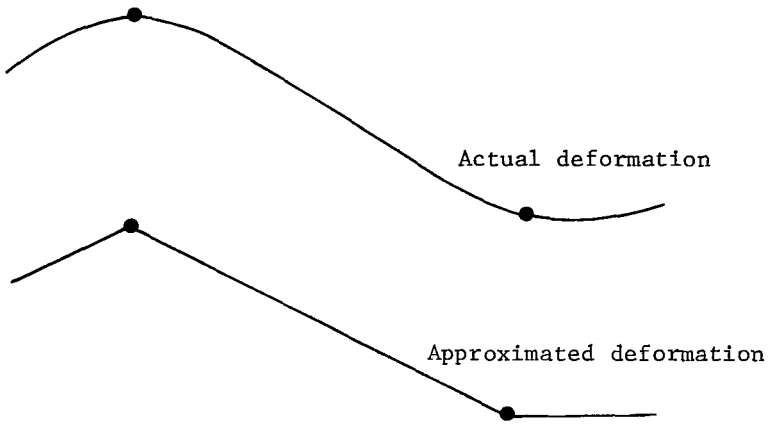

Sketch (n)

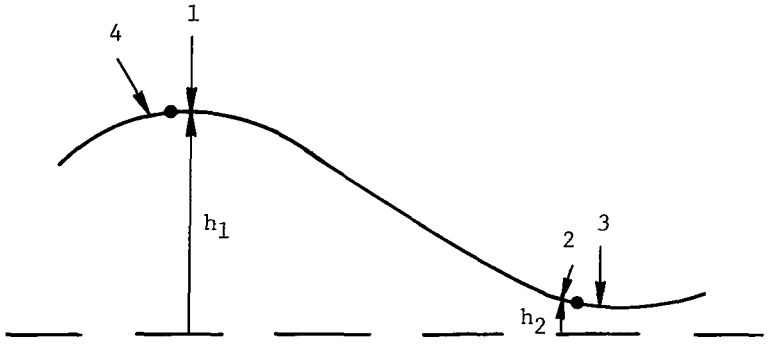

Sketch (o)

output of these two accelerometers can be processed to give α and h/b of the main part of the surface. The two rotational accelerometers, are located on the control surfaces, somewhere near the hinge line, at points 3 and 4. (See sketch (o).) Now

$$\alpha_e = \frac{h_1 - h_2}{\Delta x_{12}}$$

$$\beta_e = \alpha_4 + \alpha_e$$

$$\delta_e = \alpha_3 - \alpha_e$$

where the subscript e refers to the equivalent deformed chord deflections. (See sketch (p).) From the knowledge of α_e and h/b, the signals are processed as before to implement the control law, and then the values of the existing control deflections β_e and δ_e are subtracted while the error function is formed in the feedback loop.

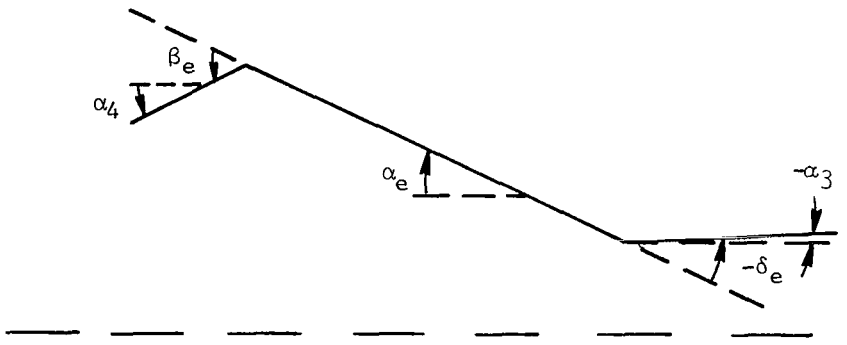

Sketch (p)

V-g Plots of a Two-Dimensional Flutter System

The results obtained were applied to a strip flutter problem, the objective being to check the control-law effectiveness in terms of a V-g plot. Figure 30(a) shows a V-g plot of the binary system previously used for the estimation of the power requirements (taken from ref. 25). The additional inertia and elastic data are

$$B_1 = \begin{bmatrix} 1.0 & 0.2 \\ 0.2 & 0.25 \end{bmatrix}$$

$$B_2 = \begin{bmatrix} 0.04 & -0.04 \\ -0.018666 & 0.050666 \end{bmatrix}$$

$$E_1 = \begin{bmatrix} 0.0625 & 0 \\ 0 & 0.25 \end{bmatrix}$$

$$E_2 = \begin{bmatrix} 0 & 0 \\ 0 & 0 \end{bmatrix}$$

the mass ratio is 4 and B_1, B_2, E_1, and E_2 are the submatrices used in appendix C. The system has a flutter speed $V_F/\omega_\alpha b$ of 1.54 and a divergence speed $V_D/\omega_\alpha b$ of 2.2.

Figure 30(b) shows the same system activated by the suggested control law; that is,

$$C = \begin{bmatrix} 0 & 5.6 \\ 0 & -1.4 \end{bmatrix}$$

$$[G] = \begin{bmatrix} 0 & 1.5 \\ 0.4 & 0.1 \end{bmatrix}$$

It can be seen that flutter has completely been suppressed and that the g values are in the order of hundreds.

Figure 30(c) shows the same system but with a very small activation that amounts to 10 percent of the suggested value. It is interesting to note the resulting major change in the V-g plot and the fairly substantial change in flutter speed. This particular result indicates that wing designs having large masses, like engines, attached near the wing trailing edge may introduce camber changes equivalent to control deflections and may lead to flutter results highly sensitive to the mode-shape definition.

Some Further Use of the Energy Approach

It has already been mentioned that the energy approach may be applied to investigate the effect of linear damping (structural, viscous or aerodynamic) on the flutter stability in terms of energy eigenvalues and energy mode shapes. It can also be used in either preliminary or advanced design to determine those mode shapes which absorb energy from the surroundings.

Determination of the Energy Absorbing Modes

For preliminary design, it is possible to represent the mode shapes of the structure in terms of either synthetic modes or some other known modes taken from a similar aircraft. Determine the matrix $[U]$ (eq. (A9)) and solve for the eigenvalues (by using eq. (A8)) to form the matrix $[\Lambda]$ and the modal matrices $[Q_R + iQ_I]$. Determine next, the smallest value of λ (generally negative) and isolate its corresponding modal columns $\{q_R + iq_I\}$. Inspection of the elements of both this q_R and q_I will yield the physical modes which participate most in this energy mode shape. If this term is the only negative λ term, design parameters like engine location, external stores locations, and so forth, can be used in a manner which will suppress those modes which contribute most to the energy mode. If there are few negative λ values this procedure can be repeated and preference can be given to those modes which correspond to the lower frequencies (smaller number of nodes) and higher negative values of λ.

For an advanced design stage where the flutter mode of vibration $\{q_F\}$ is known, equation (A10) can be used to determine the energy vector $\{\xi_R + i\xi_I\}$ at flutter. Substitution into the energy equation (eq. (A15)) yields the largest negative product of $\lambda_i\left(\xi_{R_i}^2 + \xi_{I_i}^2\right)$. This ith energy mode can then be identified as outlined previously.

In a similar manner, the reduction of the larger flutter system into a smaller system can be achieved by ignoring all those modes which either give rise to very small values of λ (preliminary design) or very small values of $\lambda_i\left(\xi_{R_i}^2 + \xi_{I_i}^2\right)$ (advanced design).

Mechanism of Flutter

An additional use of the energy equation is to further the insight into the mechanism of flutter. It is shown in appendix D that the flutter equation

$$\left(-\omega^2\left[B + \pi\rho b^4\omega^2 s\left(A_R + iA_I\right)\right] + \left[E\right]\right)\left\{q\right\} = 0$$

can be reduced to the following equation (eq. (D10)) by the use of the energy modal matrix $\left[Q_R + iQ_I\right]$ as a transformation matrix; that is,

$$\left(-\omega^2\left[N_{S1}\right] + \left[N_{S2}\right] + i\left[\frac{m_1\omega^2}{2}\Lambda - \omega^2 N_{A1} + N_{A2}\right]\right)\left\{\xi_R + i\xi_I\right\} = 0$$

where the matrices N_{S1} and N_{S2} are symmetric whereas N_{A1} and N_{A2} are antisymmetric. All the N matrices and m_1 are defined in appendix D. The form of equation (D10) is very interesting since it shows that the Λ matrix (which is diagonal) is the equivalent damping matrix. The matrices N_{A1} and N_{A2} are nondissipative matrices since they are antisymmetric and their effect is to provide out-of-phase coupling terms only in the equations of motion. Hence, any nonconservative linear problem can be reduced in a similar fashion, to a problem of considering on one hand the existence or nonexistence of some basically unstable mode shapes (negative λ terms) and on the other hand, the amount of coupling between those unstable modes and the other stable ones. It can therefore be seen that the key point for flutter to be at all possible is the existence of a mode shape with negative λ.

The relative importance of the low frequency modes over the high frequency modes, when flutter problems are considered, is widely accepted in aeroelasticity (excluding panel flutter). The analysis of an elastic system is invariably performed by considering its first few elastic modes. The normal justification, based on the responses of the system, is not convincing especially when dynamic stability problems are considered. It is, however, well known that practice provides the best justification for this approach. Inspection of figures 1 and 2 seems to provide some explanation and justification. At a certain value of flight speed, the low frequency modes will give rise to low reduced frequencies whereas the high frequency modes give rise to high values of reduced frequency. This statement means that the low frequency modes will lie on the far right-hand side of figures 1 and 2, whereas the high frequency modes will lie on the near left-hand side of

these figures. Since λ_{min} decreases in absolute value continuously and rapidly as k increases, it reaches a value of k at which λ_{min} is completely canceled by the structural damping of the system and thus makes it impossible for flutter to exist.

CONCLUDING REMARKS

The advantages of using a leading-edge—trailing-edge control system, driven by two sensors, and the usefulness of the energy approach have been demonstrated in the present work. The results obtained show that flutter can be suppressed but that great care must be exercised. It is appropriate to stress here, once again, some of the salient points which were brought to light in this work:

(1) Oscillatory aerodynamic derivatives are essential in this type of work. Furthermore, they must have good accuracy up to high values of the reduced frequency k. The accuracy of the aerodynamic derivatives used in the present work was not sufficient at the very high k values, as shown by comparison with computed exact results. Comparisons made with tabulated results, and which showed good agreement, were for values of $k < 1$ (since no higher values of k were tabulated). The results presented in this work, using numerical aerodynamic solutions, lead to somewhat smaller values of the energy eigenvalue λ in the high k range than the exact solution.

(2) Mach number effects are of a complex nature and no overall correction, like the Prandtl-Glauert correction, can be considered satisfactory. An example which showed excellent stability from the λ_{min} point of view, over an extremely large range of k, at a zero Mach number showed some very adverse effects at a Mach number of 0.9 and $k > 0.5$. Hence, the oscillatory Mach number effects must be considered.

(3) Control surface and actuator dynamics are of prime importance. Phase lags and amplitude changes can easily deprive the system of its effectiveness, especially at the low k range.

(4) All the structural modes that give rise to signals that actuate the control surfaces must be considered in the flutter analysis with active control. This statement is true irrespective of the number of structural modes required to represent the important flutter modes of the unactivated system.

It is believed that the control system which consists of the leading-edge—trailing-edge controls and which utilizes the frequency ratio ω/ω_r term (and obviates the need to determine the frequencies) is the best from the point of view of practical implementation and performance. This condition is particularly true since the very low reduced frequencies lying around the phugoid or short-period modes do not need such large positive values of λ_{min} as compared with those at the higher values of k. Further

improvements in the control law can be obtained if the k range of the system is more limited than the one treated here.

The implications of a successful flutter suppressor on design philosophy are many. They span a very wide range of problems: elastic stability, structural efficiency, structural fatigue life, and riding qualities of the aircraft. Additional work is, however, required before such a system can be incorporated into a design. Analytical work on a typical airplane can provide answers to questions relating to the number and size of surfaces required to suppress flutter for different types of airplanes and different categories of planforms. As a direct extension of this work, systematic analyses can be done on simple types of airplanes where some form of strip theory can be used. The extension using lifting surface theories requires the refinement of present numerical schemes to insure sufficient accuracy to allow partial span control at high Mach numbers and high k values. Finally, some carefully designed experimental work is required to provide support to these analytical results.

Langley Research Center,
National Aeronautics and Space Administration,
Hampton, Va., January 27, 1971.

APPENDIX A

THE ENERGY ANALYSIS

Let

$$\{F\} = \left(-\omega^2\left[B + \pi\rho b^4 s\left(A_R + iA_I\right)\right] + \left[E\right]\right)\{q\} \tag{A1}$$

where, at flutter

$$\{F\} = 0$$

and ω represents the frequency of oscillation; $\left[B\right]$, the mass matrix; $\left[A_R\right]$ and $\left[A_I\right]$, the real and imaginary parts of the aerodynamic matrix, respectively; $\left[E\right]$, the stiffness matrix; ρ, the density of the surrounding fluid; b, the half of a reference chord; $\{q\}$, the response vector; and s, the semispan of the wing.

The vector $\{q\}$ can be written as

$$\{q\} = \{q_o\} e^{i\omega t} = \{q_R + iq_I\} e^{i\omega t} \tag{A2}$$

where $\{q_o\}$ is a complex vector of amplitudes. The real part of equation (A1) is essentially the same as the imaginary part, except for the initial conditions at $t = 0$. In a harmonic motion, where no transients are treated, the real part only of equation (A1) can be considered without losing the generality of the equations. Hence, the forces $\{F\}$ which the system exerts on its surroundings are given by

$$\begin{aligned}\{F\} = &\frac{1}{2}\left(-\omega^2\left[B + \pi\rho b^4 s\left(A_R + iA_I\right)\right] + \left[E\right]\right)\{q_o\} e^{i\omega t} \\ &+ \frac{1}{2}\left(-\omega^2\left[B + \pi\rho b^4 s\left(A_R - iA_I\right)\right] + \left[E\right]\right)\{q_o^*\} e^{-i\omega t}\end{aligned} \tag{A3}$$

where the asterisk denotes the conjugate vector. The vector $\{F\}$ is clearly a real vector.

The velocity vector $\{\dot{q}\}$ can be obtained by differentiating equation (A2) to obtain

$$\{\dot{q}\} = i\omega\{q_o\} e^{i\omega t} \tag{A4}$$

The real part of this velocity vector $R\{\dot{q}\}$ is given by

$$R\{\dot{q}\} = \frac{1}{2} i\omega \{q_o\} e^{i\omega t} - \frac{1}{2} i\omega \{q_o^*\} e^{-i\omega t} \tag{A5}$$

Hence, the rate at which the system does work on its surroundings is given by $R[\dot{q}]\{F\}$ and using equations (A3) and (A5) yields

$$\begin{aligned} R[\dot{q}]\{F\} = {} & \frac{i\omega}{4}[q_o]\left(-\omega^2\left[B + \pi\rho b^4 s\left(A_R + iA_I\right)\right] + [E]\right)\{q_o\} e^{2i\omega t} \\ & - \frac{i\omega}{4}[q_o^*]\left(-\omega^2\left[B + \pi\rho b^4 s\left(A_R + iA_I\right)\right] + [E]\right)\{q_o\} \\ & + \frac{i\omega}{4}[q_o]\left(-\omega^2\left[B + \pi\rho b^4 s\left(A_R - iA_I\right)\right] + [E]\right)\{q_o^*\} \\ & - \frac{i\omega}{4}[q_o^*]\left(-\omega^2\left[B + \pi\rho b^4 s\left(A_R - iA_I\right)\right] + [E]\right)\{q_o^*\} e^{-2i\omega t} \end{aligned} \tag{A6}$$

Hence, the work $\overline{P}$ done per cycle by the system on its surroundings can be found by integrating equation (A6) between $t = 0$ to $t = \frac{2\pi}{\omega}$. Thus,

$$\begin{aligned} \overline{P} = {} & \frac{i\pi}{2}[q_o]\left(-\omega^2\left[B + \pi\rho b^4 s\left(A_R - iA_I\right)\right] + [E]\right)\{q_o^*\} \\ & - \frac{i\pi}{2}[q_o^*]\left(-\omega^2\left[B + \pi\rho b^4 s\left(A_R + iA_I\right)\right] + [E]\right)\{q_o\} \end{aligned}$$

This equation is a scalar equation and therefore the first expression on the right-hand side of this equation can be transposed to obtain ($[B]$ and $[E]$ being assumed to be symmetric)

$$\overline{P} = \frac{\pi^2 \rho b^4 \omega^2 s}{2}[q_o^*]\left[-\left(A_I + A_I^T\right) + i\left(A_R - A_R^T\right)\right]\{q_o\} \tag{A7}$$

Note that the matrices within the square brackets form a Hermitian matrix.

Now determine the eigenvalues and eigenvectors of the following Hermitian matrix $[U]$ extracted from equation (A7):

$$\lambda\{\eta\} = [U]\{\eta\} \tag{A8}$$

where

$$\left[U\right] = \left[-\left(A_I + A_I^T\right) + i\left(A_R - A_R^T\right)\right] \tag{A9}$$

and represent the vector $\left\{q_o\right\}$ in terms of the eigenvectors of equation (A8), that is,

$$\left\{q_o\right\} = \left[Q_R + iQ_I\right]\left\{\xi_R + i\xi_I\right\} \tag{A10}$$

where $\left[Q_R\right]$ and $\left[Q_I\right]$ are square matrices whose columns are the real and imaginary parts of the eigenvectors of equation (A8), and $\left\{\xi_R + i\xi_I\right\}$ are generalized modal coordinates (defined by eq. (A10)) associated with the aerodynamic energy.

All the eigenvalue and eigenvector solutions of equation (A8) can be expressed in the classical form (ref. 26, p. 6) $\left[Q_R + iQ_I\right]\left[\Lambda\right] = \left[U\right]\left[Q_R + iQ_I\right]$. Postmultiplying this equation by $\left\{\xi_R + i\xi_I\right\}$ and premultiplying it by $\left[q_o^*\right]$ or $\left[\xi_R - i\xi_I\right]\left[Q_R^T - iQ_I^T\right]$ yields

$$\left[\xi_R - i\xi_I\right]\left[Q_R^T - iQ_I^T\right]\left[Q_R + iQ_I\right]\left[\Lambda\right]\left\{\xi_R + i\xi_I\right\} = \left[\xi_R - i\xi_I\right]\left[Q_R^T - iQ_I^T\right]\left[-\left(A_I + A_I^T\right) + i\left(A_R - A_R^T\right)\right]\left[Q_R + iQ_I\right]\left\{\xi_R + i\xi_I\right\} \tag{A11}$$

where $\left[\Lambda\right]$ is the eigenvalues matrix, that is,

$$\left[\Lambda\right] = \begin{bmatrix} \lambda_1 & & & & \\ & \lambda_2 & & & \\ & & \cdot & & \\ & & & \cdot & \\ & & & & \lambda_n \end{bmatrix} \tag{A12}$$

The right-hand side of equation (A11) is identical to the right-hand side of equation (A7) except for the $\pi^2\rho b^4\omega^2 s/2$ factor. Hence, the left-hand sides of these two equations can be equated to obtain:

$$\overline{P} = \frac{\pi^2\rho b^4\omega^2 s}{2}\left[\xi_R - i\xi_I\right]\left[Q_R^T - iQ_I^T\right]\left[Q_R + iQ_I\right]\left[\Lambda\right]\left\{\xi_R + i\xi_I\right\}$$

The matrix $\left[Q_R^T - iQ_I^T\right]$ represents the modal matrix of the complex left-hand (normalized) eigenvectors and therefore (ref. 26, p. 26)

$$\left[Q_R^T - iQ_I^T\right]\left[Q_R + iQ_I\right] = \left[I\right] \tag{A13}$$

where $\left[I\right]$ is the unit matrix. Hence $\overline{P}$ reduces to the form

$$\overline{P} = \frac{\pi^2 \rho b^4 \omega^2 s}{2}\left\{\xi_R - i\xi_I\right\}\left[\Lambda\right]\left\{\xi_R + i\xi_I\right\} \tag{A14}$$

or

$$\overline{P} = \frac{\pi^2 \rho b^4 \omega^2 s}{2}\left(\left\{\xi_R\right\}\left[\Lambda\right]\left\{\xi_R\right\} + \left\{\xi_I\right\}\left[\Lambda\right]\left\{\xi_I\right\}\right) \tag{A15}$$

The energy input per cycle into the surroundings has thus been reduced to a quadratic form in terms of the generalized energy modal coordinates.

APPENDIX B

DERIVATION OF THE GENERALIZED AERODYNAMIC FORCES OF A L.E.-T.E. SYSTEM

Consider the determination of the aerodynamic forces acting on the system shown in sketch (B1)

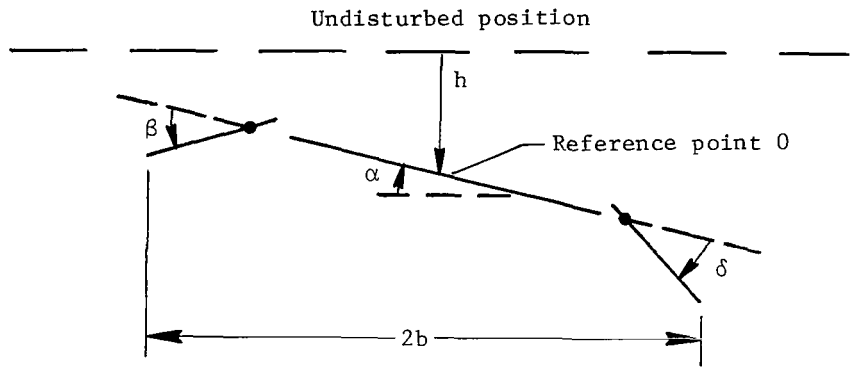

Sketch (B1)

and assume that the forces acting on a somewhat similar system (as used in ref. 16) described in sketch (B2) are known. Note the difference between the h,α,β,δ coordinates and the $\bar{h},\bar{\alpha},\bar{\beta},\bar{\delta}$ coordinates

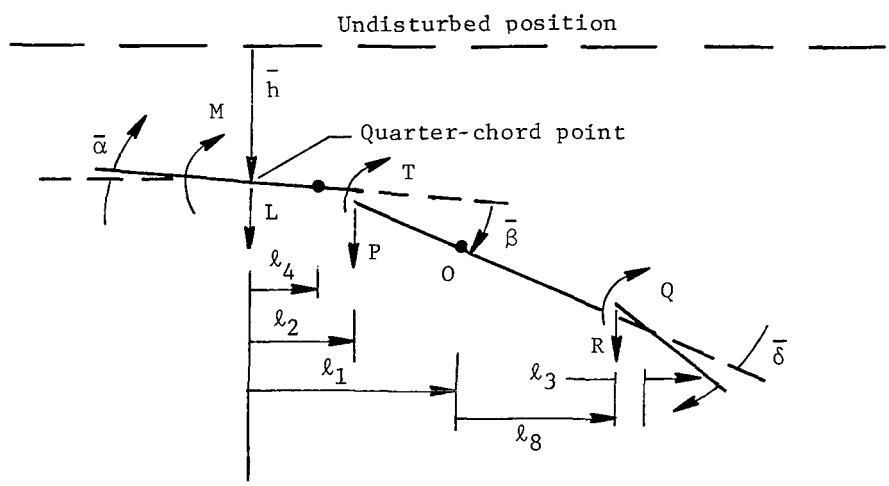

Sketch (B2)

The arrows indicate the direction of either positive displacements, distances, or forces. The symbols L and M denote the total lift and pitching moment and L is assumed to act through the quarter-chord point. The force acting on the aileron-tab combination

through the aileron L.E. point is denoted by P and the aileron-tab moment is denoted by T. The force acting on the tab through its L.E. point is R and the tab moment is Q. The forces in sketch (B2), their direction, and points of application are identical with those of Smilg and Wasserman (ref. 18) and can be determined directly from expressions appearing in the reference for $M = 0$. These expressions summarize the works of Theodorsen, Garrick, Küssner, and Schwartz (refs. 20 and 21).

The object of the following analysis is to determine the generalized forces acting on the h, α, β, and δ coordinates. This object will be accomplished by the application of the principle of virtual work. The virtual work W_h in the h coordinate is given by

$$W_h = b\frac{h}{b}L \tag{B1}$$

and therefore, the generalized force Q_h will be given by

$$Q_h = \frac{\delta W_h}{\delta(h/b)} = bL \tag{B2}$$

Similarly, the virtual work W_α in the α coordinate is given by

$$W_\alpha = M\alpha - Ll_1\alpha \tag{B3}$$

Hence, the generalized force Q_α is

$$Q_\alpha = \frac{\delta W_\alpha}{\delta\alpha} = M - Ll_1 \tag{B4}$$

The virtual work W_β in the β coordinate is given by

$$W_\beta = -\left(M - T - Pl_2\right)\beta + (L - P)l_4\beta$$

and hence

$$Q_\beta = \frac{\delta W_\beta}{\delta\beta} = P\left(l_2 - l_4\right) + Ll_4 + T - M \tag{B5}$$

Similarly,

$$W_\delta = Q\delta - Rl_3\delta$$

and hence,

$$Q_\delta = \frac{\delta W_\delta}{\delta \delta} = Q - Rl_3 \tag{B6}$$

These equations can be condensed into the following matrix equation:

$$\begin{Bmatrix} Q_h \\ Q_\alpha \\ Q_\beta \\ Q_\delta \end{Bmatrix} = \begin{bmatrix} b & 0 & 0 & 0 & 0 & 0 \\ -l_1 & 1 & 0 & 0 & 0 & 0 \\ l_4 & -1 & 1 & l_2 - l_4 & 0 & 0 \\ 0 & 0 & 0 & 0 & 1 & -l_3 \end{bmatrix} \begin{Bmatrix} L \\ M \\ T \\ P \\ Q \\ R \end{Bmatrix} \tag{B7}$$

but the forces are of the form

$$\begin{Bmatrix} L \\ M \\ T \\ P \\ Q \\ R \end{Bmatrix} = \pi \rho \omega^2 \begin{bmatrix} b^3 & & & & & \\ & b^4 & & & & \\ & & b^4 & & & \\ & & & b^3 & & \\ & & & & b^4 & \\ & & & & & b^3 \end{bmatrix} [A_O] \begin{Bmatrix} \bar{h}/b \\ \bar{\alpha} \\ \bar{\beta} \\ \bar{z}/b \\ \bar{\delta} \\ \bar{y}/b \end{Bmatrix} \tag{B8}$$

where $[A_O]$ is a 6×6 matrix and $\bar{z}$ and $\bar{y}$ define the hinge locations and are given by

$$\bar{z} = (l_2 - l_4)\bar{\beta} \tag{B9}$$

$$\bar{y} = -l_3 \bar{\delta} \tag{B10}$$

Therefore, one can write the following equation based on equations (B9) and (B10)

$$\begin{Bmatrix} \bar{h}/b \\ \bar{\alpha} \\ \bar{\beta} \\ \bar{z}/b \\ \bar{\delta} \\ \bar{y}/b \end{Bmatrix} = \begin{bmatrix} 1 & 0 & 0 & 0 \\ 0 & 1 & 0 & 0 \\ 0 & 0 & 1 & 0 \\ 0 & 0 & (l_2 - l_4)/b & 0 \\ 0 & 0 & 0 & 1 \\ 0 & 0 & 0 & -l_3/b \end{bmatrix} \begin{Bmatrix} \bar{h}/b \\ \bar{\alpha} \\ \bar{\beta} \\ \bar{\delta} \end{Bmatrix} \tag{B11}$$

Substituting equations (B8) and (B11) into equation (B7) yields

$$\begin{Bmatrix} Q_h \\ Q_\alpha \\ Q_\beta \\ Q_\delta \end{Bmatrix} = \pi\rho b^4\omega^2[A_1]\begin{Bmatrix} \bar{h}/b \\ \bar{\alpha} \\ \bar{\beta} \\ \bar{\delta} \end{Bmatrix} \tag{B12}$$

where

$$[A_1] = \begin{bmatrix} 1 & 0 & 0 & 0 & 0 & 0 \\ -l_1/b & 1 & 0 & 0 & 0 & 0 \\ l_4/b & -1 & 1 & (l_2 - l_4)/b & 0 & 0 \\ 0 & 0 & 0 & 0 & 1 & -l_3/b \end{bmatrix}[A_0]\begin{bmatrix} 1 & 0 & 0 & 0 \\ 0 & 1 & 0 & 0 \\ 0 & 0 & 1 & 0 \\ 0 & 0 & (l_2 - l_4)/b & 0 \\ 0 & 0 & 0 & 1 \\ 0 & 0 & 0 & -l_3/b \end{bmatrix} \tag{B13}$$

Comparison between the coordinates h,α,β,δ, and $\bar{h},\bar{\alpha},\bar{\beta},\bar{\delta}$ yields the following relations:

$$\bar{h} = h - l_1\alpha + l_4\beta$$

$$\bar{\alpha} = \alpha - \beta$$

$$\bar{\beta} = \beta$$

$$\bar{\delta} = \delta$$

These equations can be expressed as

$$\begin{Bmatrix} \bar{h}/b \\ \bar{\alpha} \\ \bar{\beta} \\ \bar{\delta} \end{Bmatrix} = \begin{bmatrix} 1 & -l_1/b & l_4/b & 0 \\ 0 & 1 & -1 & 0 \\ 0 & 0 & 1 & 0 \\ 0 & 0 & 0 & 1 \end{bmatrix}\begin{Bmatrix} h/b \\ \alpha \\ \beta \\ \delta \end{Bmatrix} \tag{B14a}$$

Substituting equation (B14a) into equation (B12) and rearranging finally yields

$$\begin{Bmatrix} Q_h \\ Q_\alpha \\ Q_\beta \\ Q_\delta \end{Bmatrix} = \pi\rho b^4\omega^2 [D]^T [A_0][D] \begin{Bmatrix} h/b \\ \alpha \\ \beta \\ \delta \end{Bmatrix} \tag{B14b}$$

where

$$[D] = \begin{bmatrix} 1 & -l_1/b & l_4/b & 0 \\ 0 & 1 & -1 & 0 \\ 0 & 0 & 1 & 0 \\ 0 & 0 & (l_2 - l_4)/b & 0 \\ 0 & 0 & 0 & 1 \\ 0 & 0 & 0 & -l_3/b \end{bmatrix} \tag{B15}$$

and $[D]^T$ is the transpose of $[D]$.

If

$$[H] = [D]^T [A_0][D] \tag{B16}$$

then equation (B14b) can be written in the more concise form:

$$\begin{Bmatrix} Q_h \\ Q_\alpha \\ Q_\beta \\ Q_\delta \end{Bmatrix} = \pi\rho b^4\omega^2 [H] \begin{Bmatrix} h/b \\ \alpha \\ \beta \\ \delta \end{Bmatrix} \tag{B17}$$

APPENDIX C

ESTIMATION OF THE POWER REQUIRED TO ACTIVATE THE CONTROL SURFACES

Consider the equations of motion of a L.E.-T.E. wing strip of unit span which is allowed to oscillate in bending and torsion in addition to its control-surface deflections; that is,

$$\left(-\omega^2\left[B + \pi\rho b^4 H\right] + \left[E\right]\right)\{q\} = \begin{Bmatrix} 0 \\ 0 \\ f_\beta \\ f_\delta \end{Bmatrix} \tag{C1}$$

where f_β and f_δ are external forces applied by the control system on the control surfaces and the matrices are of order 4×4. The first algebraic equations in the matrix equations (C1) have already been used in the energy analysis in conjunction with the control law defined by equation (2). The last two equations, when used with the control law, yield the forces required for the implementation of the control law.

Denote

$$\left.\begin{aligned} \left[B\right] &= \left[\begin{array}{c|c} B_1 & B_2 \\ \hline B_3 & B_4 \end{array}\right] \\ \left[E\right] &= \left[\begin{array}{c|c} E_1 & E_2 \\ \hline E_3 & E_4 \end{array}\right] \\ \left[H\right] &= \left[\begin{array}{c|c} H_1 & H_2 \\ \hline H_3 & H_4 \end{array}\right] \end{aligned}\right\} \tag{C2}$$

where all the submatrices are of order 2×2. Substitute the control law in the last two equations of equation (C1) to obtain

$$\left(-\omega^2\left[B_3 + B_4C + iB_4G + \pi\rho b^4\left(H_3 + H_4C + iH_4G\right)\right] + E_3 + E_4C + iE_4G\right)\begin{Bmatrix} h/b \\ \alpha \end{Bmatrix} = \begin{Bmatrix} f_\beta \\ f_\delta \end{Bmatrix} \tag{C3}$$

By denoting

$$\left[F_1\right] = -\omega^2\left[B_3 + B_4C + iB_4G + \pi\rho b^4\left(H_3 + H_4C + iH_4G\right)\right] + \left[E_3 + E_4C + iE_4G\right] \tag{C4}$$

equation (C3) can be written in the form

$$\begin{Bmatrix} f_\beta \\ f_\delta \end{Bmatrix} = \left[F_1\right]\begin{Bmatrix} h/b \\ \alpha \end{Bmatrix} \tag{C5a}$$

The matrix $\begin{Bmatrix} f_\beta \\ f_\delta \end{Bmatrix}$ is complex. Its real part will be given by

$$R\begin{Bmatrix} f_\beta \\ f_\delta \end{Bmatrix} = \frac{1}{2}\left[F_1\right]\begin{Bmatrix} h/b \\ \alpha \end{Bmatrix} + \frac{1}{2}\left[F_1^*\right]\begin{Bmatrix} h^*/b \\ \alpha^* \end{Bmatrix} \tag{C5b}$$

where the asterisks denote complex conjugates. The angular velocities of the control surfaces are obtained by differentiating equation (8); that is,

$$\begin{Bmatrix} \dot\beta \\ \dot\delta \end{Bmatrix} = \left(\left[C\right] + i\left[G\right]\right)\begin{Bmatrix} \dot h/b \\ \dot\alpha \end{Bmatrix} \tag{C6}$$

The maximum instantaneous power requirement $\overline{P}_{1,max}$ is given by

$$\overline{P}_{1,max} = \left(R\left[\dot\beta,\dot\delta\right]R\begin{Bmatrix} f_\beta \\ f_\delta \end{Bmatrix}\right)_{max}$$

or

$$\overline{P}_{1,max} = \left(R\left[\dot\beta,\dot\delta\right]\right)_{max}\left(R\begin{Bmatrix} f_\beta \\ f_\delta \end{Bmatrix}\right)_{max} \tag{C7}$$

Equation (C6) indicates that the maximum possible value of $R\left[\dot{\beta},\dot{\delta}\right]$ will be given by

$$\left(R\left[\dot{\beta},\dot{\delta}\right]\right)_{max} = \omega\left[\left|h_o/b\right|,\left|\alpha_o\right|\right]\left[\left|C^T + iG^T\right|\right] \tag{C8}$$

where the notation $|\ |$ means the modulus of the complex number written within the lines, and

$$\begin{Bmatrix} h/b \\ \alpha \end{Bmatrix} = \begin{Bmatrix} h_o/b \\ \alpha_o \end{Bmatrix} e^{i\omega t} \tag{C9}$$

Similarly, using equation (C5) yields

$$\left(R\begin{Bmatrix} f_\beta \\ f_\delta \end{Bmatrix}\right)_{max} = \left[\left|F_1\right|\right]\begin{Bmatrix} \left|h_o/b\right| \\ \left|\alpha_o\right| \end{Bmatrix} \tag{C10}$$

Substitution of equations (C8) and (C10) into equation (C7) finally yields

$$\overline{P}_{1,max} = \omega\left[\left|h_o/b\right|,\left|\alpha_o\right|\right]\left[\left|C^T + iG^T\right|\right]\left[\left|F_1\right|\right]\begin{Bmatrix} \left|h_o/b\right| \\ \left|\alpha_o\right| \end{Bmatrix} \tag{C11}$$

Equation (C11) formed the basis upon which the power estimates were made.

APPENDIX D

TRANSFORMATION OF THE FLUTTER EQUATIONS USING THE ENERGY MODE SHAPES MATRIX

The flutter equation

$$\left(-\omega^2\left[B + m_1\left(A_R + iA_I\right)\right] + \left[E\right]\right)\left\{q\right\} = 0 \tag{D1}$$

where

$$m_1 = \pi\rho b^4 s \tag{D2}$$

can be transformed to an interesting special form by the use of the energy modal matrix $\left[Q_R + iQ_I\right]$ as a transformation matrix, that is,

$$\left\{q\right\} = \left[Q_R + iQ_I\right]\left\{\xi_R + i\xi_I\right\} \tag{D3}$$

Substitute equation (D3) into equation (D1) and premultiply the resulting equation by $\left[Q_R^T - iQ_I^T\right]$ to obtain

$$\left[Q_R^T - iQ_I^T\right]\left(-\omega^2\left[B + m_1\left(A_R + iA_I\right)\right] + \left[E\right]\right)\left[Q_R + iQ_I\right]\left\{\xi_R + i\xi_I\right\} = 0 \tag{D4}$$

Denote

$$\left.\begin{aligned}\left[A_R\right] &= \frac{1}{2}\left[A_R + A_R^T\right] + \frac{1}{2}\left[A_R - A_R^T\right] \\ \left[A_I\right] &= \frac{1}{2}\left[A_I + A_I^T\right] + \frac{1}{2}\left[A_I - A_I^T\right]\end{aligned}\right\} \tag{D5}$$

where the first matrix on the right-hand side of equations (D5) is symmetric whereas the second is antisymmetric. Substituting equations (D5) into equation (D4) and making use of equations (A11) and (A13) yields

$$\frac{i\omega^2 m_1}{2}[\Lambda]\{\xi_R + i\xi_I\} + \left[Q_R^T - iQ_I^T\right]\left(-\omega^2\left[B + \frac{m_1}{2}\left(A_R + A_R^T\right) + \frac{im_1}{2}\left(A_I - A_I^T\right)\right]\right.$$

$$\left. + [E]\right)[Q_R + iQ_I]\{\xi_R + i\xi_I\} = 0 \tag{D6}$$

Denote

$$\left.\begin{aligned} T_{S1} &= B + \frac{m_1}{2}\left(A_R + A_R^T\right) \\ T_{S2} &= E \\ T_{A1} &= \frac{m_1}{2}\left(A_I - A_I^T\right) \end{aligned}\right\} \tag{D7}$$

where T_{S1} and T_{S2} are symmetric matrices and T_{A1} is an antisymmetric matrix. Substituting equations (D7) into equation (D6) yields

$$\left(\frac{i\omega^2 m_1}{2}[\Lambda] + \left[Q_R^T - iQ_I^T\right]\left[-\omega^2\left(T_{S1} + iT_{A1}\right) + T_{S2}\right][Q_R + iQ_I]\right)\{\xi_R + i\xi_I\} = 0 \tag{D8}$$

Denote

$$\left.\begin{aligned} [N_{S1}] &= \left[Q_R^T T_{S1} Q_R + Q_I^T T_{S1} Q_I\right] - \left[Q_R^T T_{A1} Q_I - Q_I^T T_{A1} Q_R\right] \\ [N_{S2}] &= \left[Q_R^T T_{S2} Q_R + Q_I^T T_{S2} Q_I\right] \\ [N_{A1}] &= \left[Q_R^T T_{S1} Q_I - Q_I^T T_{S1} Q_R\right] + \left[Q_R^T T_{A1} Q_R + Q_I^T T_{A1} Q_I\right] \\ [N_{A2}] &= \left[Q_R^T T_{S2} Q_I - Q_I^T T_{S2} Q_R\right] \end{aligned}\right\} \tag{D9}$$

where $[N_{S1}]$ and $[N_{S2}]$ are symmetric and $[N_{A1}]$ and $[N_{A2}]$ are antisymmetric. Rearranging equation (D8) and making use of the notations defined in equation (D9) yields

$$\left(-\omega^2[N_{S1}] + [N_{S2}] + i\left[\frac{m_1\omega^2}{2}\Lambda - \omega^2 N_{A1} + N_{A2}\right]\right)\{\xi_R + i\xi_I\} = 0 \tag{D10}$$

It should be noted that all the real square matrices in equation (D10) are symmetric whereas all the imaginary square matrices are antisymmetric, except for $[\Lambda]$ which is diagonal.

REFERENCES

1. Connor, Roger J.; Hawk, John; and Levy, Charles: Dynamic Analyses for the C-47 Airplane Gust Load Alleviation System. Rep. No. SM-14456, Douglas Aircraft Co., Inc., July 29, 1952.

2. Knowles, J. A.; and Shockley, E. J.: Flight Tests of the C-47 Airplane Equipped With a Gust Alleviation Device. Rep. No. Dev-947 (Contract AF-33(038)-6655), Douglas Aircraft Co., Inc., Nov. 25, 1952.

3. Kraft, Christopher C., Jr.: Initial Results of a Flight Investigation of a Gust-Alleviation System. NACA TN 3612, 1956.

4. Hunter, Paul A., Kraft, Christopher C., Jr.; and Alford, William L.: A Flight Investigation of an Automatic Gust-Alleviation System in a Transport Airplane. NASA TN D-532, 1961.

5. Dempster, John B.; and Roger, Kenneth L.: Evaluation of B-52 Structural Response to Random Turbulence With Various Stability Augmentation Systems. AIAA Pap. No. 66-998, Nov.-Dec. 1966.

6. Dempster, John B.; and Arnold, James I.: Flight Test Evaluation of an Advanced Stability Augmentation System for the B-52 Aircraft. AIAA Pap. No. 68-1068, Oct. 1968.

7. Davis, H. Max; and Swaim, Robert L.: Controlling Dynamic Response in Rough Air. AIAA Pap. No. 66-997, Nov.-Dec. 1966.

8. Wykes, John H.: Structural Dynamic Stability Augmentation and Gust Alleviation of Flexible Aircraft. AIAA Pap. No. 68-1067, Oct. 1968.

9. Smith, Ralph E.; and Lum, Evan L. S.: Linear Optimal Theory Applied to Active Structural Bending Control. AIAA Pap. No. 66-970, Nov.-Dec. 1966.

10. Wykes, John H.; and Mori, Alva S.: Techniques and Results of an Analytical Investigation Into Controlling the Structural Modes of Flexible Aircraft. AIAA Symposium of Structural Dynamics and Aeroelasticity, Aug.-Sept. 1965, pp. 419-433.

11. Broadbent, E. G.; and Williams, Margaret: The Effect of Structural Damping on Binary Flutter. R.&M. 3169, British A.R.C., 1960.

12. Done, G. T. S.: The Effect of Linear Damping on Flutter Speed. R.&M. No. 3396, British A.R.C., 1965.

13. Nissim, E.: Effect of Linear Damping on Flutter Speed. Part I: Binary Systems. Aeronaut. Quart., vol. XVI, Pt. 2, May 1965, pp. 159-178.

14. Theissen, J. G.; and Robinette, W. C.: Servo Control of Flutter. AIAA Structural Dynamics and Aeroelasticity Specialist Conference and ASME/AIAA 10th Structures, Structural Dynamics and Materials Conference (New Orleans, La.), Apr. 1969, pp. 228-240.

15. Moon, F. C.; and Dowell, E. H.: The Control of Flutter Instability in a Continuous Elastic System Using Feedback. AIAA/ASME 11th Structures, Structural Dynamics, and Materials Conference (Denver, Colo.), Apr. 1970, pp. 48-65.

16. Garrick, I. E.: Propulsion of a Flapping and Oscillating Airfoil. NACA Rep. 567, 1936.

17. Duncan, W. J.: Introductory Survey. Vol. I of AGARD Manual on Aeroelasticity, W. P. Jones, ed., 1959.

18. Smilg, Benjamin; and Wasserman, Lee S.: Application of Three-Dimensional Flutter Theory to Aircraft Structures. ACTR No. 4798, Material Div., Army Air Corps, July 9, 1942.

19. Wasserman, Lee S.; Mykytow, Walter J.; and Spielberg, Irvin: Tab Flutter Theory and Applications. AAF TR No. 5153, Air Technical Service Command, Army Air Forces, Sept. 1, 1944.

20. Küssner, H. G.; and Schwartz, L.: The Oscillating Wing With Aerodynamically Balanced Elevator. NACA TM 991, 1941.

21. Theodorsen, Theodore; and Garrick, I. E.: Nonstationary Flow About a Wing-Aileron-Tab Combination Including Aerodynamic Balance. NACA Rep. 736, 1942.

22. Bisplinghoff, Raymond L.; Ashley, Holt; and Halfman, Robert L.: Aeroelasticity. Addison-Wesley Pub. Co., Inc., c.1955.

23. Turner, M. J.; and Rabinowitz, S.: Aerodynamic Coefficients for an Oscillating Airfoil With Hinged Flap, With Tables for a Mach Number of 0.7. NACA TN 2213, 1950.

24. Van der Vooren, A. I.: The Theodorsen Circulation Function Aerodynamic Coefficients. Collected Tables and Graphs, Pt. VI of AGARD Manual on Aeroelasticity, W. P. Jones, ed., 1964.

25. Theodorsen, T.; and Garrick, I. E.: Mechanism of Flutter – A Theoretical and Experimental Investigation of the Flutter Problem. NACA Rep. 685, 1940.

26. Wilkinson, J. H.: The Algebraic Eigenvalue Problem. Clarendon Press (Oxford), 1965.

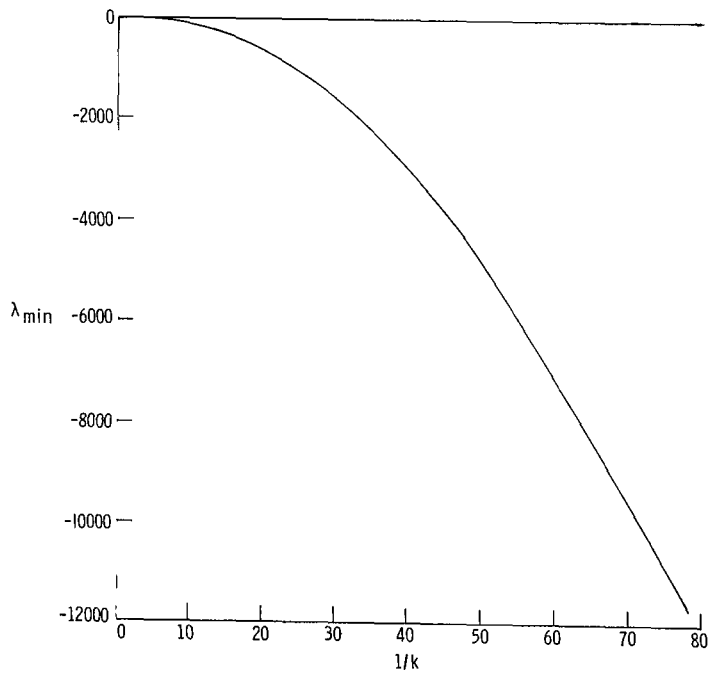

(a) λ_{min}.

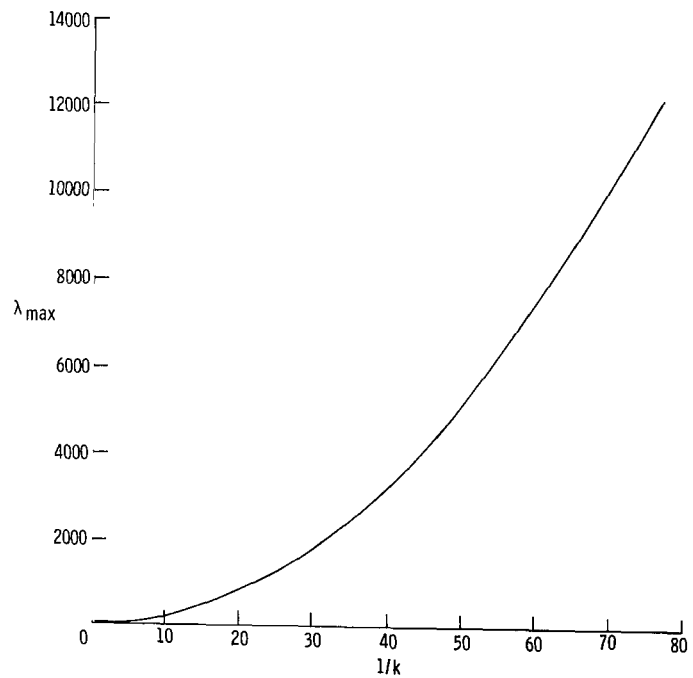

(b) λ_{max}.

Figure 1.- Variation of λ with $1/k$ of a wing strip with no control surfaces.

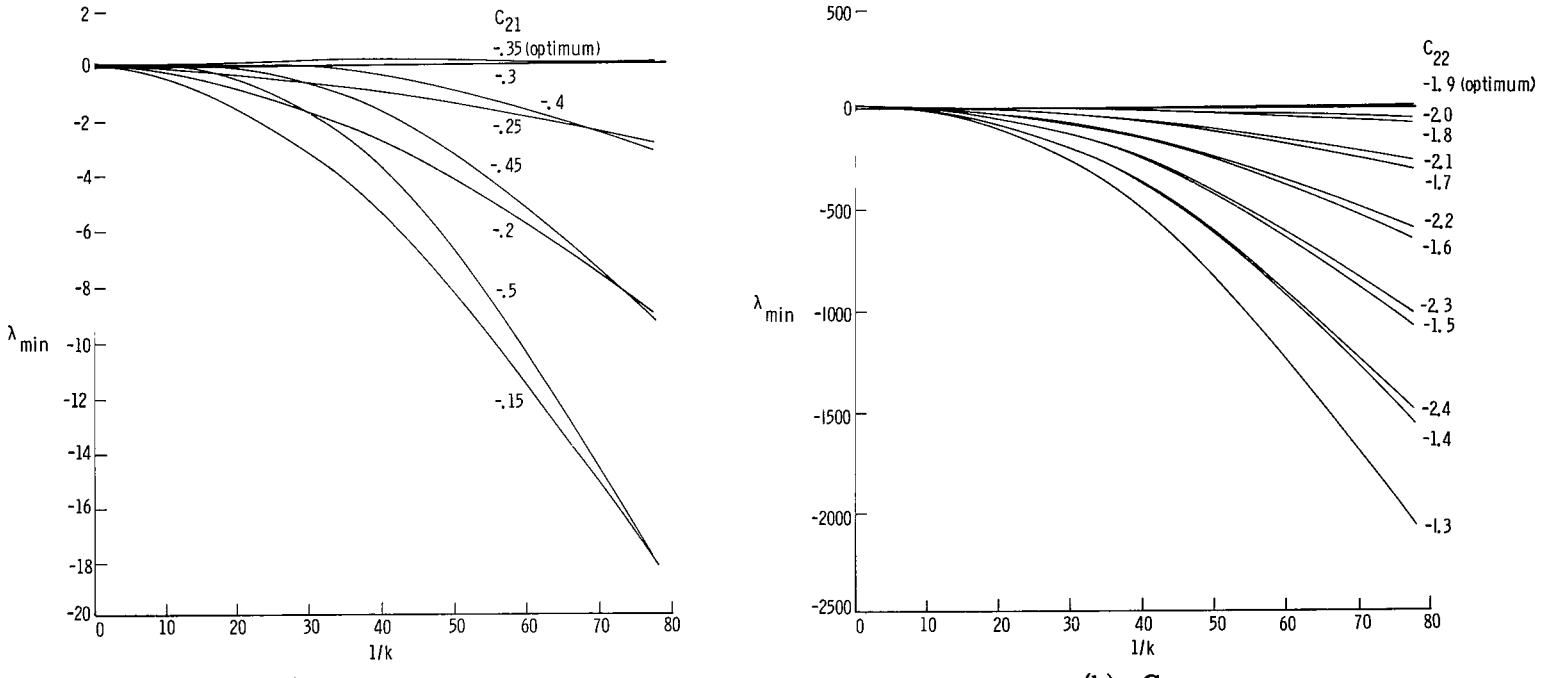

(a) C_{21}.

(b) C_{22}.

Figure 2.- The effects on λ_{min} of variation of T.E. control system parameters around their optimum values.

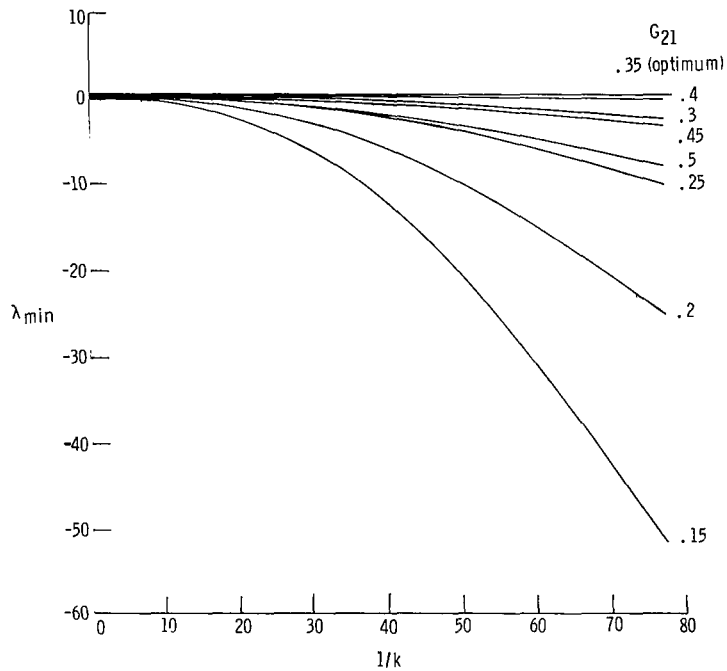

(c) G_{21}.

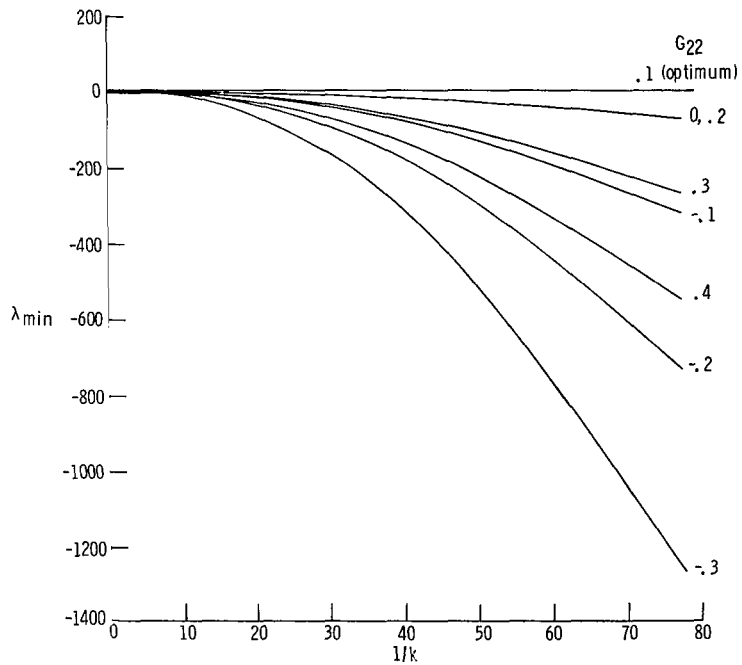

(d) G_{22}.

Figure 2.- Concluded.

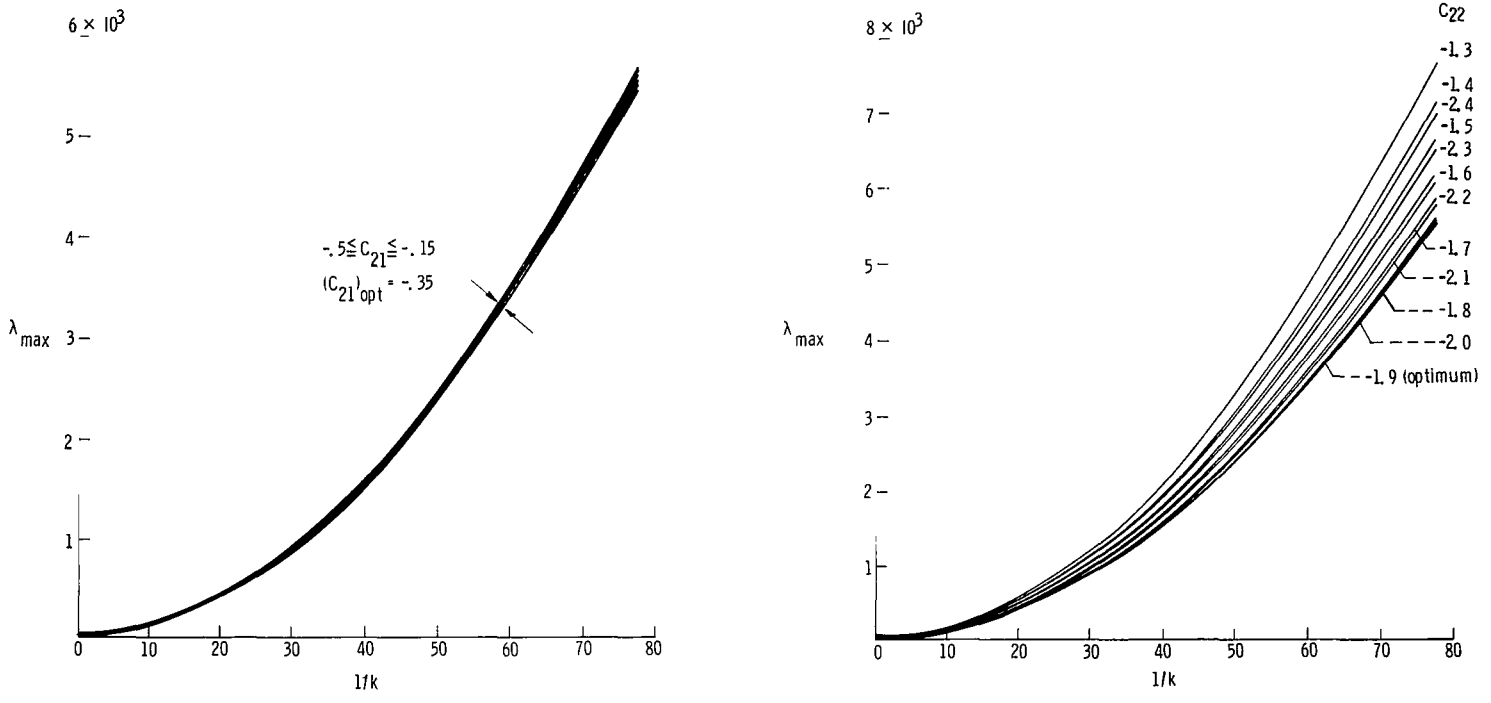

(a) C_{21}.

(b) C_{22}.

Figure 3.- The effects on λ_{max} of variation of the T.E. control system parameters around their optimum values.

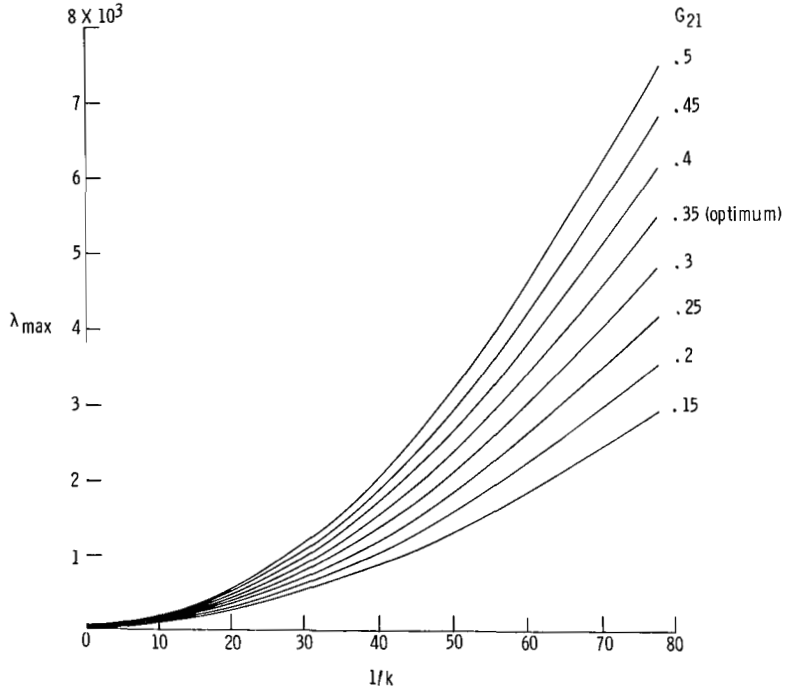

(c) G_{21}.

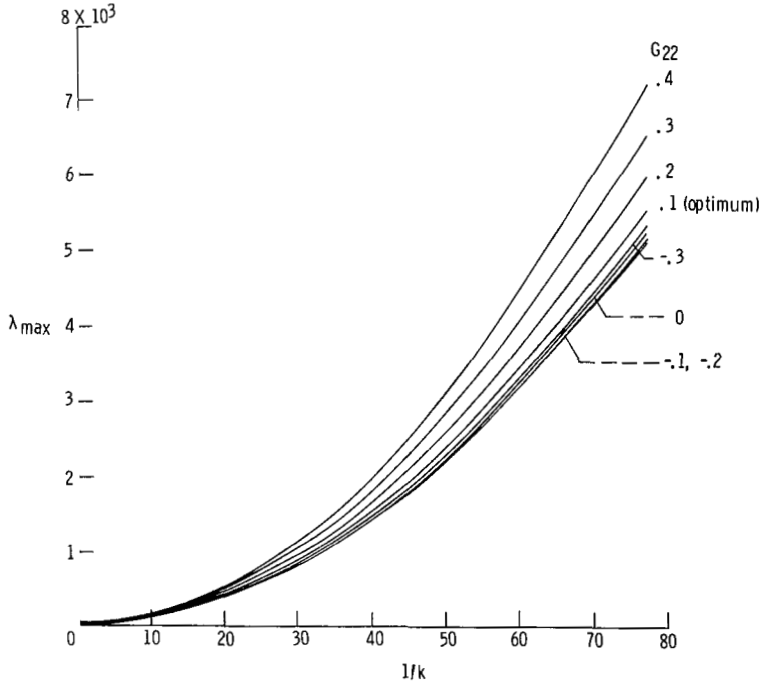

(d) G_{22}.

Figure 3.- Concluded.

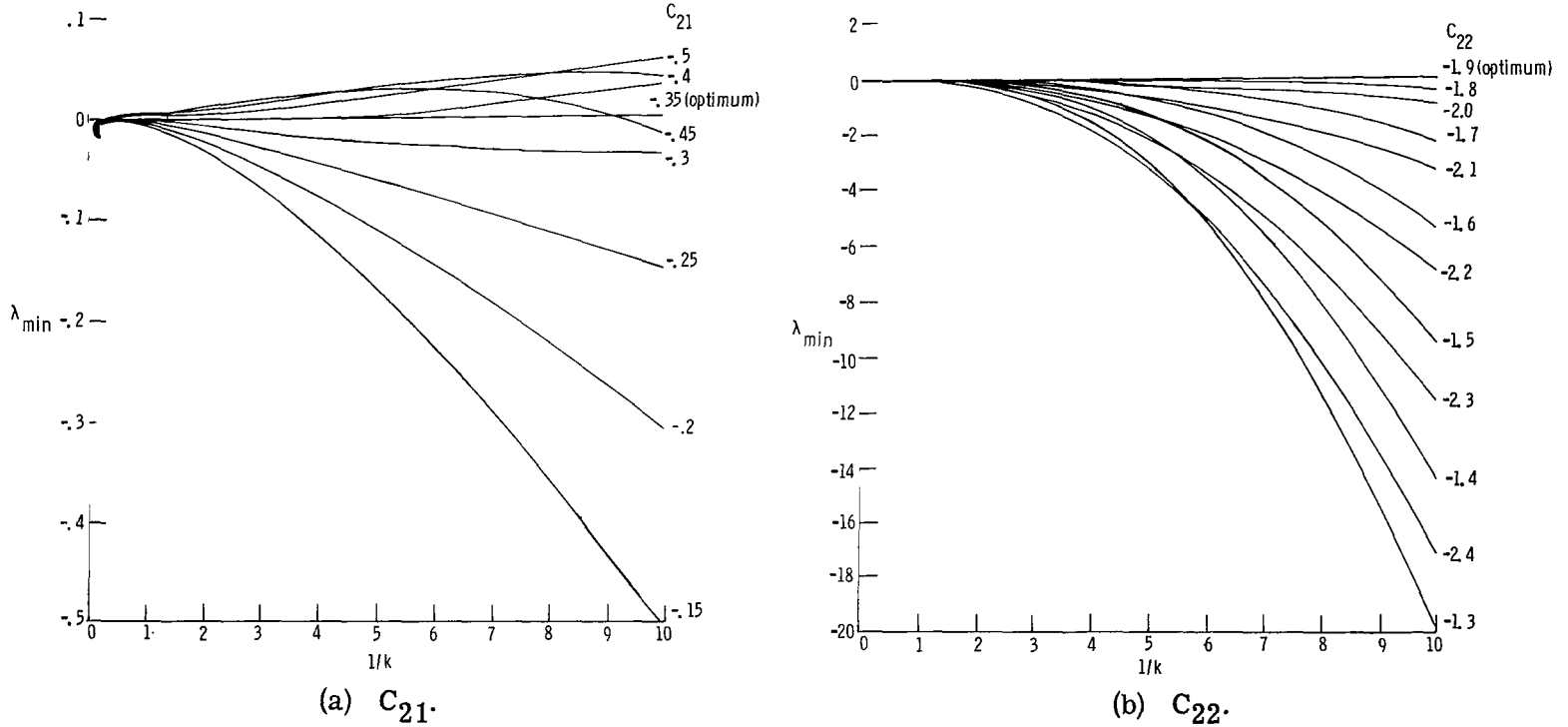

(a) C_{21}.

(b) C_{22}.

Figure 4.- The effects on λ_{min} of variation of the T.E. control system parameters around their optimum values.

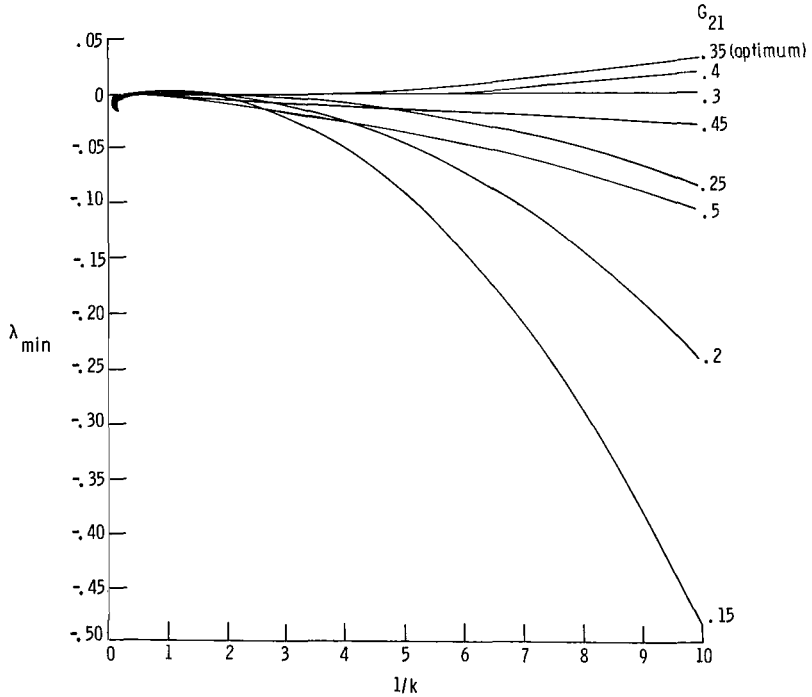

(c) G_{21}.

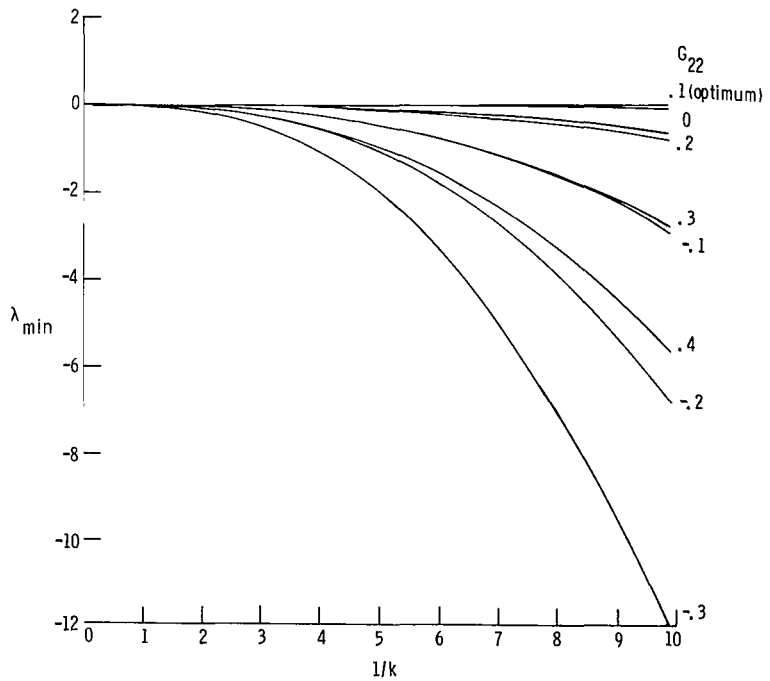

(d) G_{22}.

Figure 4.- Concluded.

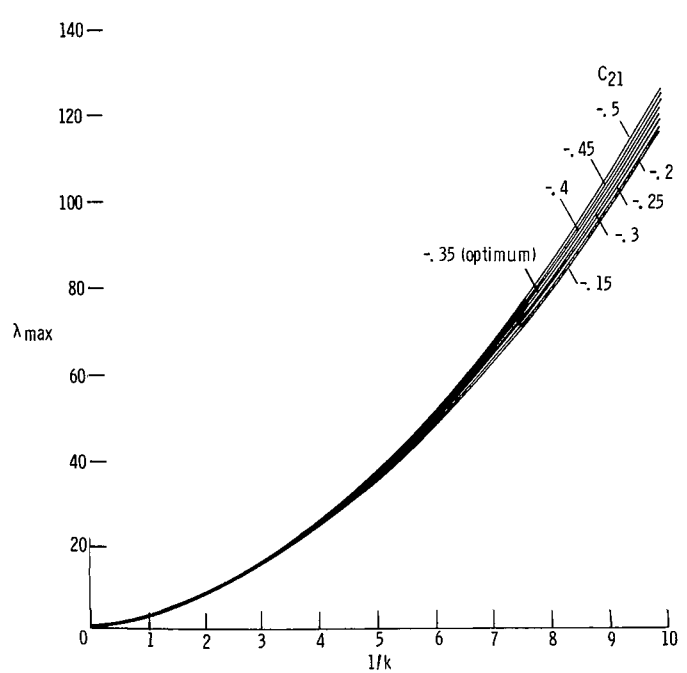

(a) C_{21}.

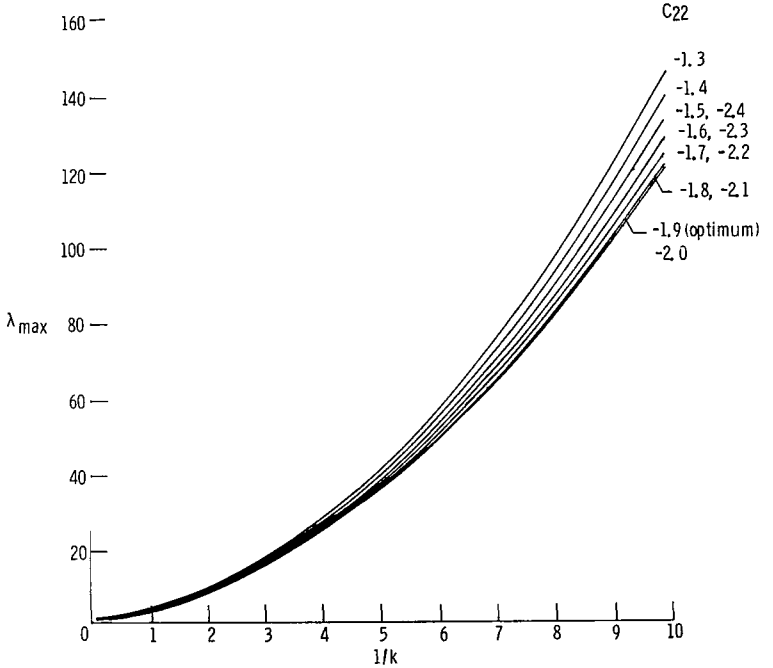

(b) C_{22}.

Figure 5.- The effects on λ_{max} of variation of the T.E. control system parameters about their optimum values.

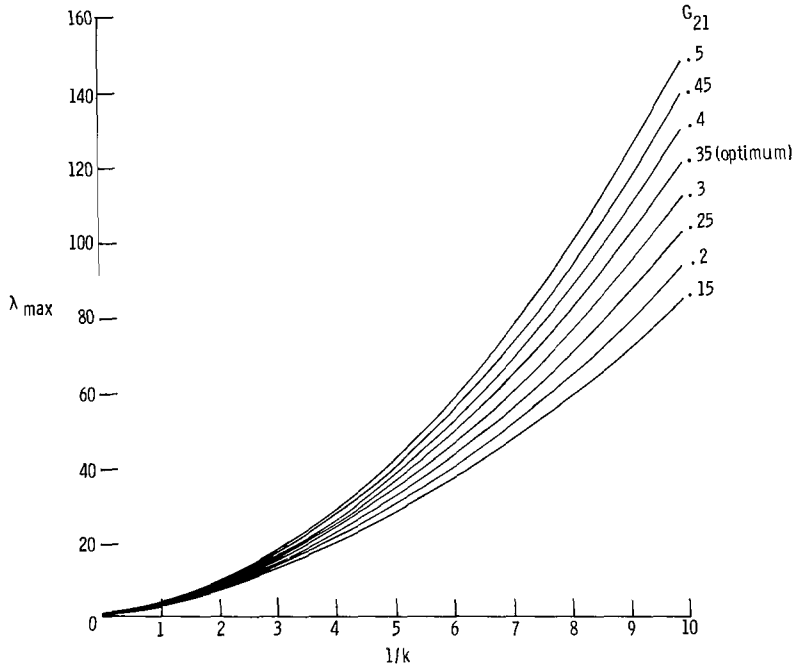

(c) G_{21}.

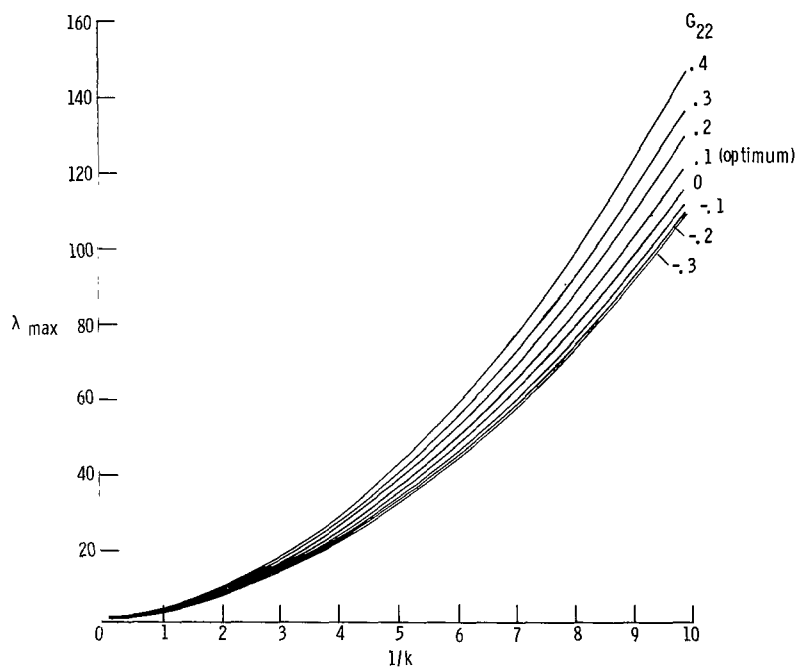

(d) G_{22}.

Figure 5.- Concluded.

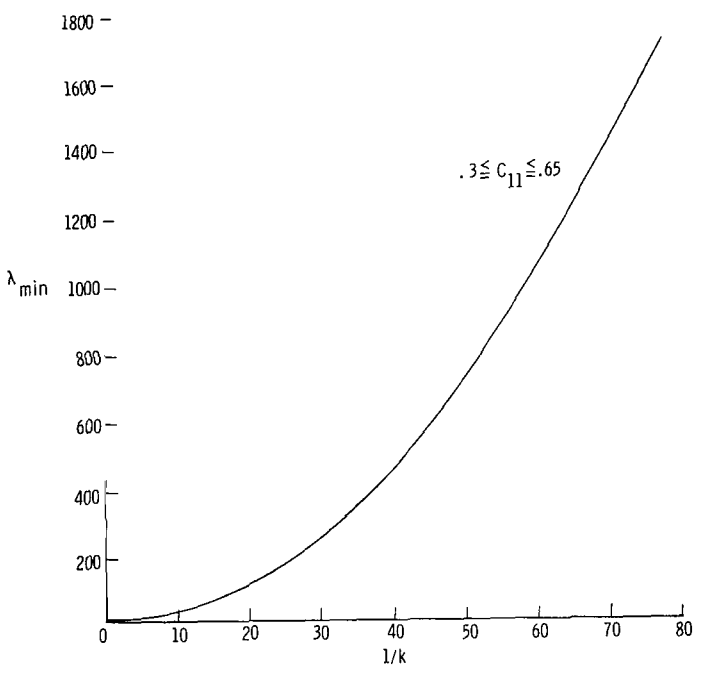

(a) C_{11}.

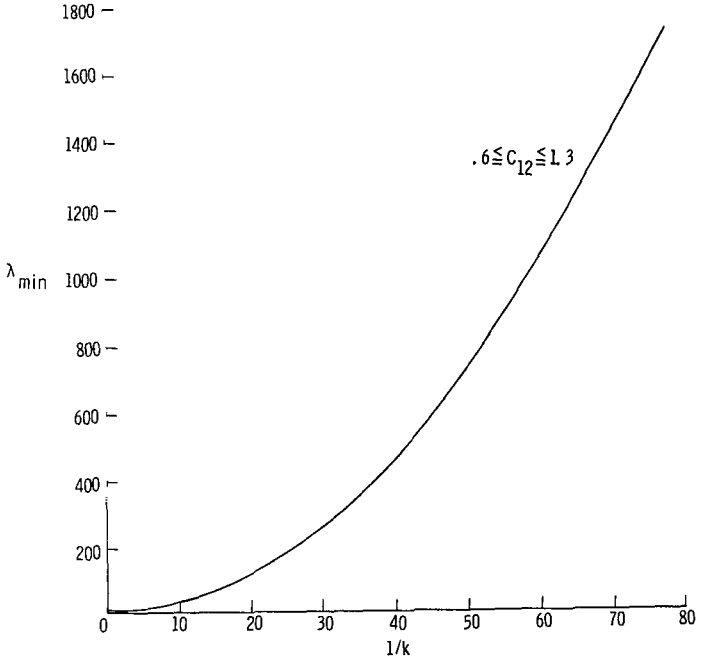

(b) C_{12}.

Figure 6.- The effects on λ_{min} of variation of the L.E.-T.E. control system parameters around their optimum values.

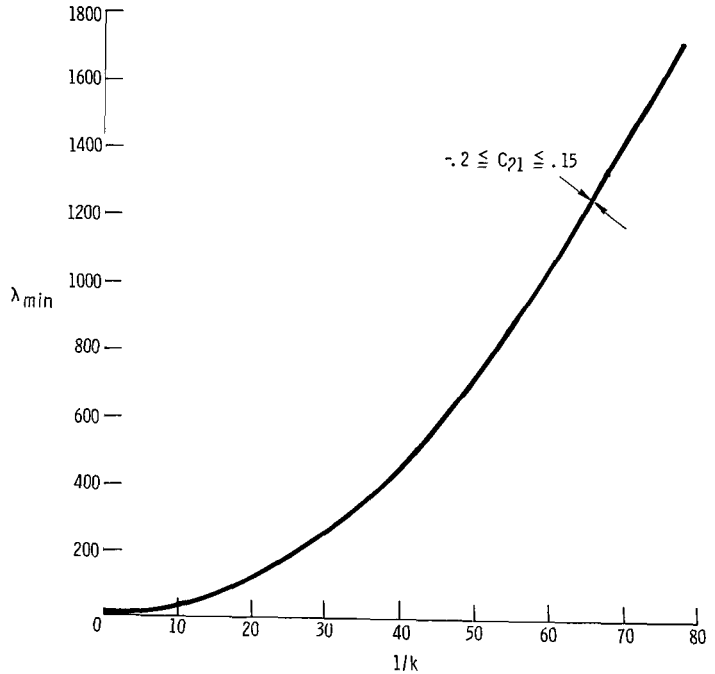

(c) C_{21}.

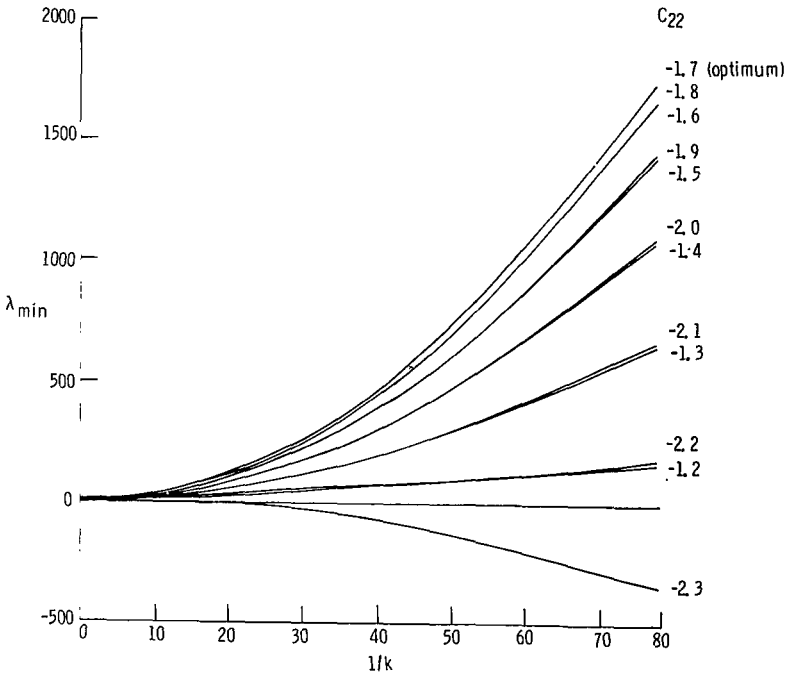

(d) C_{22}.

Figure 6.- Continued.

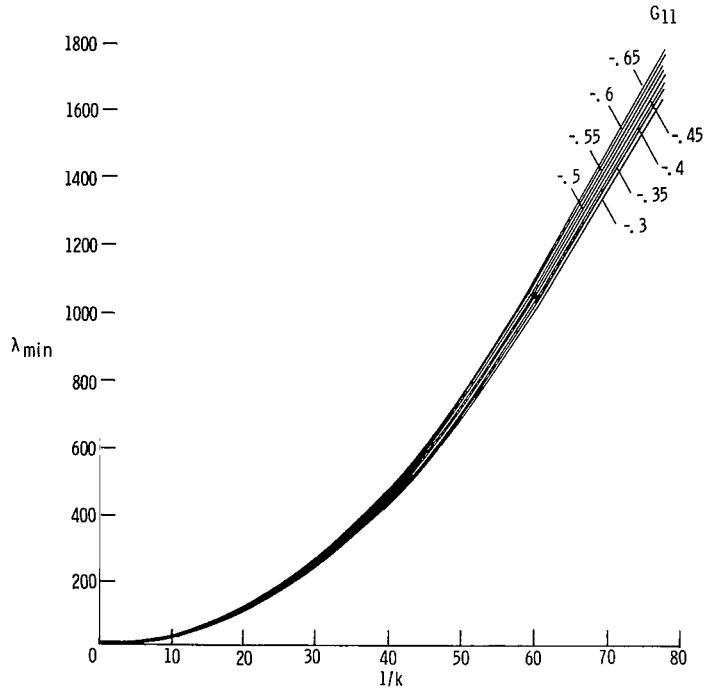

(e) G_{11}.

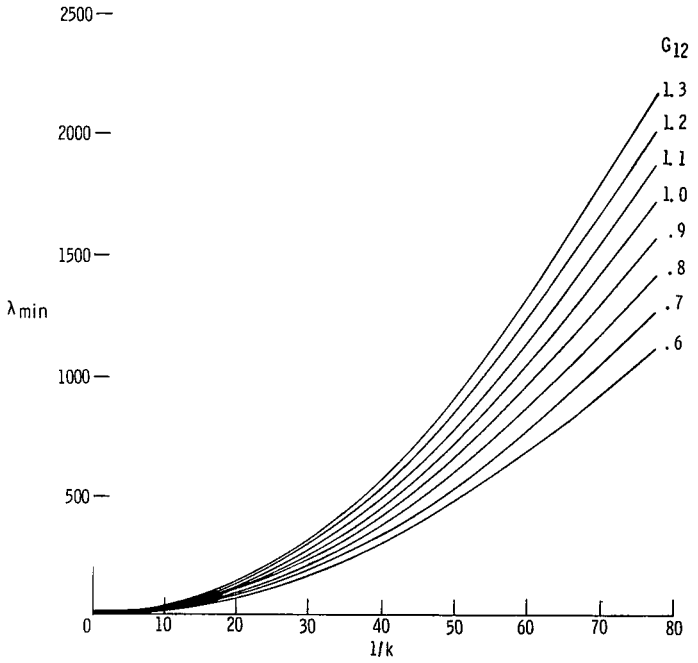

(f) G_{12}.

Figure 6.- Continued.

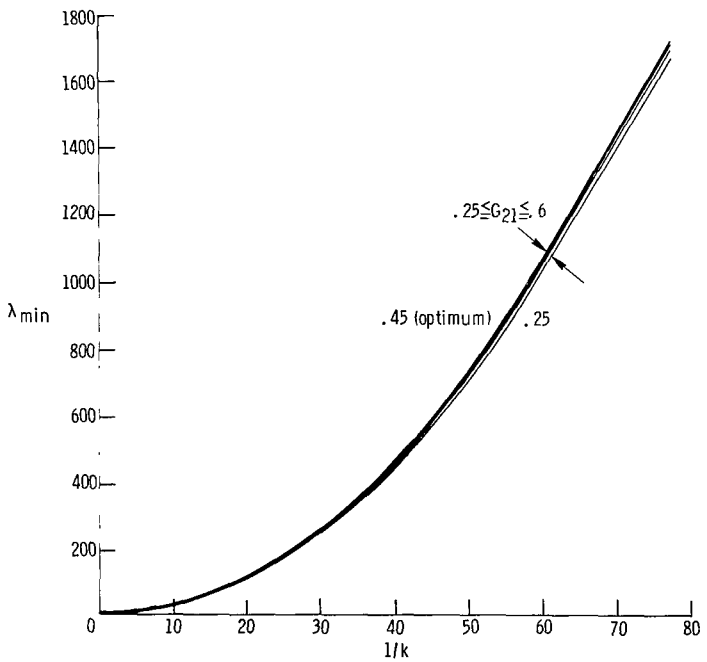

(g) G_{21}.

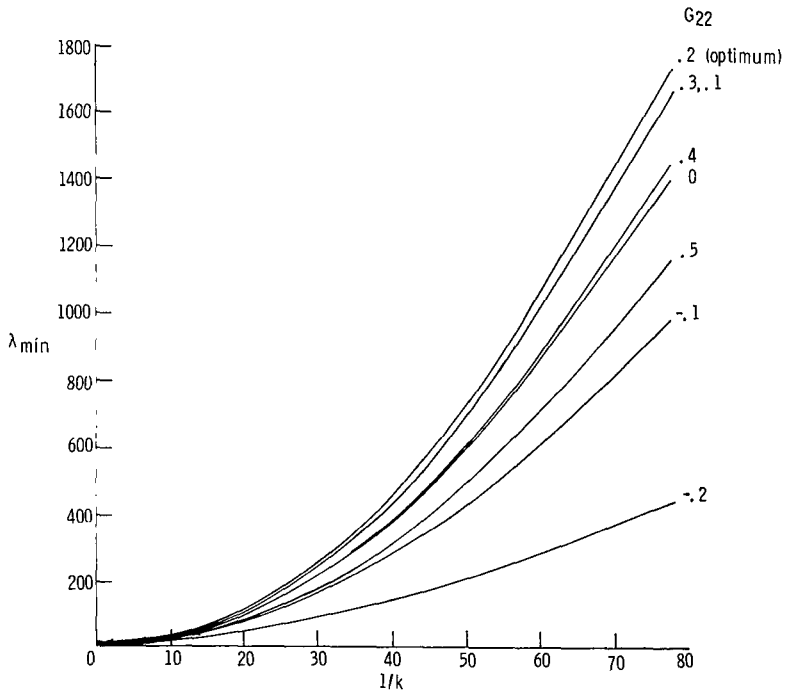

(h) G_{22}.

Figure 6.- Concluded.

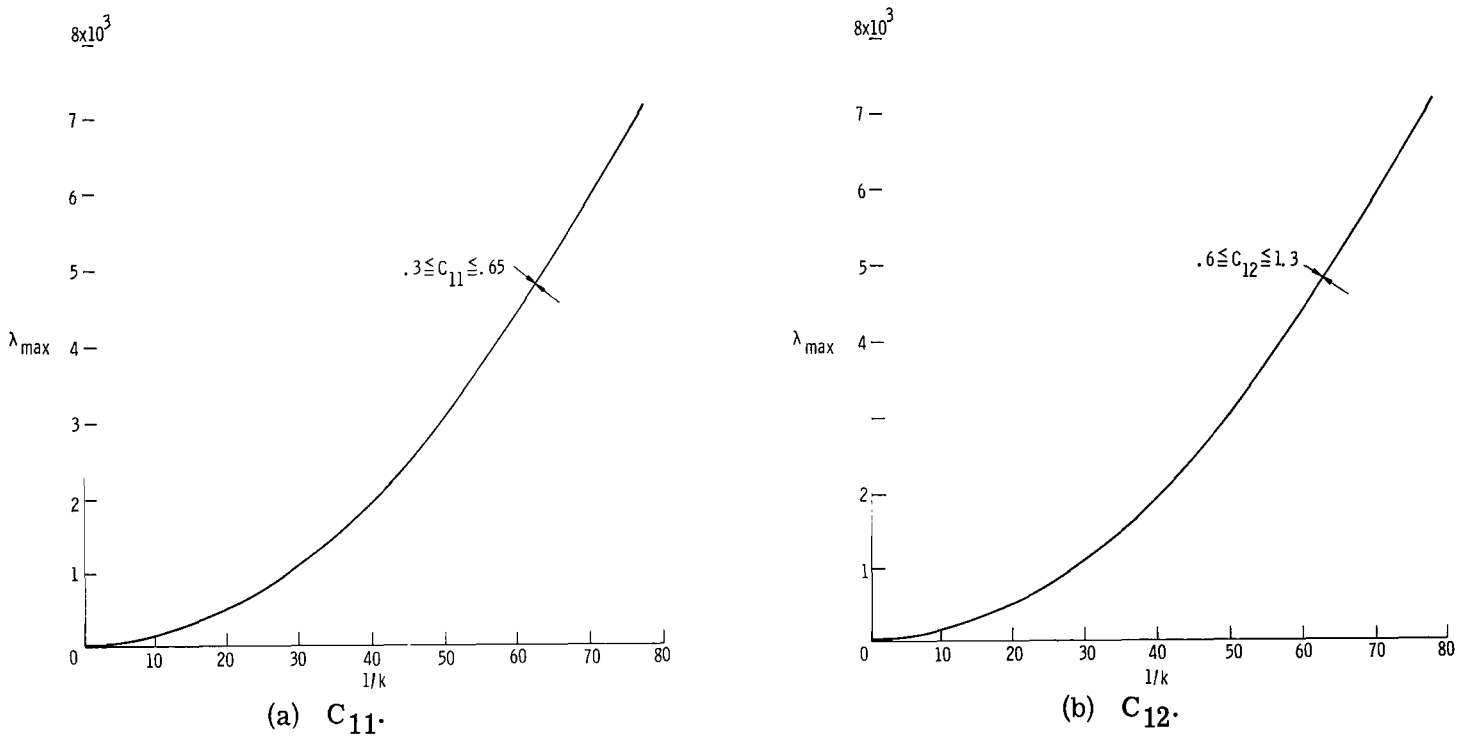

(a) C_{11}.

(b) C_{12}.

Figure 7.- The effects on λ_{max} of variation of the L.E.-T.E. control system parameters around their optimum values.

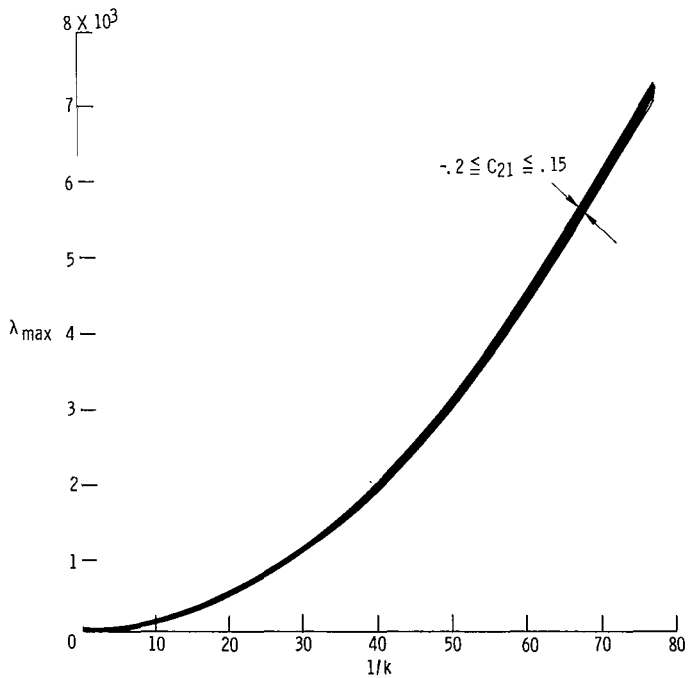

(c) C_{21}.

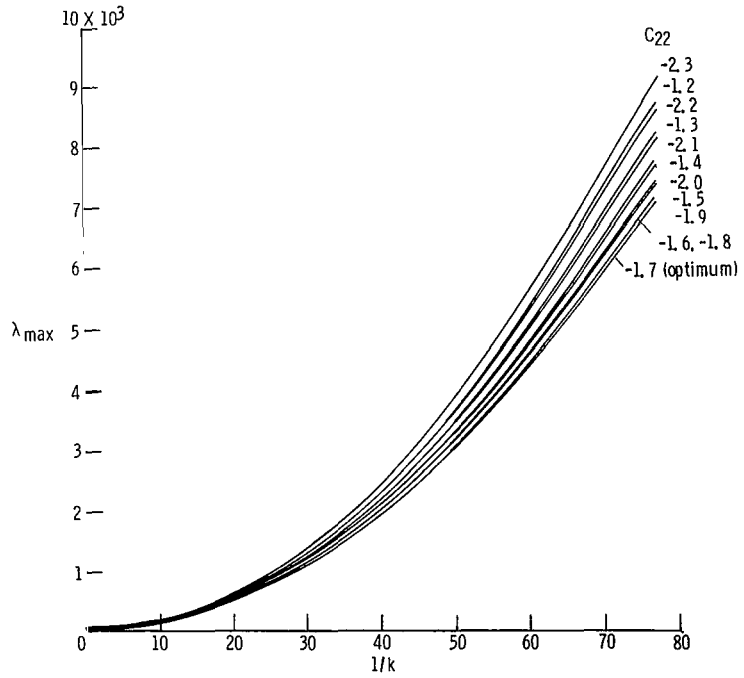

(d) C_{22}.

Figure 7.- Continued.

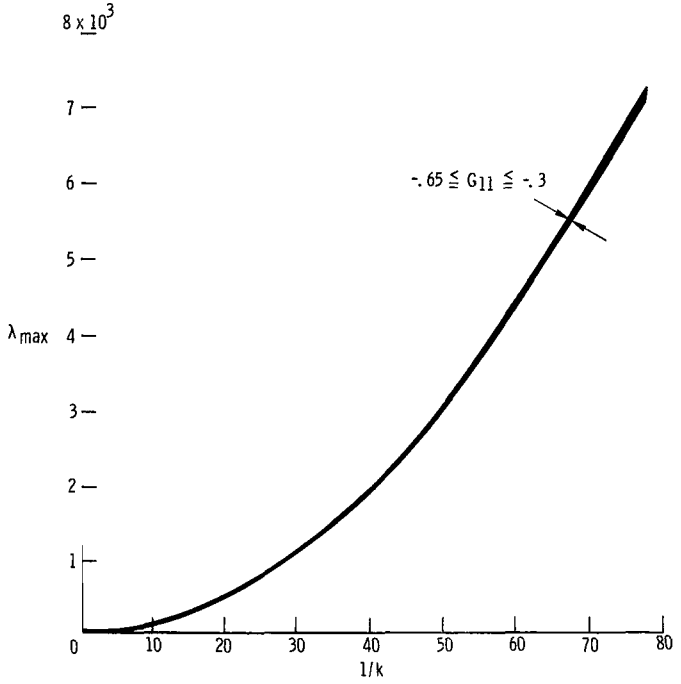

(e) G_{11}.

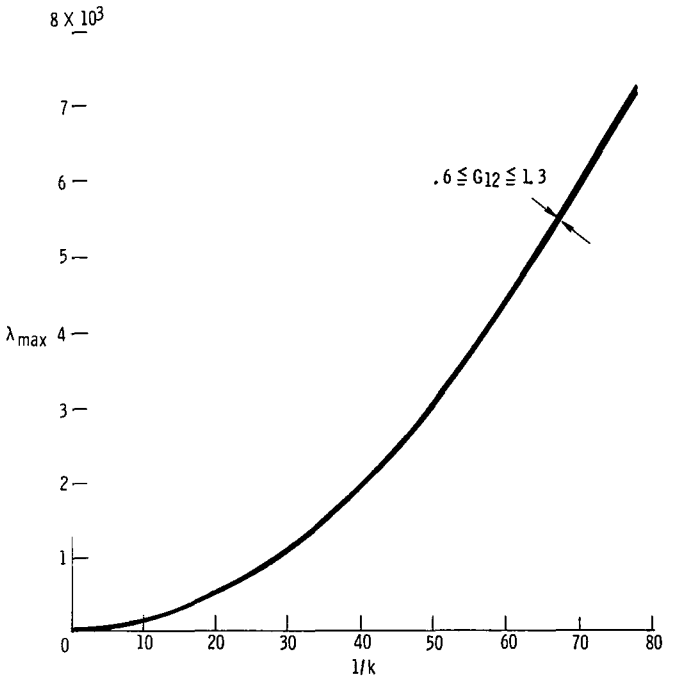

(f) G_{12}.

Figure 7.- Continued.

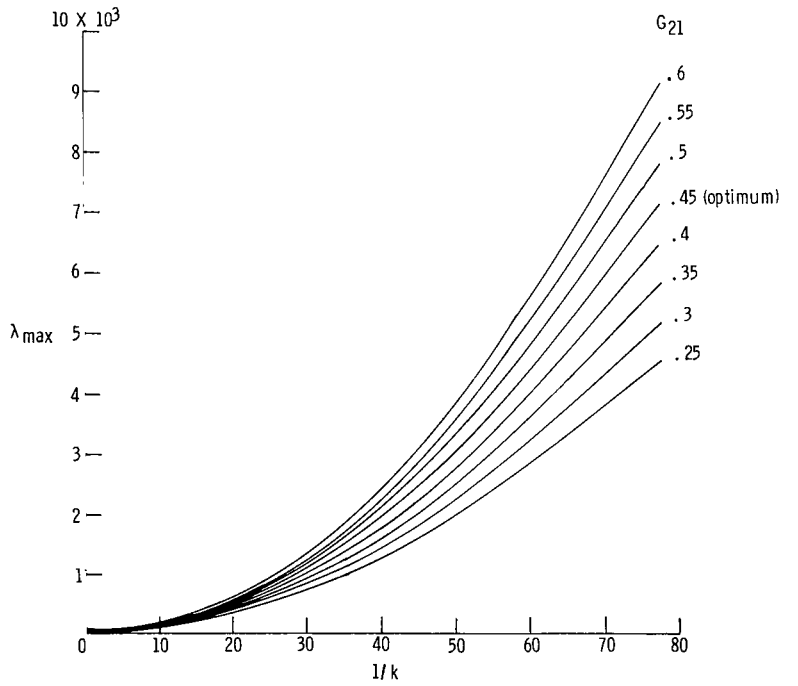

(g) G_{21}.

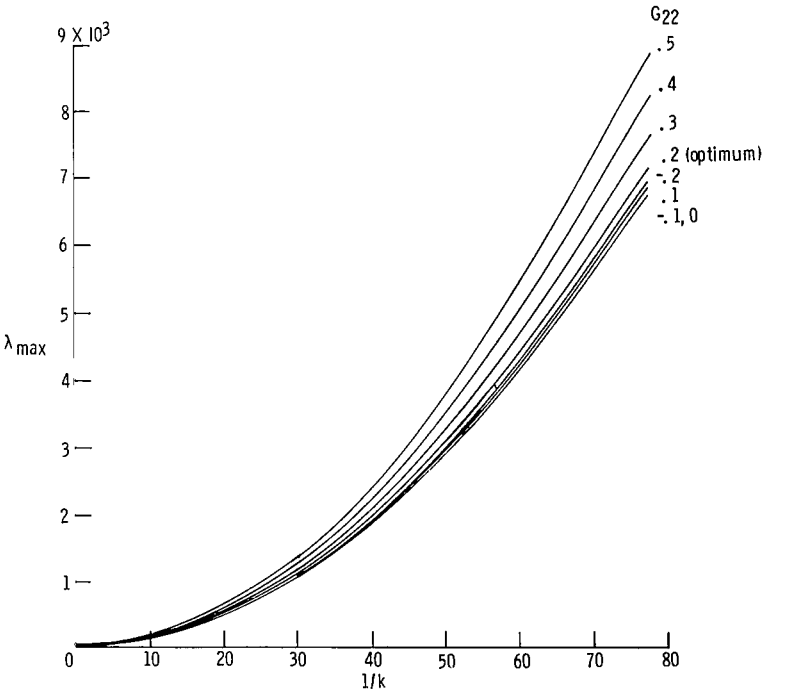

(h) G_{22}.

Figure 7.- Concluded.

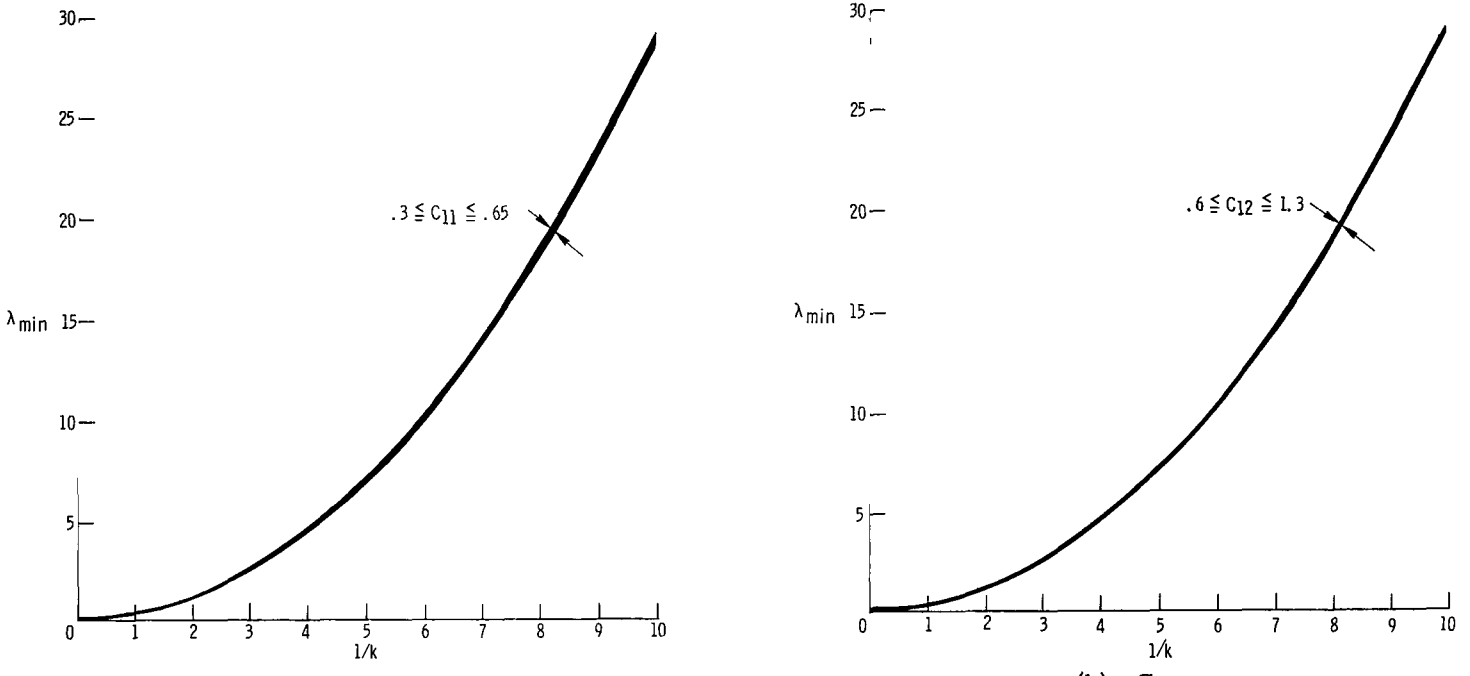

Figure 8.- The effects on λ_{min} of variation of the L.E.-T.E. control system parameters around their optimum values.

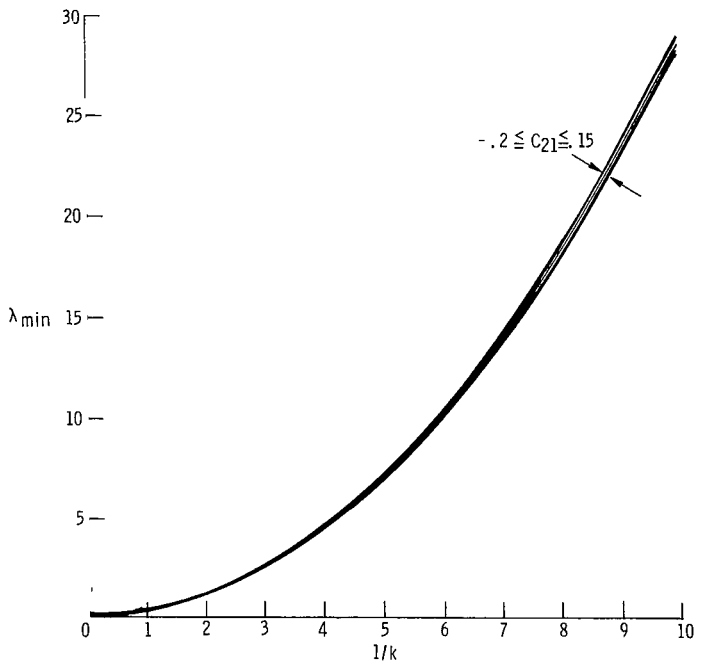

(c) C_{21}.

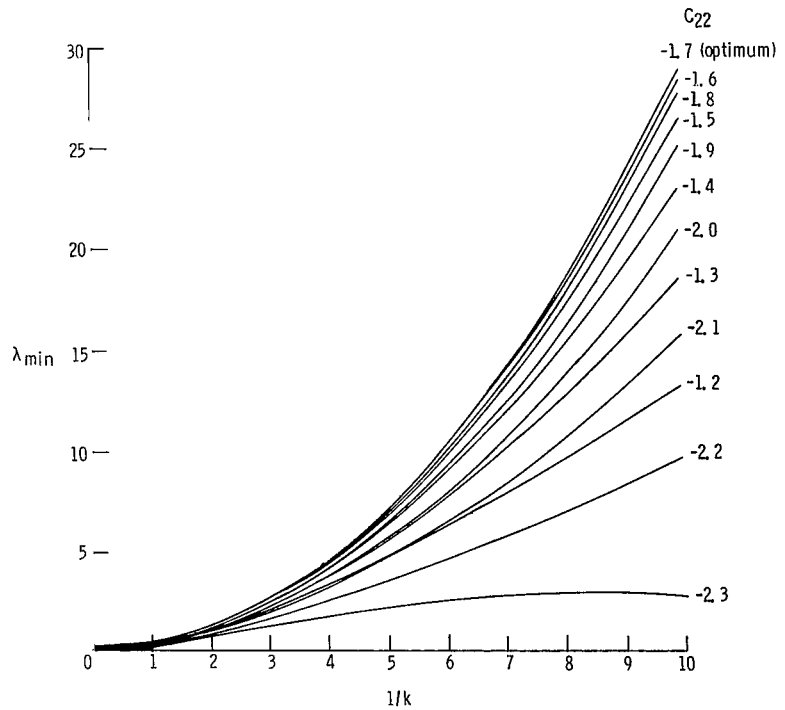

(d) C_{22}.

Figure 8.- Continued.

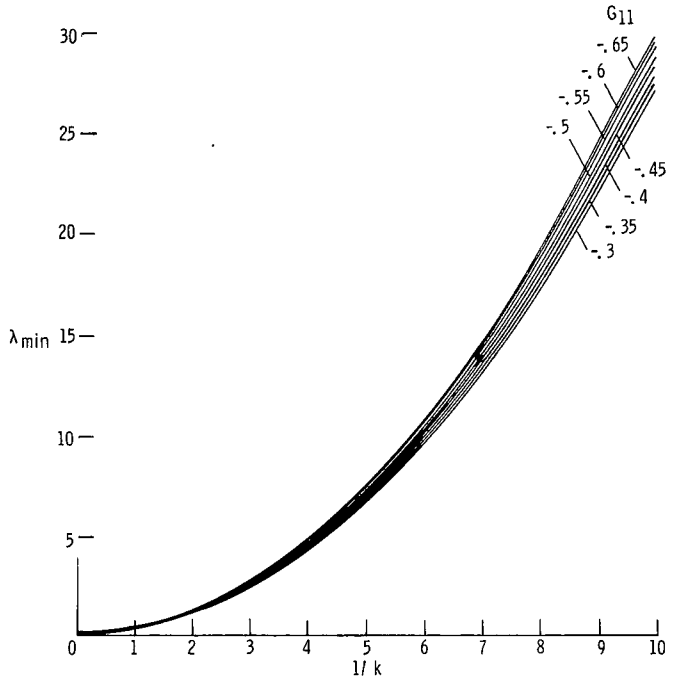

(e) G_{11}.

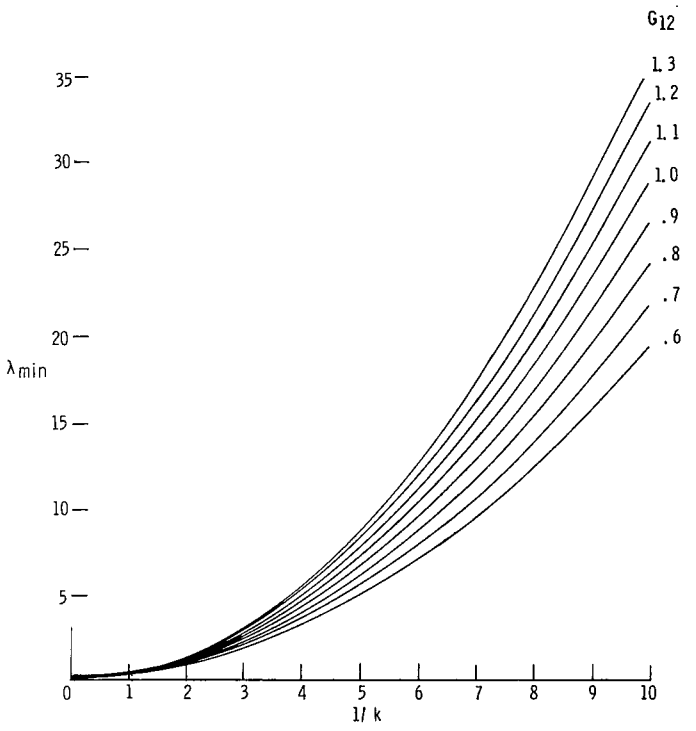

(f) G_{12}.

Figure 8.- Continued.

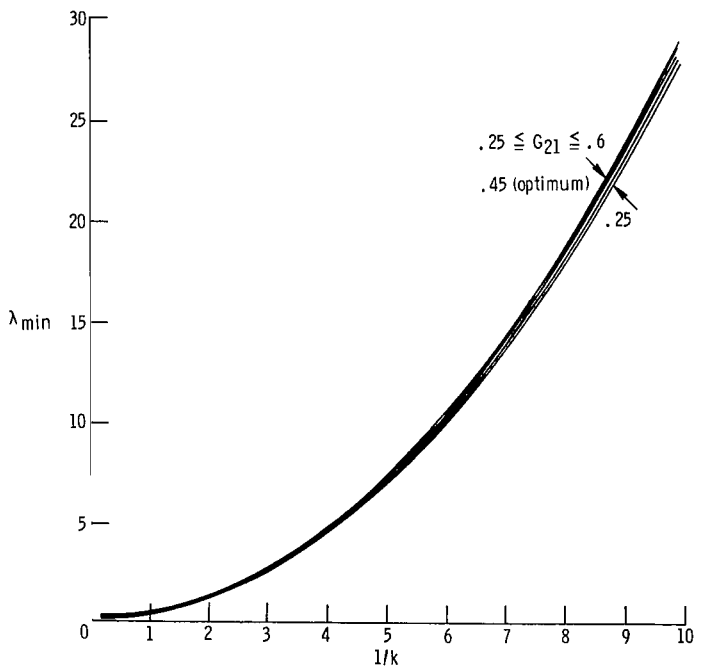

(g) G_{21}.

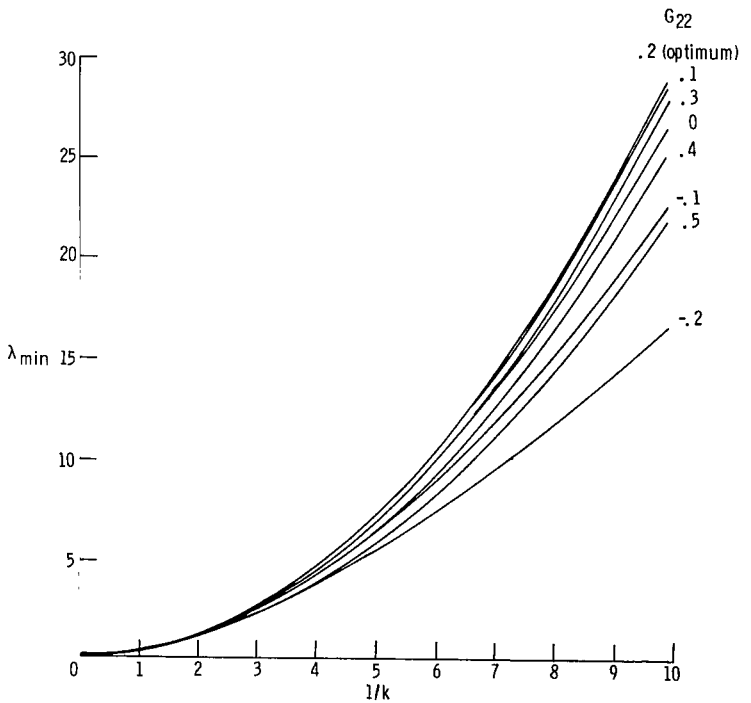

(h) G_{22}.

Figure 8.- Concluded.

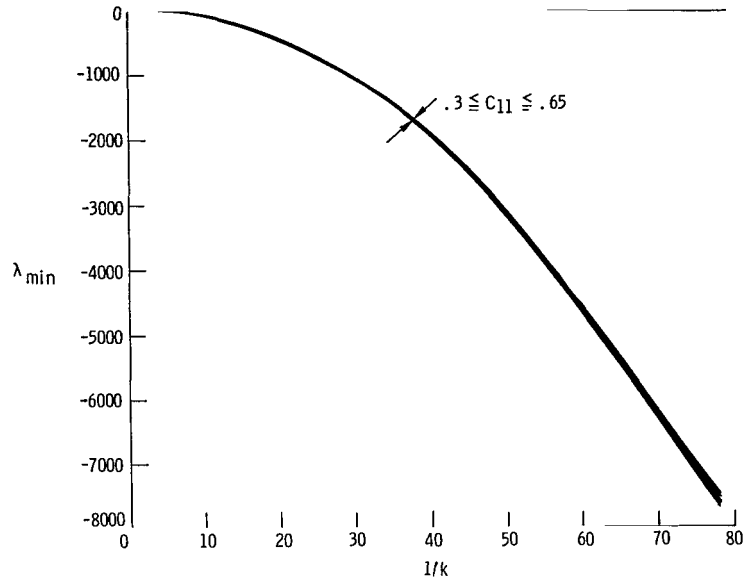

Figure 9.- The effects on λ_{min} of variation of C_{11} around the optimum of the L.E.-T.E. system $(C_{12} = C_{22} = G_{12} = G_{22} = 0)$ driven by a linear sensor only.

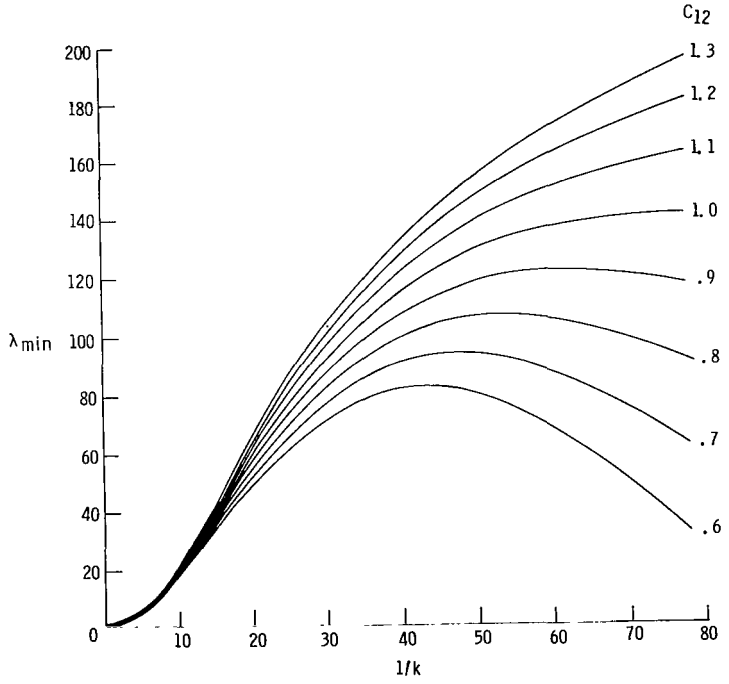

Figure 10.- The effects on λ_{min} of variation of C_{12} around the optimum of the L.E.-T.E. system $(C_{11} = C_{21} = G_{11} = G_{21} = 0)$ driven by a rotational sensor only.

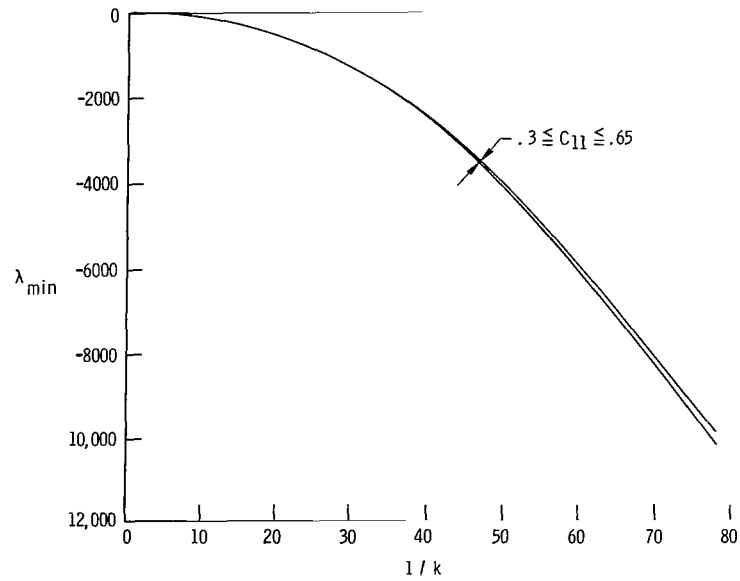

Figure 11.- The effects on λ_{min} of variation of C_{11} around the optimum of the L.E. system.

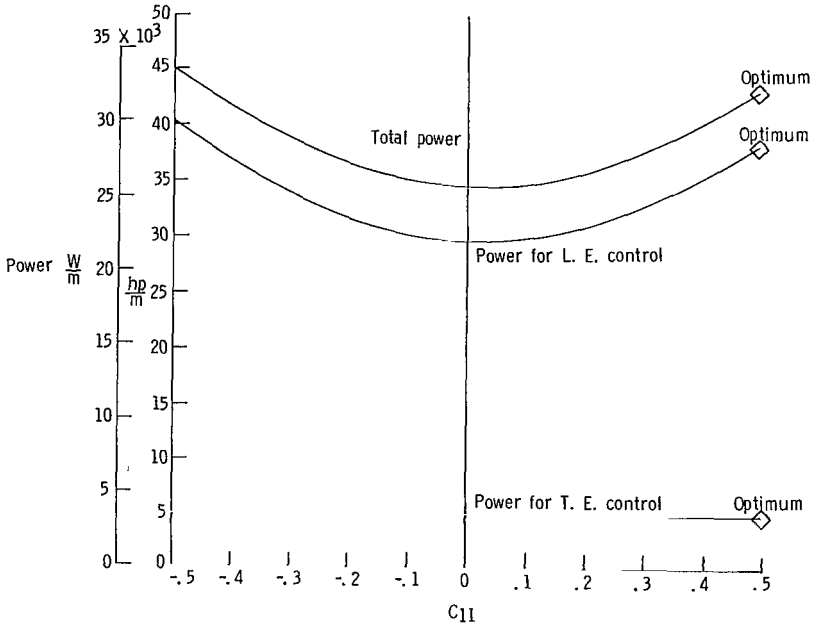

(a) C_{11}.

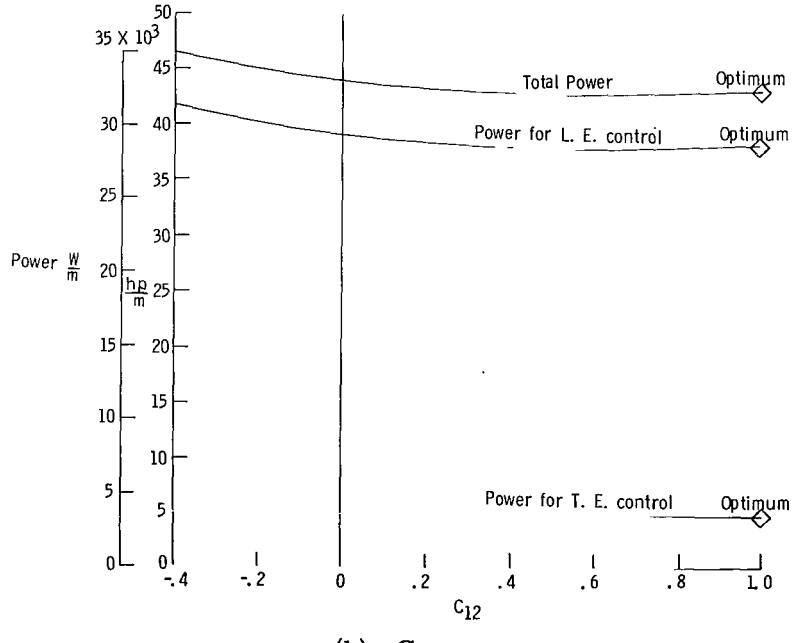

(b) C_{12}.

Figure 12.- The effects on the power requirement of variation of L.E.-T.E. control system parameters around their optimum values. k = 0.075; V = 243.84 m/sec.

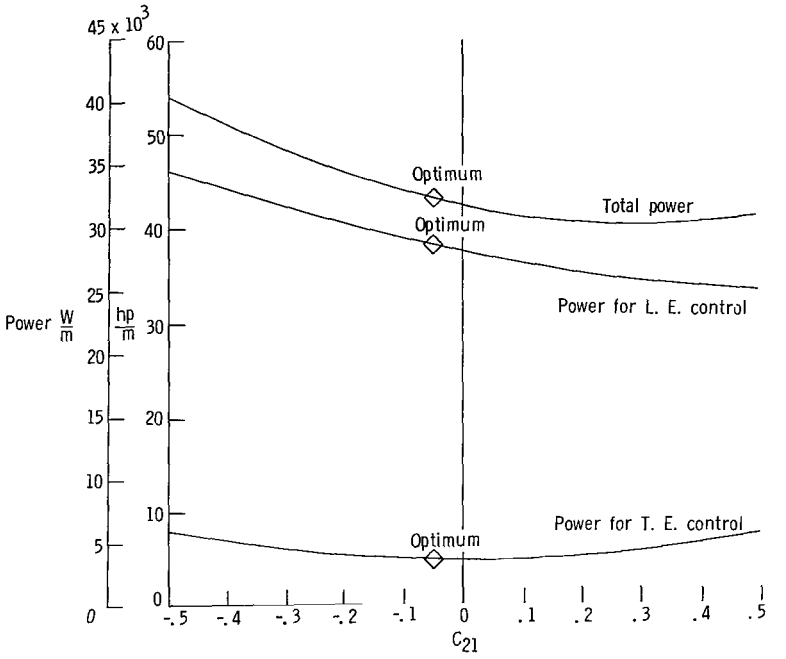

(c) C_{21}.

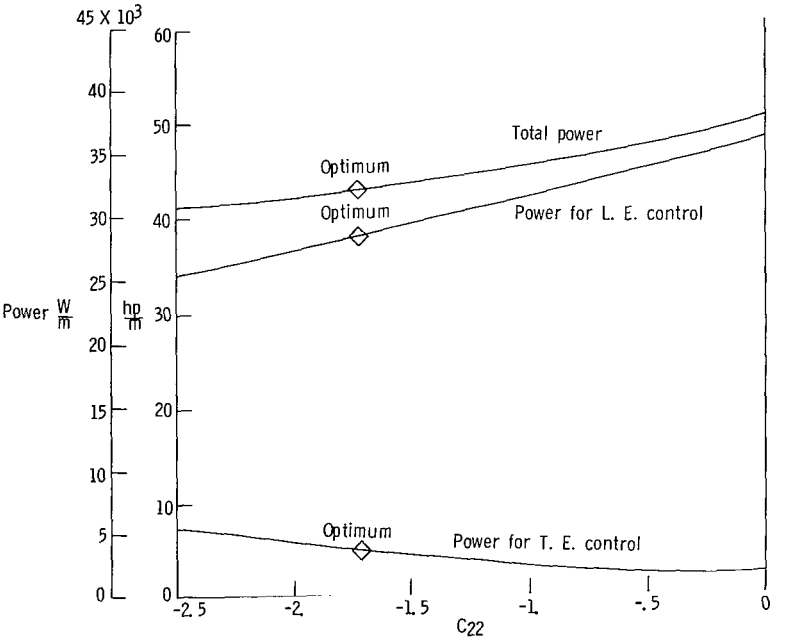

(d) C_{22}.

Figure 12.- Continued.

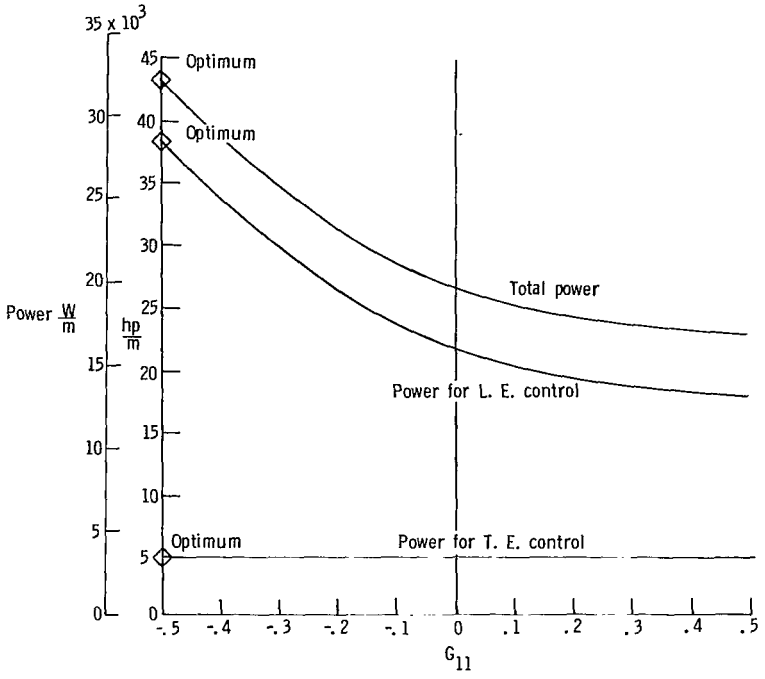

(e) G_{11}.

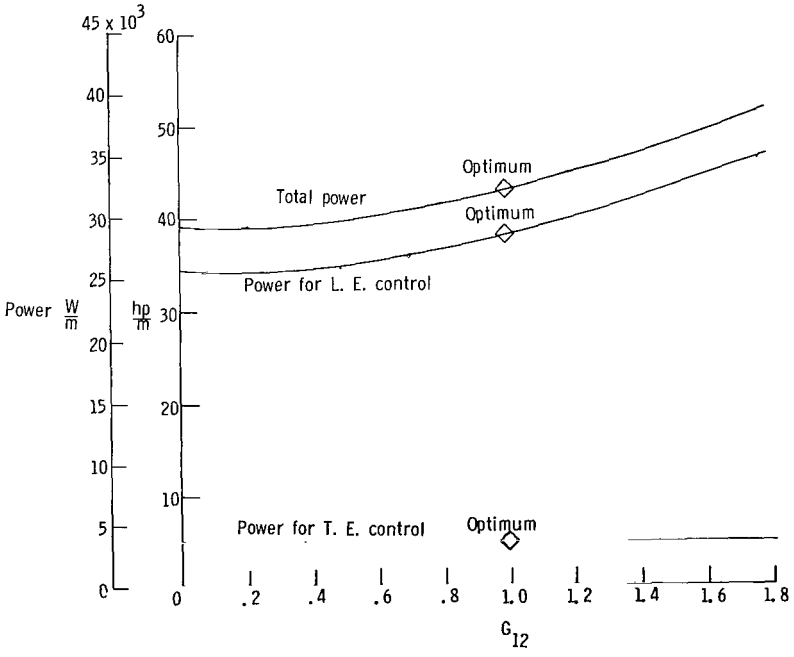

(f) G_{12}.

Figure 12.- Continued.

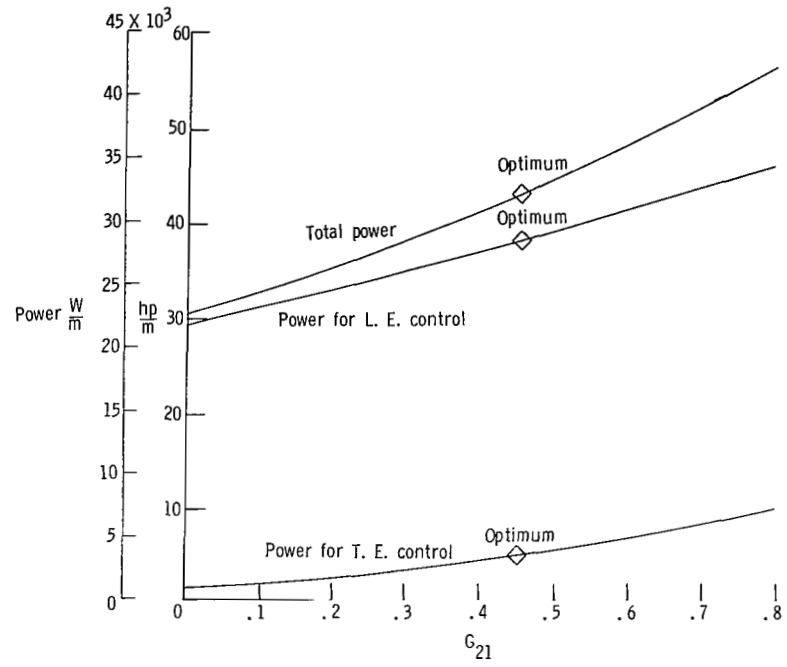

(g) G_{21}.

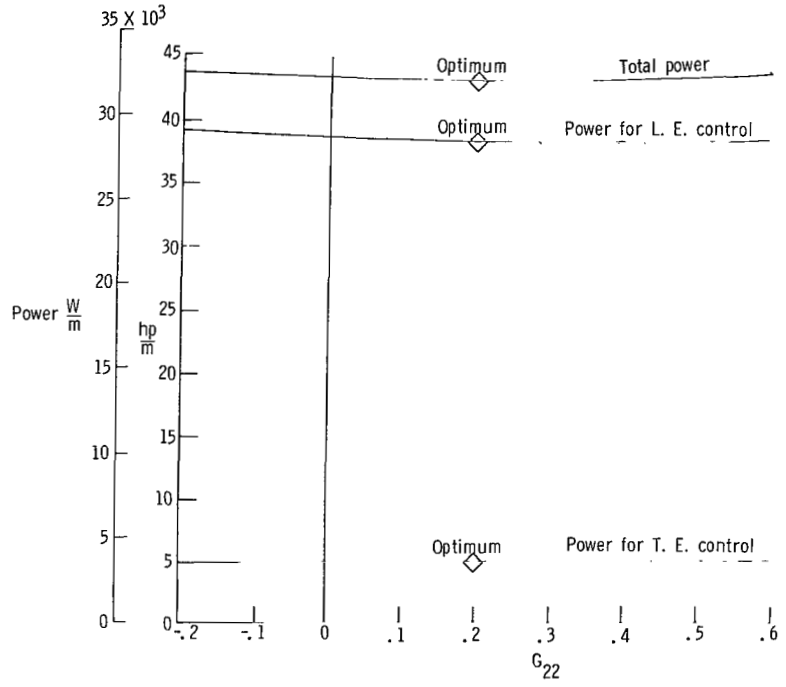

(h) G_{22}.

Figure 12.- Concluded.

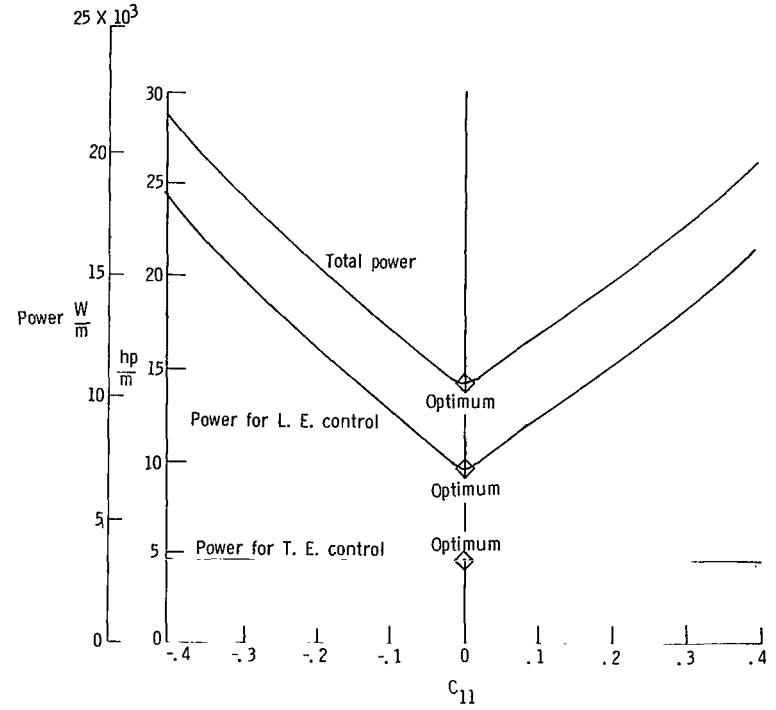

(a) C_{11}.

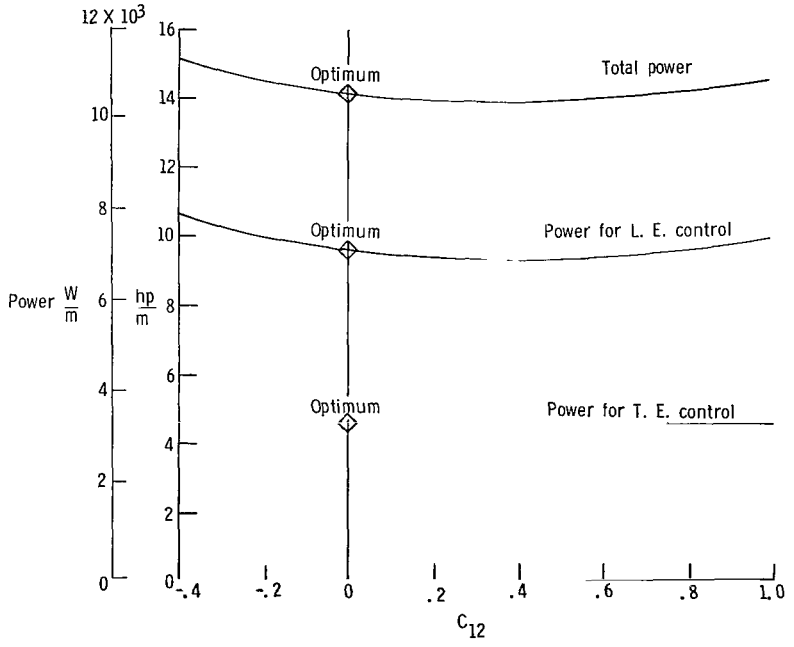

(b) C_{12}.

Figure 13.- The effects on the power requirements of variation of the L.E.-T.E. control system parameters around their optimum values. k = 0.075; V = 243.84 m/sec.

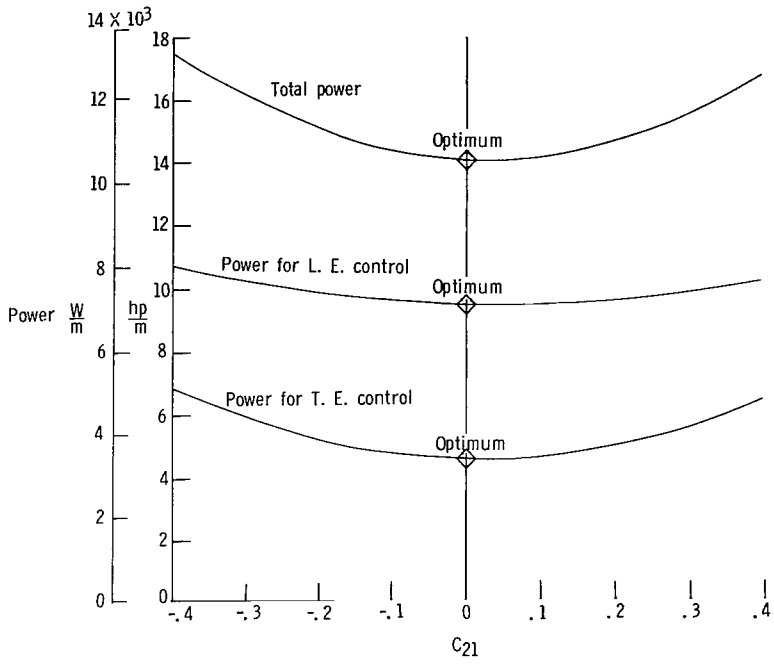

(c) C_{21}.

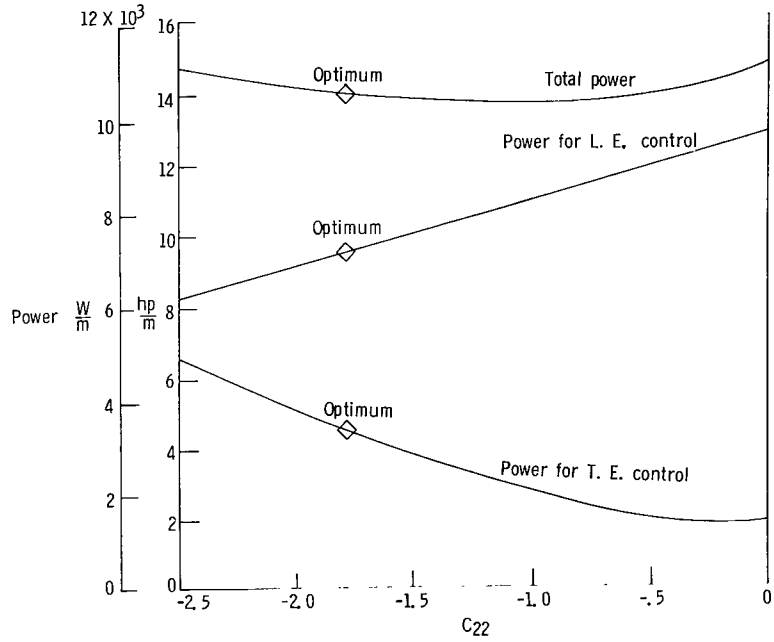

(d) C_{22}.

Figure 13.- Continued.

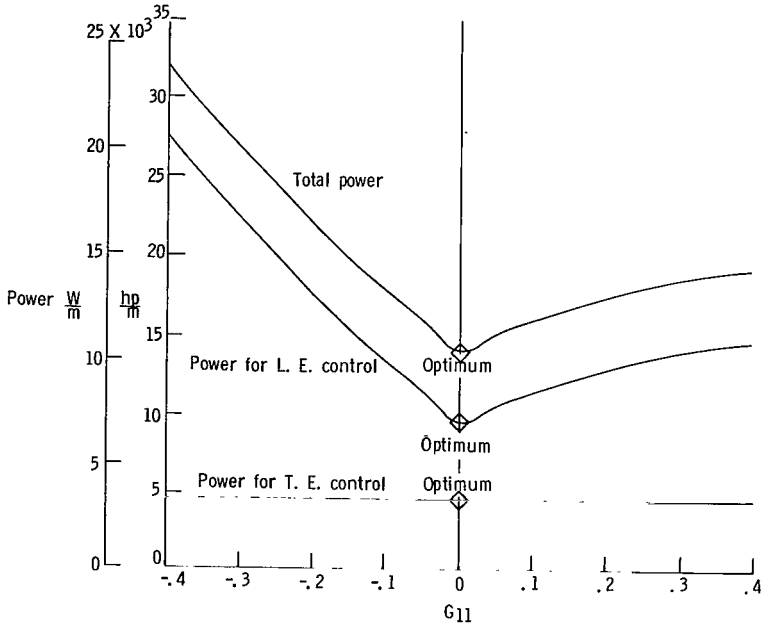

(e) G_{11}.

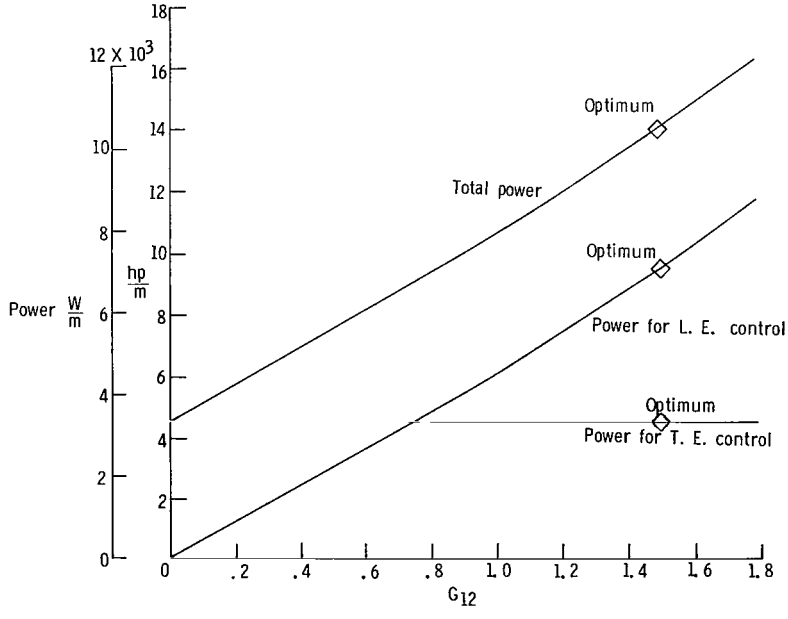

(f) G_{12}.

Figure 13.- Continued.

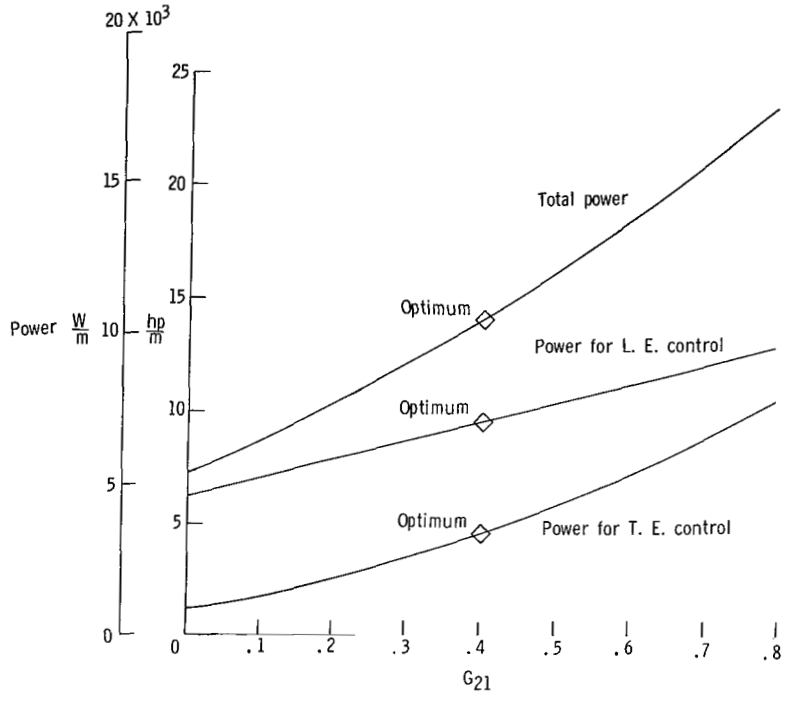

(g) G_{21}.

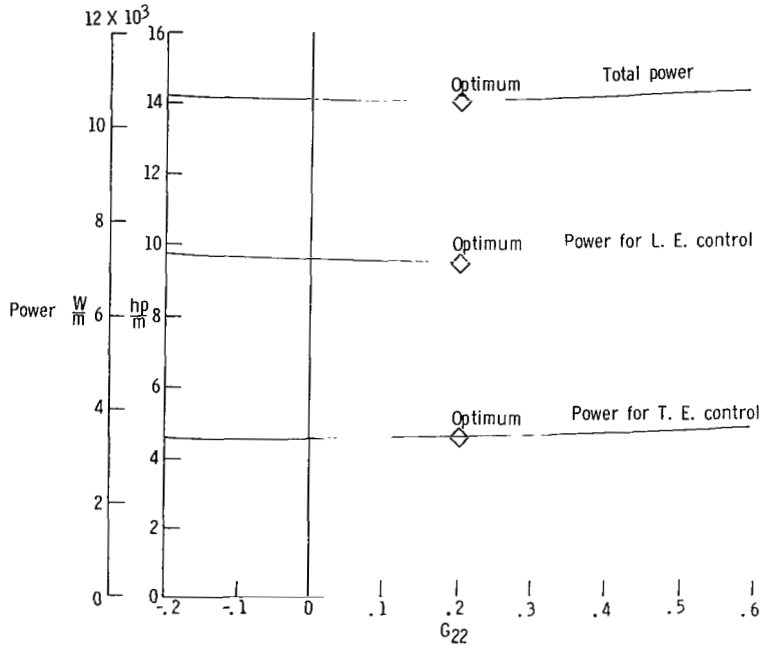

(h) G_{22}.

Figure 13.- Concluded.

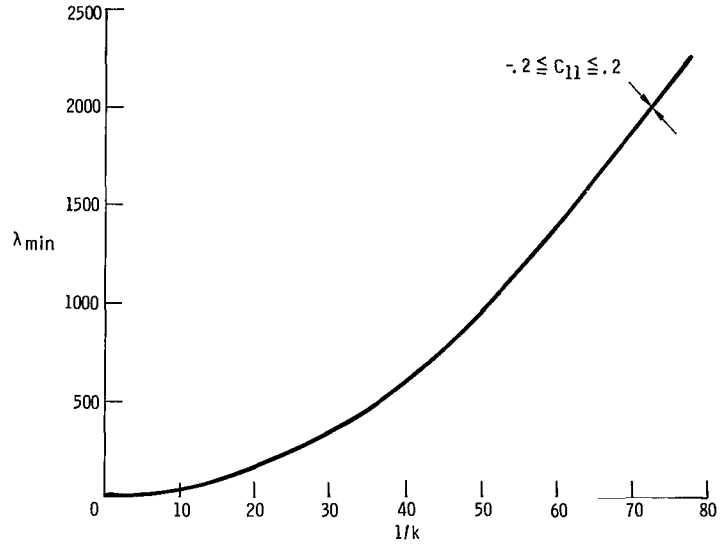

Figure 14.- The effects on λ_{min} of variation of C_{11} around optimum of L.E.-T.E. system (optimum with $C_{11} = C_{12} = C_{21} = G_{11} = 0$, $G_{21} = 0.4$).

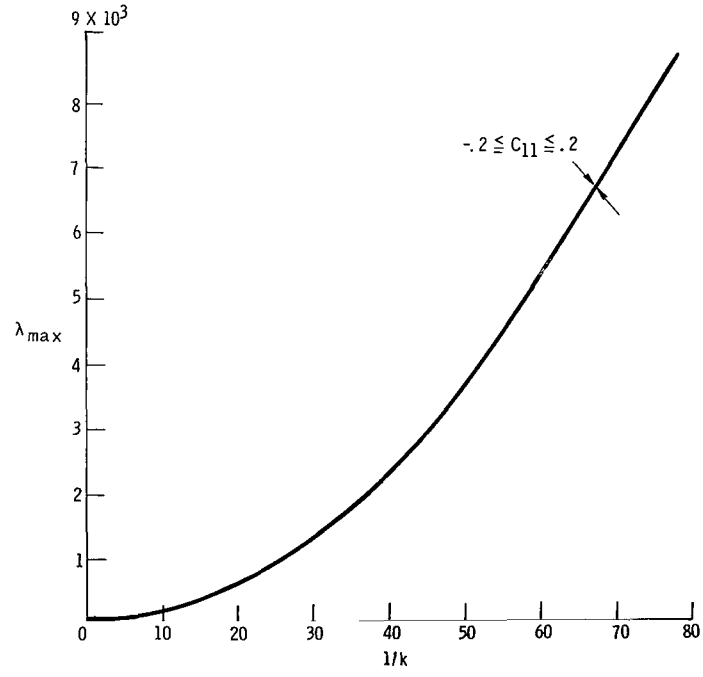

Figure 15.- The effects on λ_{max} of variation of C_{11} around optimum of L.E.-T.E. system (optimum with $C_{11} = C_{12} = C_{21} = G_{11} = 0$, $G_{21} = 0.4$).

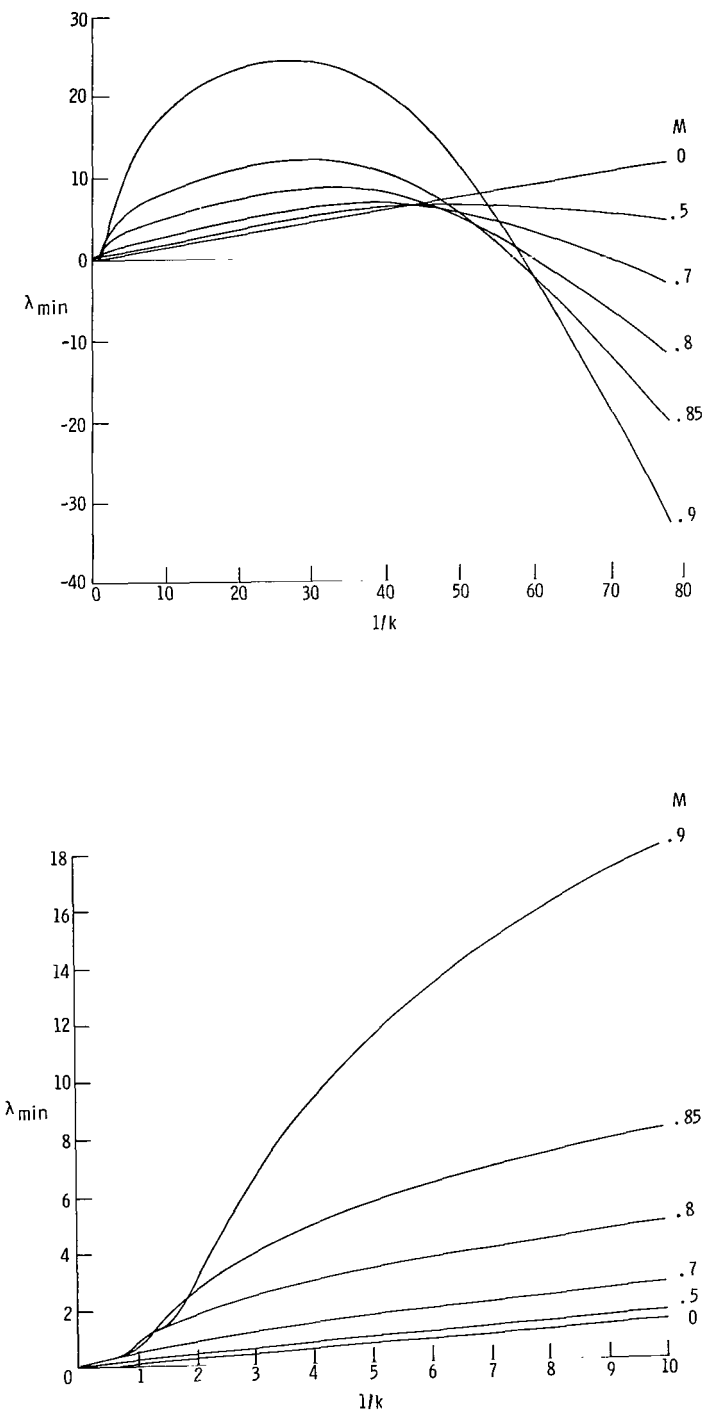

Figure 16.- Compressibility effects of the T.E. system.

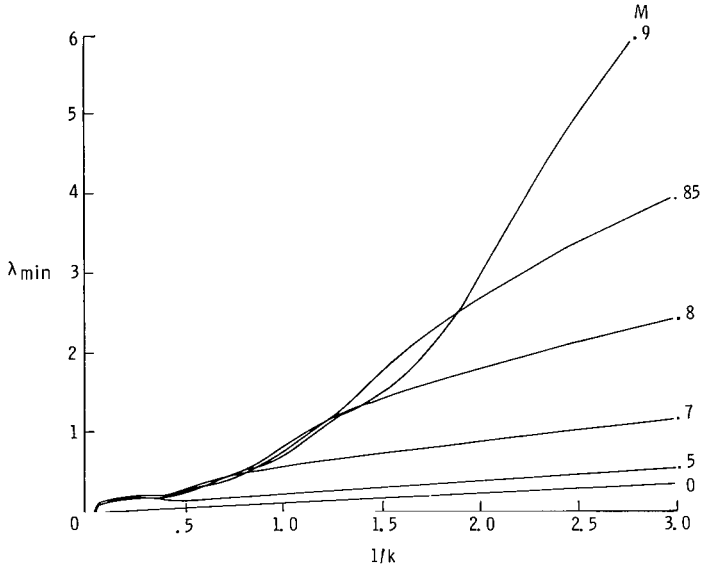

Figure 16.- Concluded.

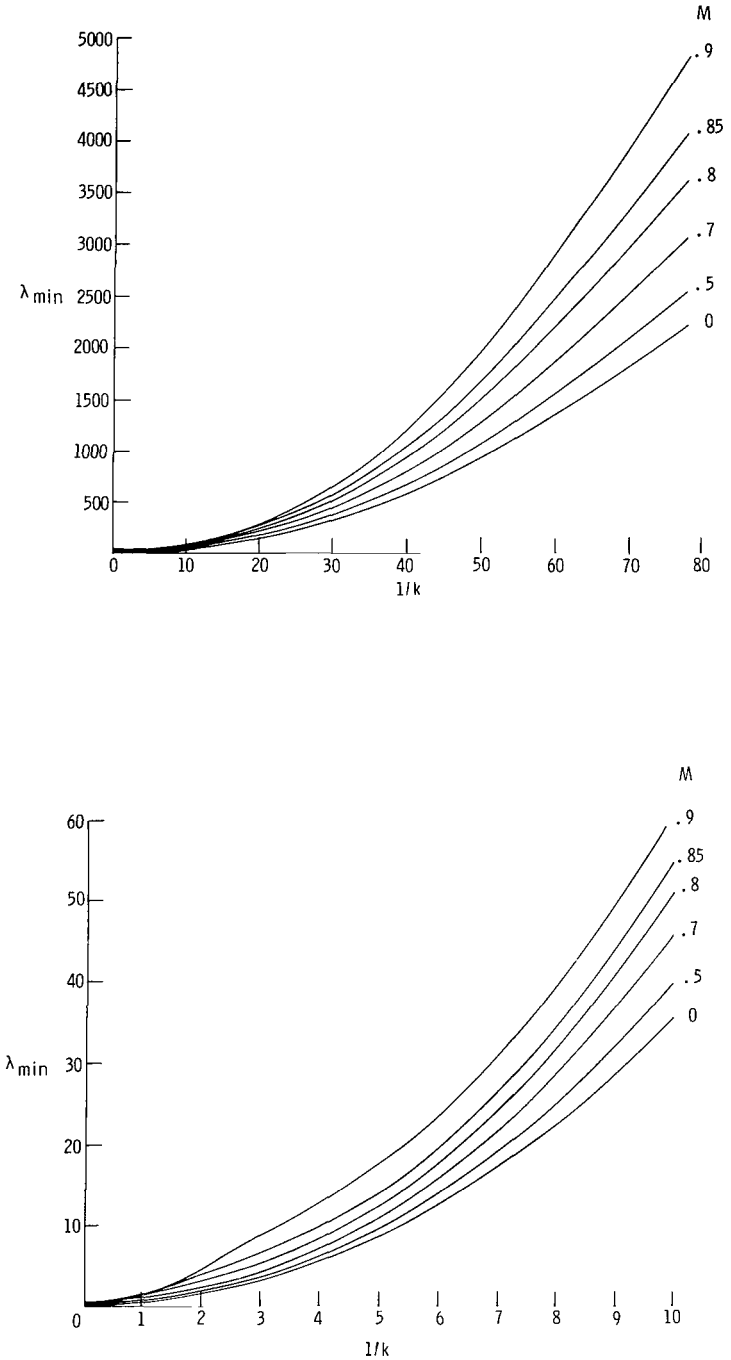

Figure 17.- Compressibility effects of the optimized L.E.-T.E. system.

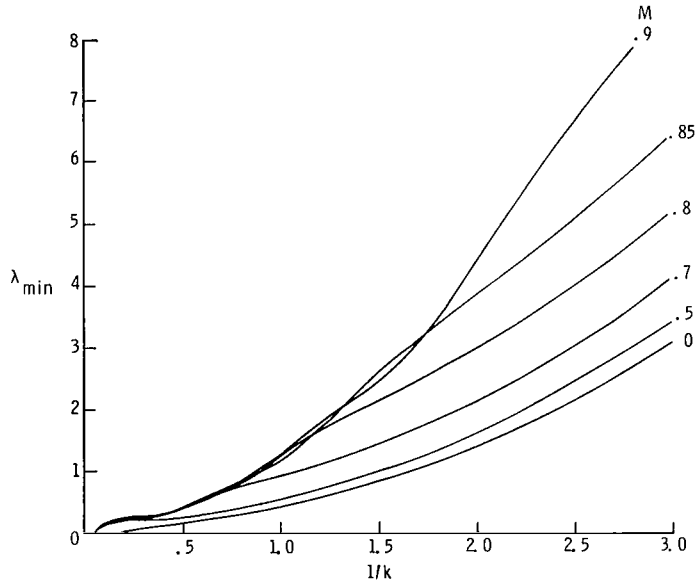

Figure 17.- Concluded.

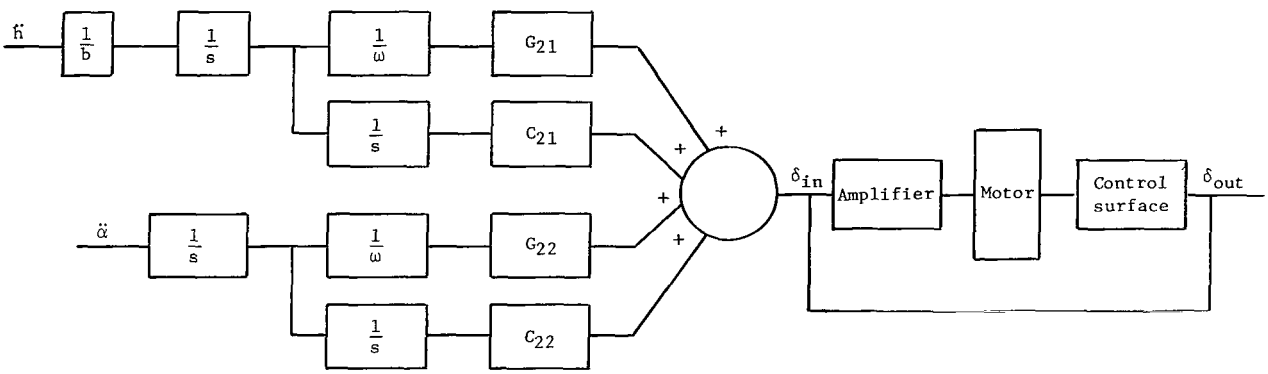

Figure 18.- Block diagram of the T.E. control system.

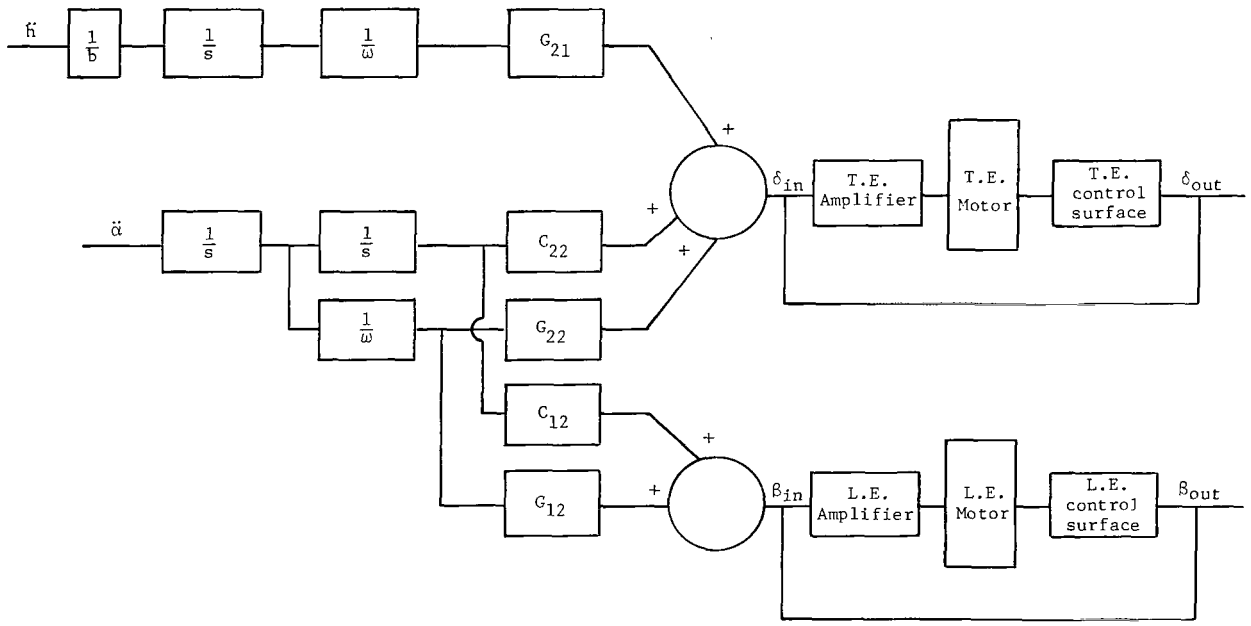

Figure 19.- Block diagram of the L.E.-T.E. control system.

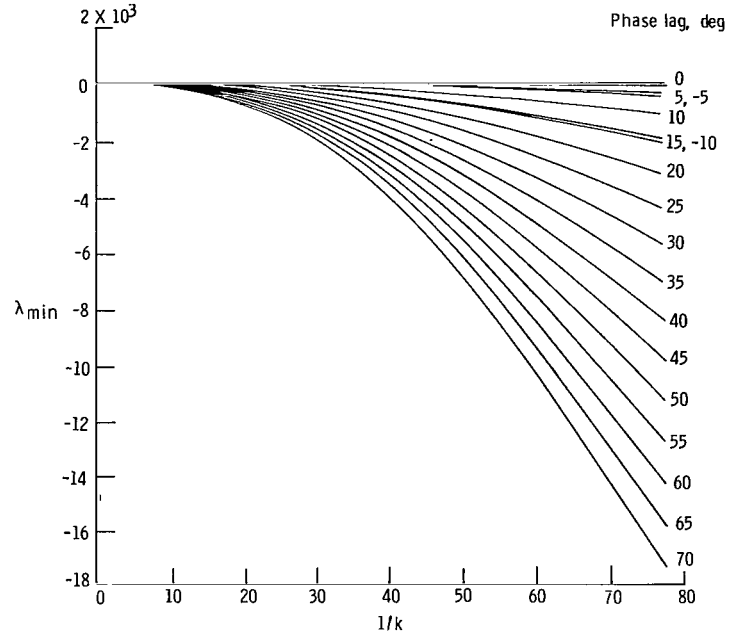

(a) Wide k^{-1} range.

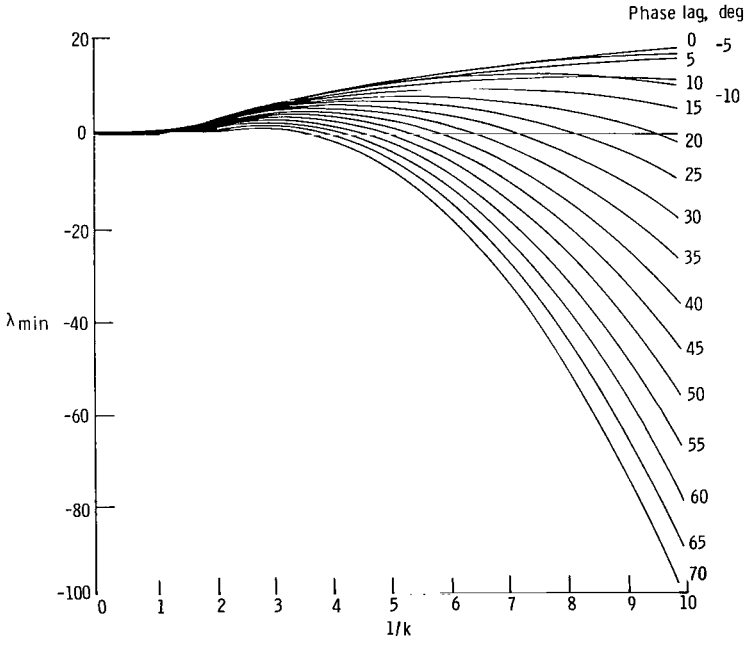

(b) Reduced k^{-1} range.

Figure 20.- Variation of λ_{min} with phase lag by use of optimum values of C and G from M = 0.9 results (T.E. system).

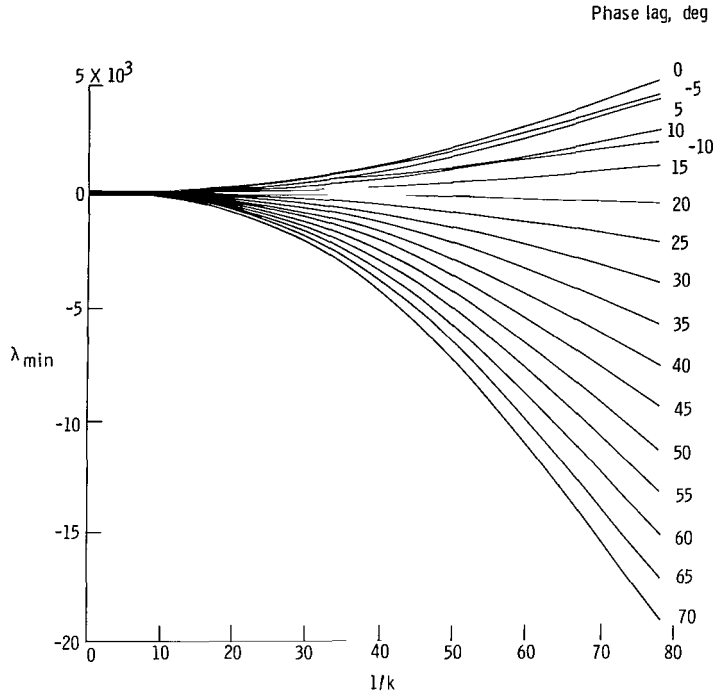

(a) Wide k^{-1} range.

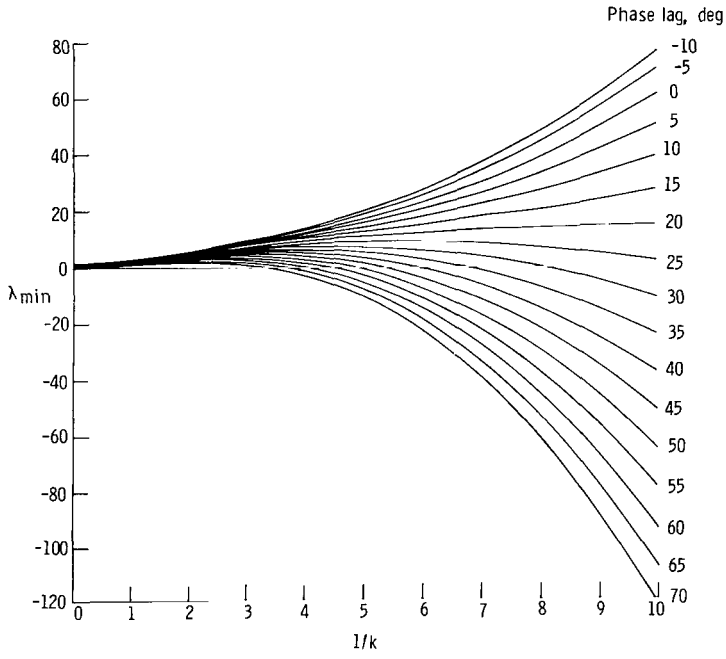

(b) Reduced k^{-1} range.

Figure 21.- Variation of λ_{min} with phase lag by use of optimum values of C and G from M = 0.9 results (L.E.-T.E. system).

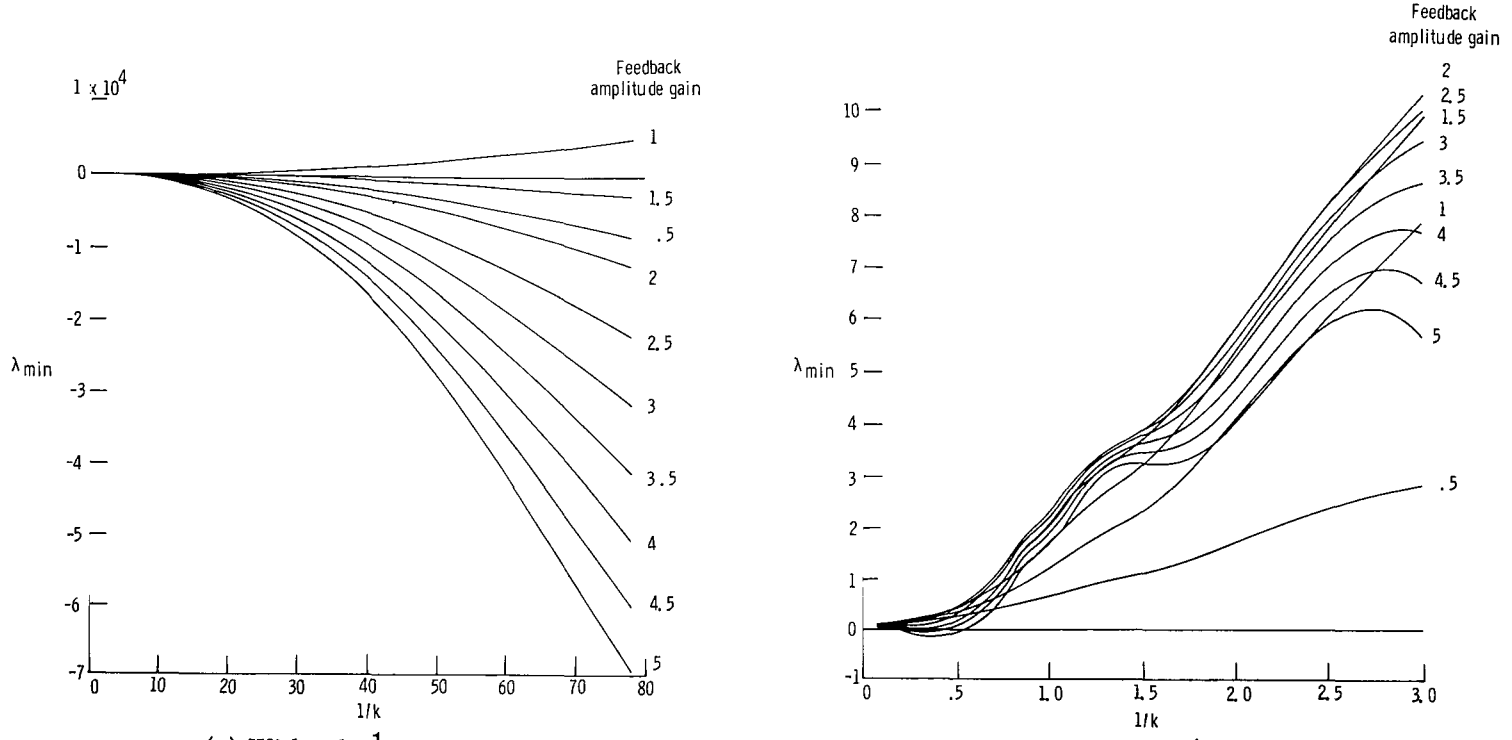

(a) Wide k^{-1} range.

(b) Reduced k^{-1} range.

Figure 22.- Variation of λ_{min} with feedback amplitude gain using the optimum values of C and G. M = 0.9; L.E.-T.E. system.

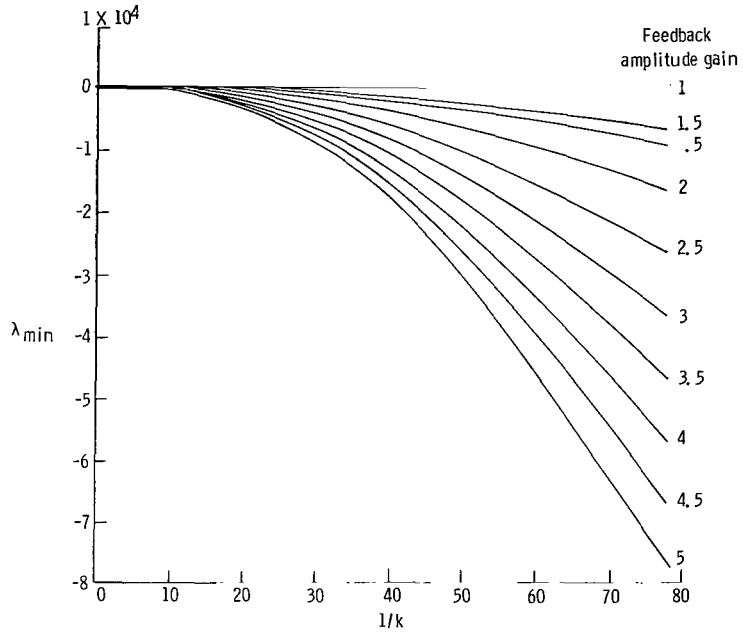

Figure 23.- Variation of λ_{min} with feedback amplitude gain using the optimum values of C and G. M = 0.9; T.E. system.

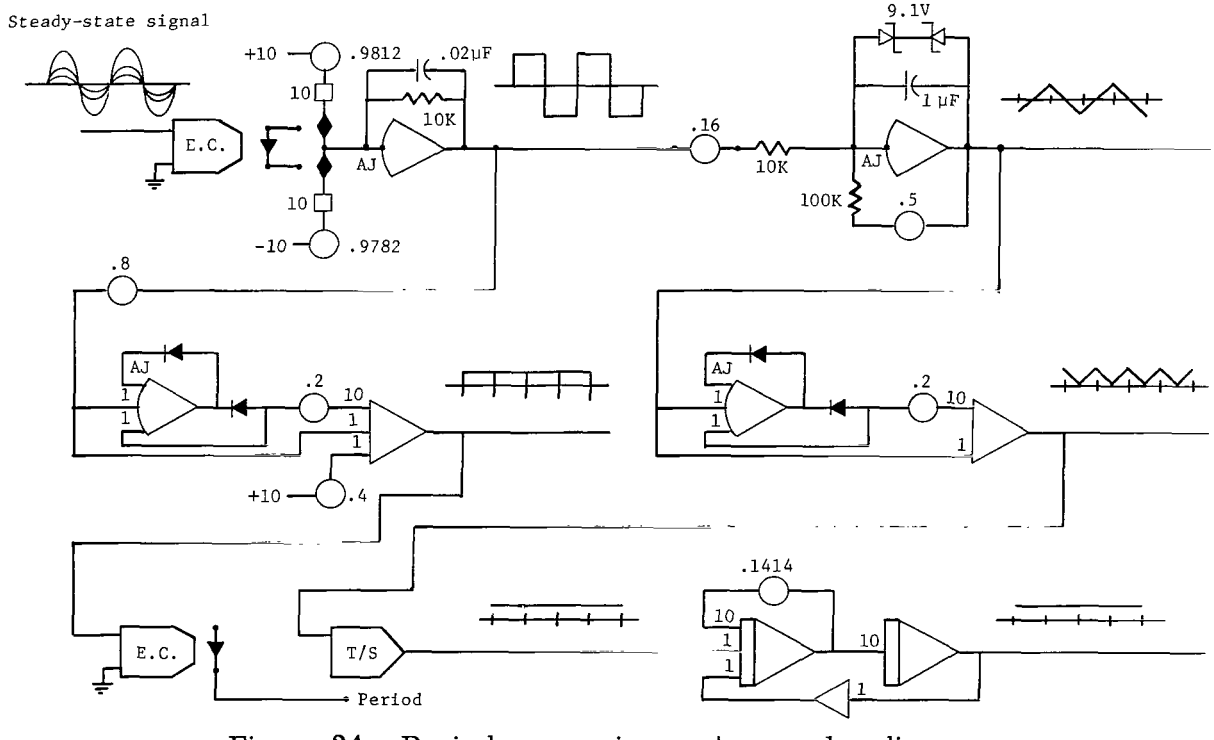

Figure 24.- Period-measuring system analog diagram and signal sketches.

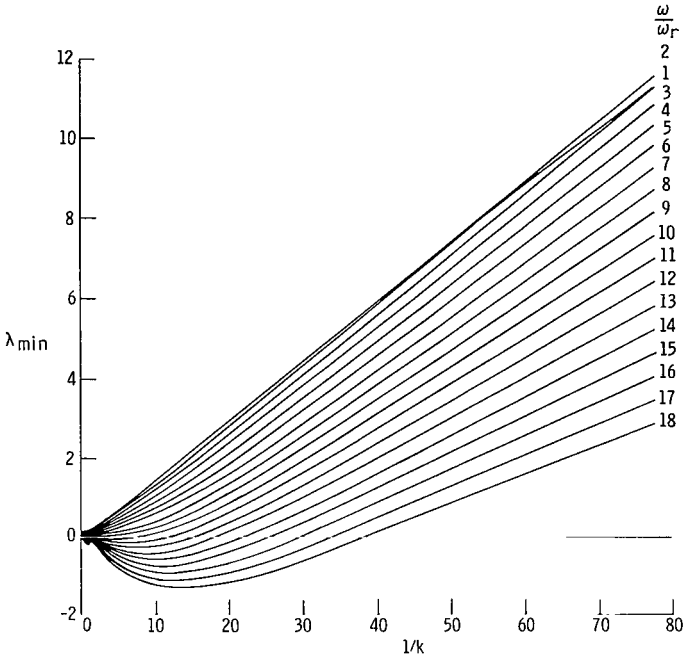

(a) $\frac{\omega}{\omega_r} \geqq 1$; wide k^{-1} range.

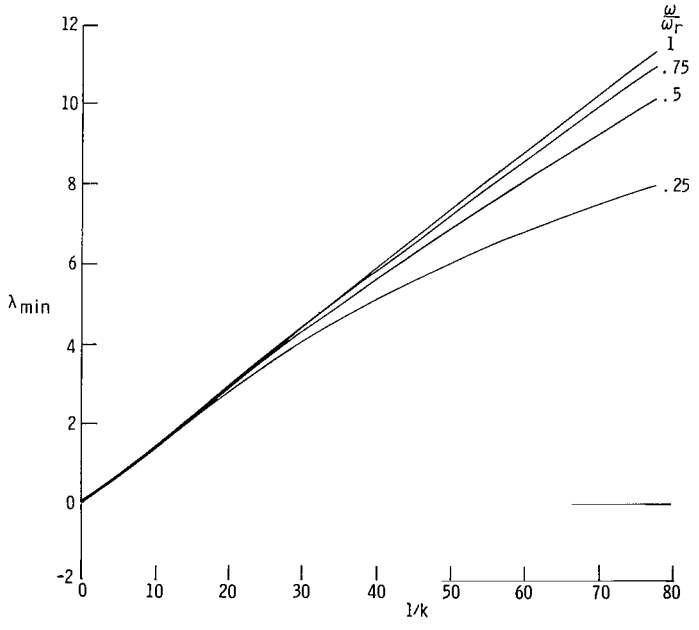

(b) $\frac{\omega}{\omega_r} \leqq 1$; wide k^{-1} range.

Figure 25.- Variation of λ_{min} with ω/ω_r using the optimum values of C and G from the M = 0 results (T.E. system).

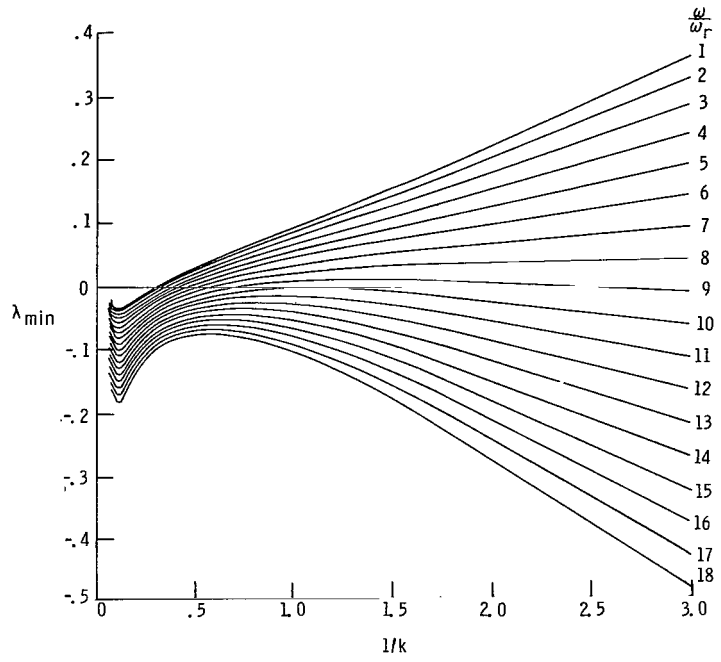

(c) $\frac{\omega}{\omega_r} \geqq 1$; reduced k^{-1} range.

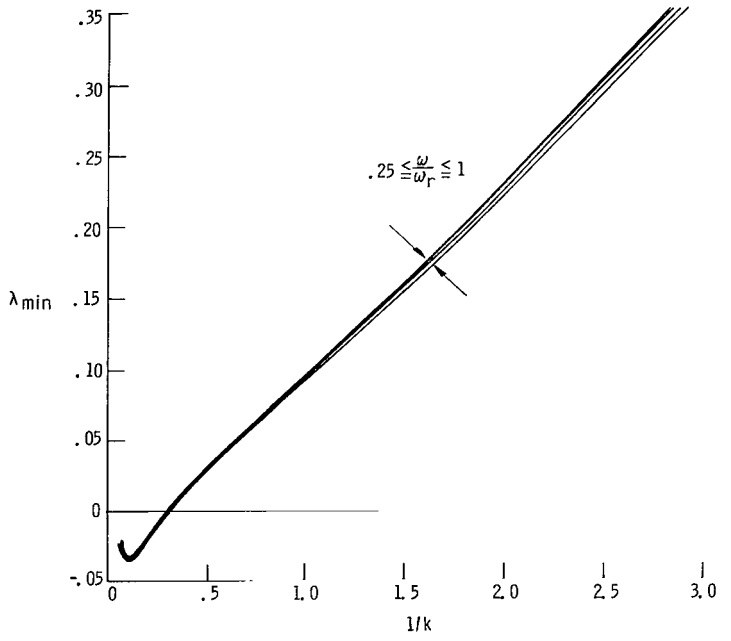

(d) $\frac{\omega}{\omega_r} \leqq 1$; reduced k^{-1} range.

Figure 25.- Concluded.

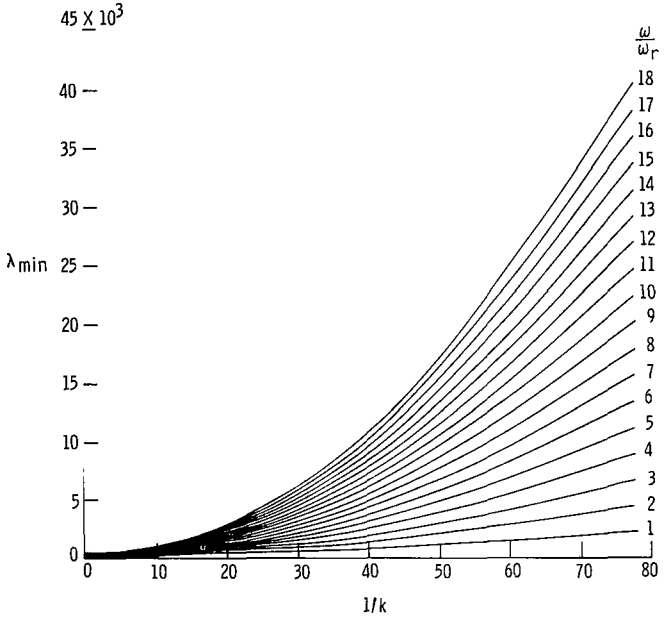

(a) $\frac{\omega}{\omega_r} \geqq 1$; wide k^{-1} range.

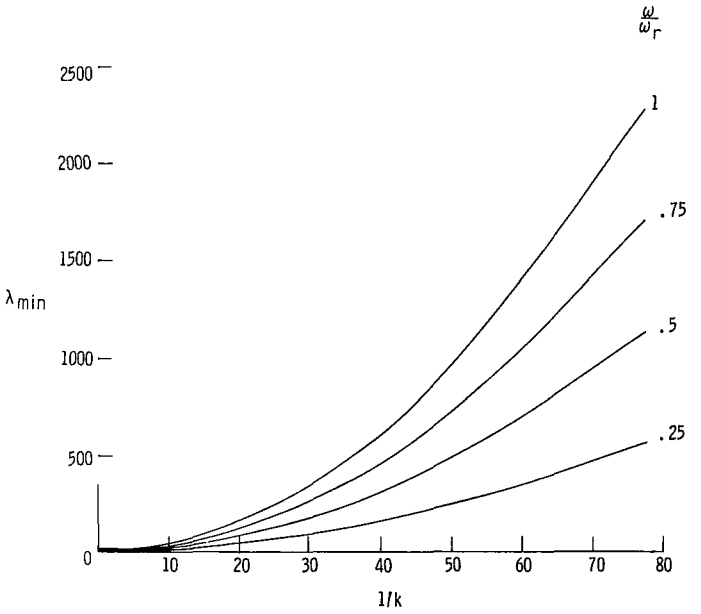

(b) $\frac{\omega}{\omega_r} \leqq 1$; wide k^{-1} range.

Figure 26.- Variation of λ_{min} with ω/ω_r using the optimum values of C and G from the M = 0 results (L.E.-T.E. system).

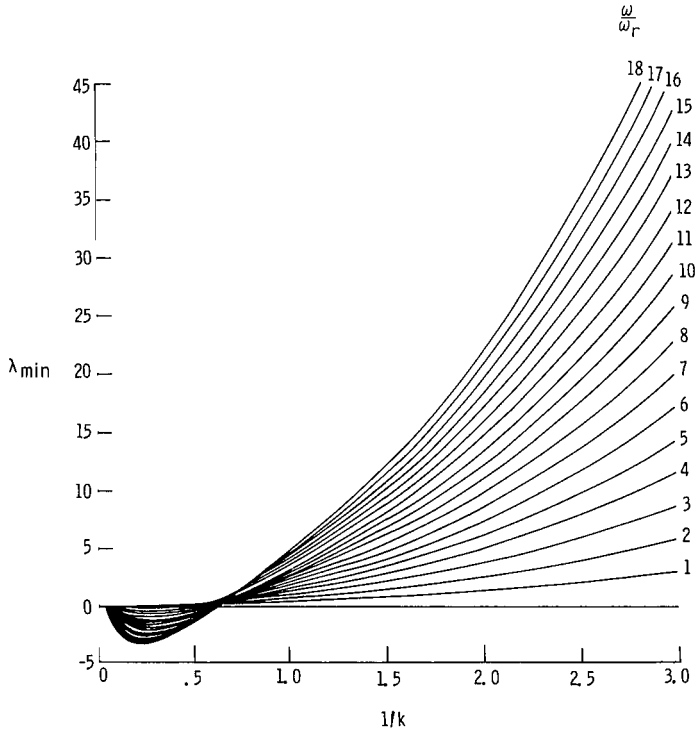

(c) $\frac{\omega}{\omega_r} \geqq 1$; reduced k^{-1} range.

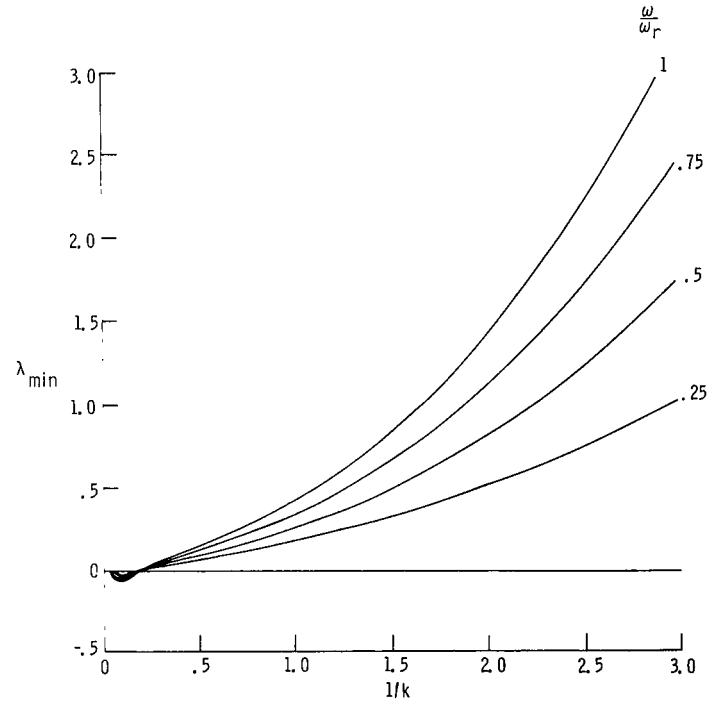

(d) $\frac{\omega}{\omega_r} \leqq 1$; reduced k^{-1} range.

Figure 26.- Concluded.

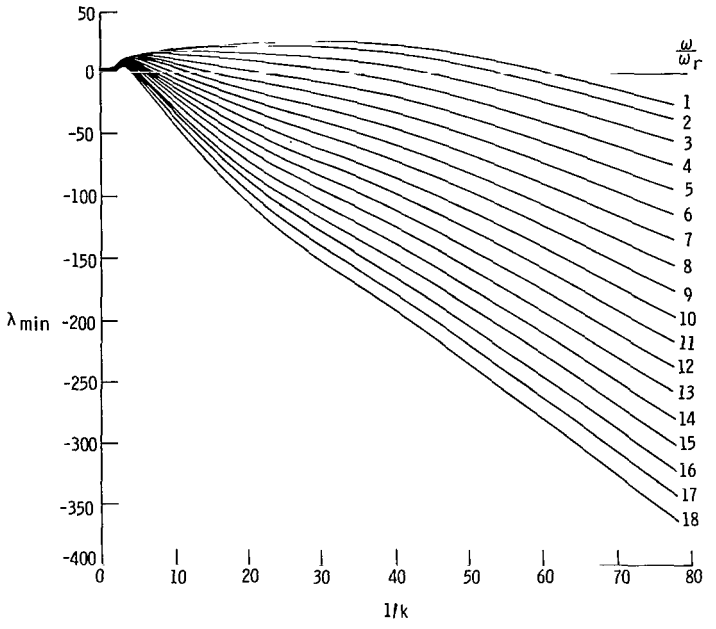

(a) $\frac{\omega}{\omega_r} \geqq 1$; wide k^{-1} range.

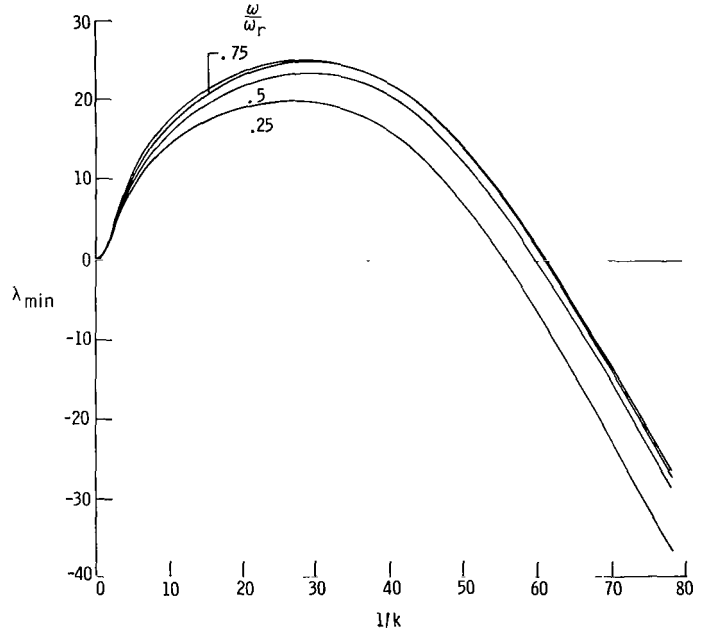

(b) $\frac{\omega}{\omega_r} \leqq 1$; wide k^{-1} range.

Figure 27.- Variation of λ_{min} with ω/ω_r using the optimum values of C and G from the M = 0.9 results (T.E. system).

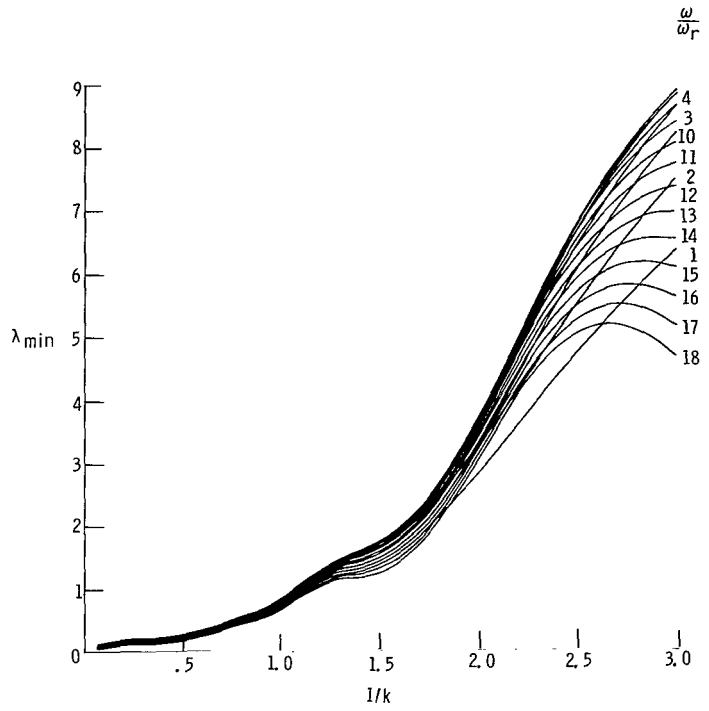

(c) $\frac{\omega}{\omega_r} \geqq 1$; reduced k^{-1} range.

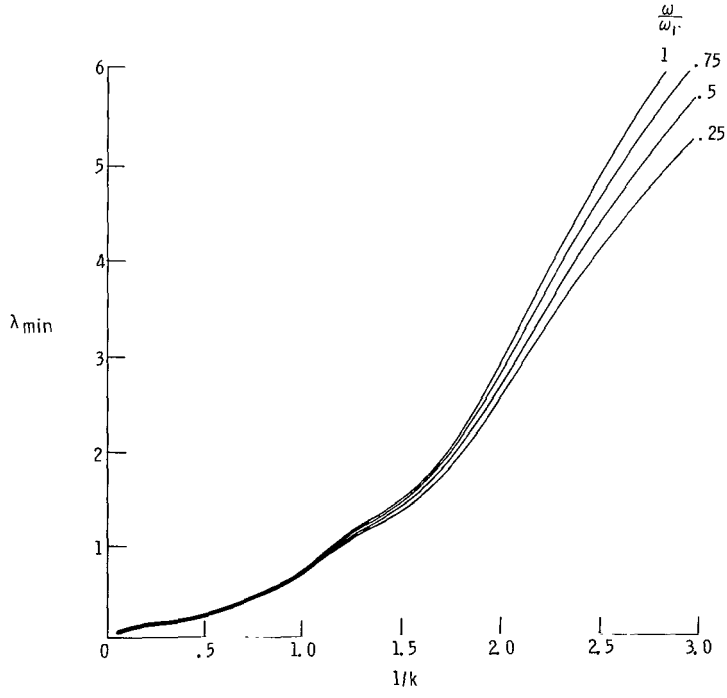

(d) $\frac{\omega}{\omega_r} \leqq 1$; reduced k^{-1} range.

Figure 27.- Concluded.

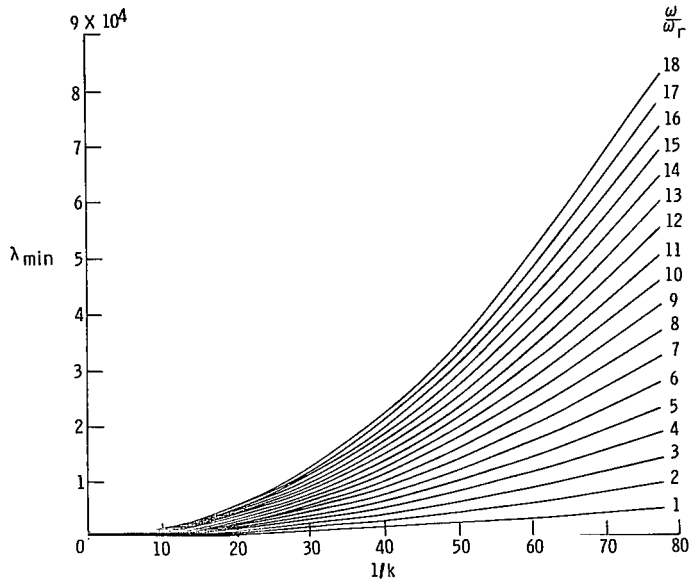

(a) $\frac{\omega}{\omega_r} \geqq 1$; wide k^{-1} range.

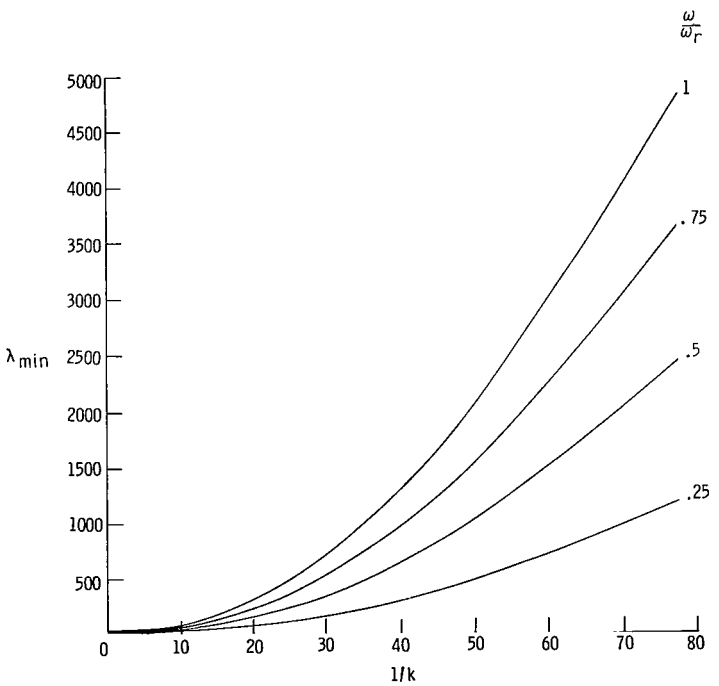

(b) $\frac{\omega}{\omega_r} \leqq 1$; wide k^{-1} range.

Figure 28.- Variation of λ_{min} with ω/ω_r using the optimum values of C and G from the M = 0.9 results (L.E.-T.E. system).

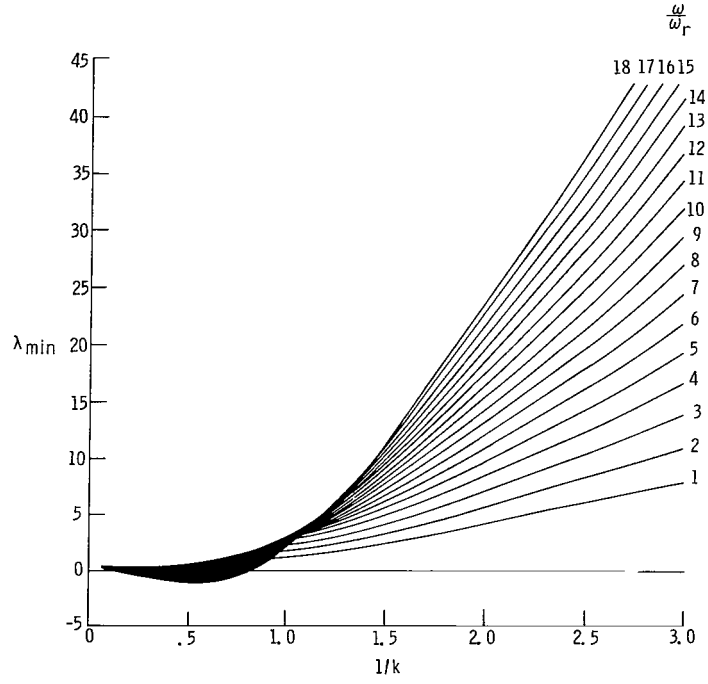

(c) $\frac{\omega}{\omega_r} \geqq 1$; reduced k^{-1} range.

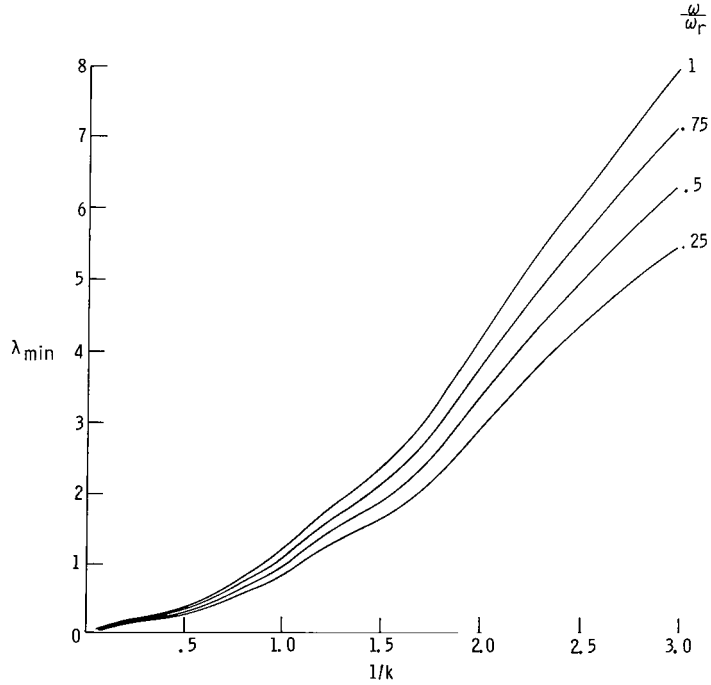

(d) $\frac{\omega}{\omega_r} \leqq 1$; reduced k^{-1} range.

Figure 28.- Concluded.

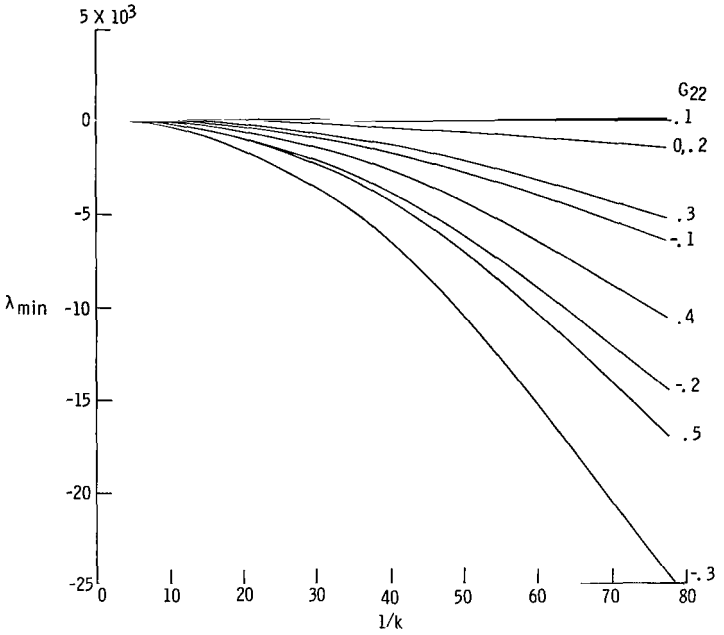

(a) Variation of G_{22}; T.E. system.

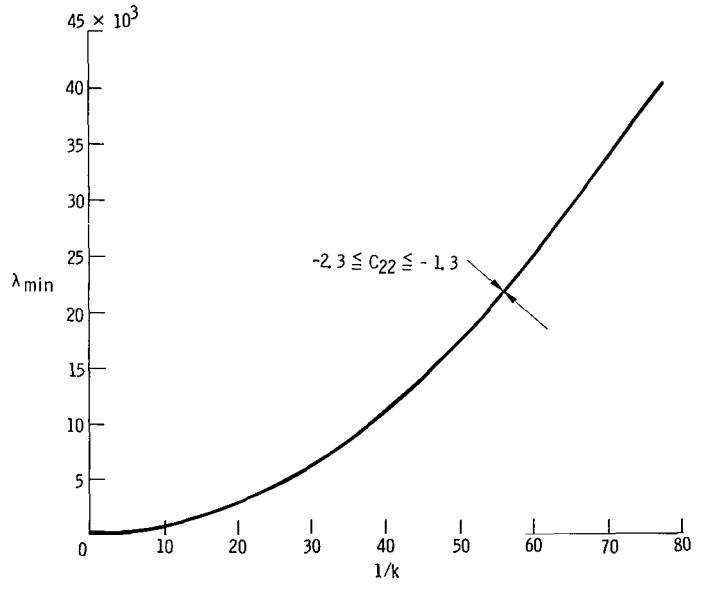

(b) Variation of C_{22}; L.E.-T.E. system.

Figure 29.- The effects on λ_{min} of variation of the control system parameters around their optimum values. $C_{11} = C_{12} = G_{11} = G_{12} = 0$; $C_k = 18$; $M = 0$.

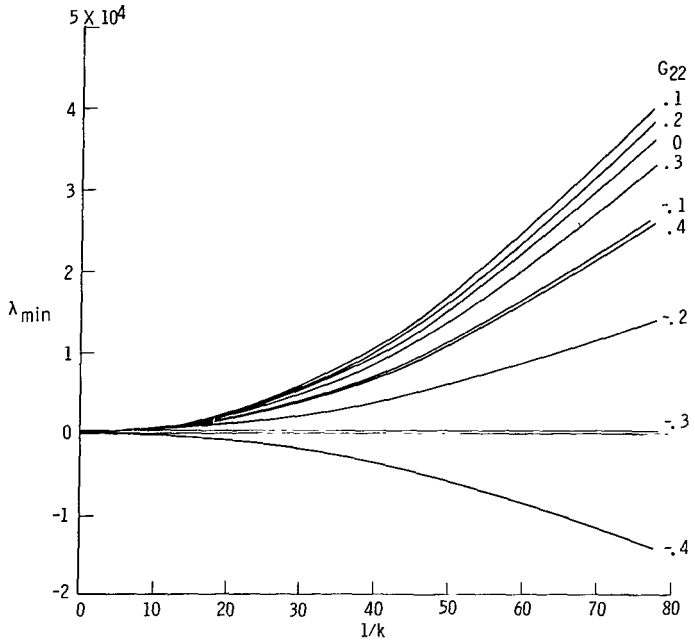

(c) Variation of G_{22}; L.E.-T.E. system.

Figure 29.- Concluded.

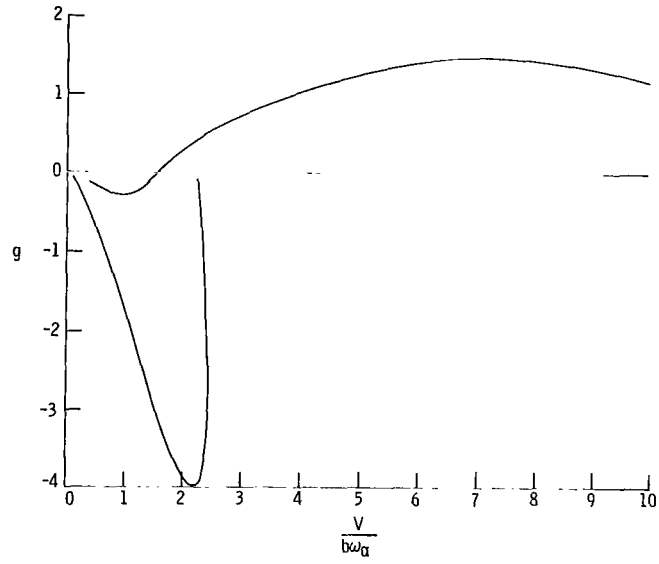

(a) Basic binary system; no active controls.

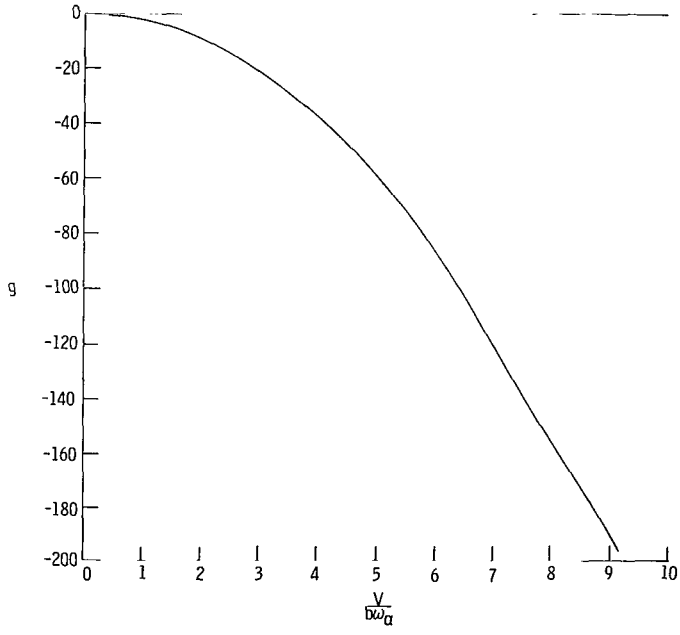

(b) Binary system with optimized control law; L.E.-T.E. system.

Figure 30.- V-g plots of a two-dimensional, two-degrees-of-freedom (bending-torsion) system.

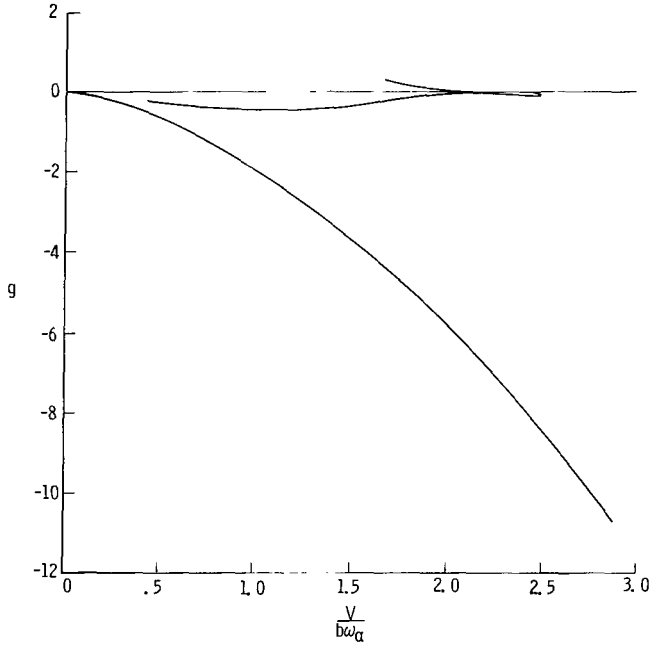

(c) Binary system with 0.1 of optimized control law values; L.E.-T.E. system.

Figure 30.- Concluded.

NASA-Langley, 1971 — 1 L-7525

"The aeronautical and space activities of the United States shall be conducted so as to contribute . . . to the expansion of human knowledge of phenomena in the atmosphere and space. The Administration shall provide for the widest practicable and appropriate dissemination of information concerning its activities and the results thereof."

— NATIONAL AERONAUTICS AND SPACE ACT OF 1958

NASA SCIENTIFIC AND TECHNICAL PUBLICATIONS

TECHNICAL REPORTS: Scientific and technical information considered important, complete, and a lasting contribution to existing knowledge.

TECHNICAL NOTES: Information less broad in scope but nevertheless of importance as a contribution to existing knowledge.

TECHNICAL MEMORANDUMS: Information receiving limited distribution because of preliminary data, security classification, or other reasons.

CONTRACTOR REPORTS: Scientific and technical information generated under a NASA contract or grant and considered an important contribution to existing knowledge.

TECHNICAL TRANSLATIONS: Information published in a foreign language considered to merit NASA distribution in English.

SPECIAL PUBLICATIONS: Information derived from or of value to NASA activities. Publications include conference proceedings, monographs, data compilations, handbooks, sourcebooks, and special bibliographies.

TECHNOLOGY UTILIZATION PUBLICATIONS: Information on technology used by NASA that may be of particular interest in commercial and other non-aerospace applications. Publications include Tech Briefs, Technology Utilization Reports and Technology Surveys.

Details on the availability of these publications may be obtained from:

SCIENTIFIC AND TECHNICAL INFORMATION OFFICE

NATIONAL AERONAUTICS AND SPACE ADMINISTRATION

Washington, D.C. 20546